Comparison of Boltzmann Kinetics with Quantum Dynamics for Relativistic Quantum Fields

Doctoral Thesis in Physics

submitted by

Markus Michael Müller

July 2006

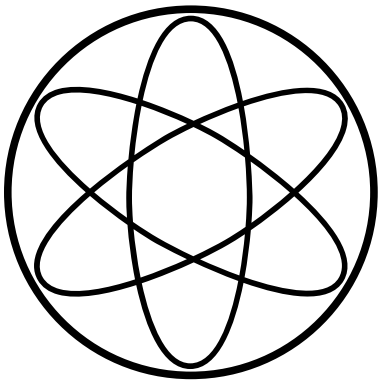

Physik-Department T30d

Technische Universität München

Prof. Dr. Manfred Lindner

Physik-Department
Technische Universität München
T30d Theoretische Elementarteilchenphysik

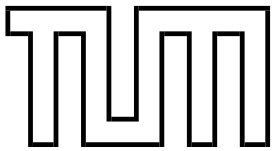

Comparison of Boltzmann Kinetics with Quantum Dynamics for Relativistic Quantum Fields

Dipl.-Phys. Univ. Markus Michael Müller

Vollständiger Abdruck der von der Fakultät für Physik der Technischen Universität München zur Erlangung des akademischen Grades eines

Doktors der Naturwissenschaften (Dr. rer. nat.)

genehmigten Dissertation.

Vorsitzender:	Univ.-Prof. Dr. Klaus Schreckenbach
Prüfer der Dissertation:	
1.	Prof. Dr. Manfred Lindner, Ruprecht-Karls-Universität Heidelberg
2.	Univ.-Prof. Dr. Wolfram Weise

Die Dissertation wurde am 26.7.2006 bei der Technischen Universität München eingereicht und durch die Fakultät für Physik am 8.8.2006 angenommen.

Comparison of Boltzmann Kinetics with Quantum Dynamics for Relativistic Quantum Fields

Abstract

Boltzmann equations are often used to study the thermal evolution of particle reaction networks. Prominent examples are the computation of the baryon asymmetry of the universe and the evolution of the quark-gluon plasma after a relativistic heavy ion collision. However, Boltzmann equations are only a classical approximation of the quantum thermalization process which is described by the so-called Kadanoff-Baym equations. This raises the question how reliable Boltzmann equations are as approximations to the full Kadanoff-Baym equations. Therefore, we present in this thesis a detailed comparison of Boltzmann and Kadanoff-Baym equations in the framework of relativistic quantum field theories in 3+1 space-time dimensions. In a first step, for simplicity we consider a real scalar Φ^4 quantum field theory and in a second step we generalize our results to a chirally invariant Yukawa-type quantum field theory including fermions. The obtained numerical solutions reveal significant discrepancies in the results predicted by both types of equations. Apart from quantitative discrepancies, on a qualitative level the universality respected by Kadanoff-Baym equations is severely restricted in the case of Boltzmann equations. Furthermore, Kadanoff-Baym equations strongly separate the time scales between kinetic and chemical equilibration. This separation of time scales is absent for Boltzmann equations.

Contents

Chapter 1

Introduction and Overview

"The story so far:

In the beginning the Universe was created. This has made a lot of people very angry and been widely regarded as a bad move."

Douglas Adams
The Restaurant at the End of the Universe

Nonequilibrium dynamics is part of numerous interesting phenomena in the field of (astro-)particle physics. For example, one of the most attractive frameworks to explain the matter-antimatter asymmetry of the universe is the so-called leptogenesis mechanism [1–3]. According to this scenario, lepton number violating interactions in the early universe produce a lepton asymmetry which is subsequently converted to the observed baryon asymmetry by so-called sphaleron processes. For the dynamical generation of the lepton asymmetry it is necessary, that the universe was in a state out of thermal equilibrium [4]. The standard means to deal with this nonequilibrium situation are Boltzmann equations. However, it is well known that (classical) Boltzmann equations suffer from several shortcomings as compared to their quantum mechanical generalizations, the so-called Kadanoff-Baym equations. This motivates a comparison of Boltzmann and Kadanoff-Baym equations in order to assess the reliability of quantitative predictions of leptogenesis scenarios.

Apart from leptogenesis, additional motivation to study the connection between Boltzmann and Kadanoff-Baym equations is furnished by relativistic heavy ion collision experiments which aim at probing the quark-gluon plasma. In these experiments the quark-gluon plasma is produced in a state far from equilibrium. Recently, however, experiments claimed that the approach to thermal equilibrium should happen very fast, and that the evolution of the quark-gluon plasma could even be described by hydrodynamic equations [5–8], which arise as approximations to Boltzmann equations [9, 10]. In this context it is important to note that different quantities effectively thermalize on different time scales [11]. Thus, one might face the situation that, although the full approach to thermal equilibrium

takes a very long time, certain quantities, which are sufficient to describe the quark-gluon plasma with hydrodynamic equations, approach their equilibrium values on considerably shorter time scales.

What are the shortcomings of Boltzmann equations? First we would like to note that Boltzmann equations should work well for a gas of particles which behave sufficiently classical. For example, the explosions in the pistons of a car engine or atmospheric turbulences can well be described by Boltzmann equations. However, once quantum mechanics comes into play, which is certainly the case for elementary particles starring in phenomena like leptogenesis or the quark-gluon plasma, things change drastically. The quantum dynamics of such systems is described by the so-called Kadanoff-Baym equations. In order to pinpoint the insufficiencies of Boltzmann equations, we note that they arise as approximations to the Kadanoff-Baym equations[1]. As a matter of fact, one has to employ a whole cascade of approximations, among them a first-order gradient expansion, a Wigner transformation and a quasi-particle (or on-shell) approximation [14–18].

It is known, that the gradient expansion cannot be justified for early times. Consequently, one might expect that Boltzmann equations fail to describe the early-time evolution and that errors accumulated for early times cannot be remedied at late times.

Of course, a Wigner transformation itself is not at all an approximation, but in order to make it available, one has to send the initial time to the remote past. Boltzmann equations imply the assumption of molecular chaos ("Stoßzahlansatz") [19–21], which introduces irreversibility: Two particles are considered uncorrelated before their collision, i.e. their history is discarded completely. In contrast to this Kadanoff-Baym equations take these memory effects into account and keep the information on the details of the initial conditions. Numerical solutions of Kadanoff-Baym equations revealed that this memory is lost gradually. Consequently, for late times it is indeed justifiable to send the initial time to the remote past. For early times, however, this is certainly not the case. The damping of correlations increases with coupling constants and the average effective particle number density of the system. Therefore, the assumption of molecular chaos seems to contradict the weak-coupling and dilute-gas approximations, which are also implied by standard Boltzmann equations.

As a consequence of the quasi-particle approximation, the conservation of momentum and energy prevents Boltzmann equations from describing thermalization in $1+1$ space-time dimensions. In contrast to this, it has been shown in the framework of a scalar Φ^4 quantum field theory that this is feasible with Kadanoff-Baym equations [22]. The reason for this qualitative discrepancy is that Kadanoff-Baym equations take off-shell effects into account [23], which are neglected in Boltzmann equations. Of course, in 3+1 dimensions both types of equations

[1]The connection between Boltzmann equations and classical field theory has been treated in Refs. [12, 13].

are capable of describing thermalization. It is important to note, however, that Kadanoff-Baym equations respect full universality: For systems with identical (conserved) average energy density the late-time behavior coincides irrespective of the details of the initial conditions. In contrast to this, the quasi-particle approximation introduces fake constants of motion for the corresponding Boltzmann equations, which severely restricts the evolution of the particle number densities. As a result, Boltzmann equations only respect a restricted universality: Only systems for which the average energy density as well as all fake constants of motion agree from the very beginning share the same late-time results. In the case of leptogenesis the on-shell character of the Boltzmann equation leads to a further inconsistency: All leptogenesis scenarios share the fact that some heavy particles decay out of thermal equilibrium into the particles which we observe in the universe today. The spectral function of a particle that can decay into other particles is given by a Breit-Wigner curve with a non-vanishing width. The quasi-particle approximation reduces the decay width of these particles to zero, i.e. a Boltzmann equation can only describe systems consisting of stable quasi-particles. After all, how does the on-shell character of the Boltzmann equation affect the description of quantum fields out of thermal equilibrium in $3+1$ dimensions?

When applying Boltzmann equations to the description of leptogenesis, the standard technique to construct the collision integrals — before employing further approximations — is to take the usual bosonic and fermionic statistical gain and loss terms multiplied with the S-matrix element for the respective reaction [24,25]. Generally these S-matrix elements are computed using perturbation theory, which is justifiable only for a consideration in vacuum, and one may wonder of which significance they are for a quantum mechanical many-particle system.

All these shortcomings of Boltzmann equations lead to the conclusion that one should perform a detailed comparison of Boltzmann and Kadanoff-Baym equations [26–32], such that one can explicitly see how large the quantum mechanical corrections are.

Due to the complexity of the problem, in a first step we restrict ourselves to a real scalar Φ^4 quantum field theory in $3+1$ space-time dimensions [31, 32]. Of course, in this framework one can neither describe the phenomenon of leptogenesis nor thermalization of the quark-gluon plasma after a relativistic heavy ion collision. Nevertheless, it certainly permits to present a detailed comparison of Boltzmann and Kadanoff-Baym equations, which may reveal interesting phenomena to be investigated in more realistic theories. We found considerable discrepancies in the results predicted by the Boltzmann and Kadanoff-Baym equations: On a quantitative level, we found that the Boltzmann equation predicts significantly larger thermalization times than the corresponding Kadanoff-Baym equations. On a qualitative level we could verify that Kadanoff-Baym equations respect full universality [33, 34] and strongly separate the time scales between kinetic and chemical equilibration [11]. In the case of a real scalar Φ^4 quantum field theory the Boltzmann equation artificially conserves the total particle num-

ber, which severely constrains the evolution of the particle number density. As a result, the Boltzmann equation respects only a restricted universality, fails to describe the process of chemical equilibration, and does not separate any time scales.

In a second step, we generalized our results to the case of a chirally invariant Yukawa model including fermions. We found the same results: Kadanoff-Baym equations respect universality including the process of quantum chemical equilibration and separate the time scales between kinetic and chemical equilibration [11, 35]. Again, the corresponding Boltzmann equations comprise fake constants of motion and therefore maintain only a restricted universality, fail to describe quantum chemical equilibration and do not separate any time scales.

Before we get to the gory details of the above considerations, in the next chapter we introduce important concepts for an efficient treatment of quantum fields in and out of thermal equilibrium. In this sense the following chapter serves as a second — more technical — introduction to this thesis.

The third and fourth chapters are devoted to the afore mentioned comparisons of Boltzmann and Kadanoff-Baym equations. In general, when studying systems out of thermal equilibrium by means of Kadanoff-Baym equations, it is crucial to start from a Φ-derivable approximation, since these approximations guarantee the conservation of energy and global charges [36–38]. The 2PI effective action [39–41] furnishes such a Φ-derivable approximation and has proven to be an efficient and reliable tool for the description of quantum fields out of thermal equilibrium in numerous previous treatments [22,33,35,42,43]. Consequently, in chapters 3 and 4 the 2PI effective action will be our starting point. The Kadanoff-Baym equations can be derived by requiring that the 2PI effective action be stationary with respect to variations of the complete connected two-point functions [22, 35, 40, 41]. In order to derive the corresponding Boltzmann equations, subsequently one has to employ a first-order gradient expansion, a Wigner transformation, the Kadanoff-Baym ansatz and the quasi-particle approximation [14–18]. While Boltzmann equations describe the time evolution of particle number distributions, Kadanoff-Baym equations describe the evolution of the complete quantum mechanical two-point functions of the system. However, one can define effective particle number distributions which are given by the complete propagators and their time derivatives evaluated at equal times [22, 35]. Finally, we solve the Boltzmann and the Kadanoff-Baym equations numerically for spatially homogeneous and isotropic systems in 3+1 space-time dimensions and compare their predictions on the evolution of these systems for various initial conditions.

We conclude this thesis in the fifth chapter. The appendix exhibits the details of the rather sophisticated computational algorithms underlying our numerical solutions of the Boltzmann and Kadanoff-Baym equations.

Throughout this work we use the Minkowski metric where the time-time component is negative and units where Planck's constant, the speed of light and Boltzmann's constant are taken to be unity [44].

Chapter 2

Basic Concepts

In this chapter we introduce important concepts for an efficient treatment of quantum fields in and out of thermal equilibrium. In the first section, we review the derivation of some results in thermal field theory which will be particularly important in subsequent chapters, when we derive Boltzmann equations from Kadanoff-Baym equations. As already mentioned in the introduction this derivation requires a whole cascade of approximations, some of which are motivated by equilibrium considerations. In the second section we will introduce the so-called closed Schwinger-Keldysh real-time contour, which is the basic tool for a description of quantum fields out of thermal equilibrium. Eventually, the third section is devoted to the 2PI effective action. In subsequent chapters the 2PI effective action will be the starting point of our considerations, namely when we derive Kadanoff-Baym equations by requiring that the 2PI effective action be stationary with respect to variations of the full connected two-point functions.

2.1 Quantum Fields in Thermal Equilibrium

In this section we consider a closed system in thermal equilibrium [18,45–48] with time-independent Hamiltonian

$$H = \int d^3x \left[\bar{\Psi}\gamma^j \partial_j \Psi + \frac{1}{2}\delta^{\mu\nu} \left(\partial_\mu \Phi\right) \left(\partial_\nu \Phi\right) + \frac{m^2}{2}\Phi^2 + V\left(\Phi, \Psi, \bar{\Psi}\right) \right] \tag{2.1.1}$$

and temperature $T = \frac{1}{\beta}$. $\Psi(x)$ is a fermionic Dirac field, $\Phi(x)$ is a real scalar quantum field and V contains terms describing the interactions of these quantum fields, which we need not specify explicitly for the purposes of this section. For simplicity we restrict our considerations to systems for which the average net charge density vanishes, such that we can work with the canonical density operator

$$\mathcal{D} = \frac{1}{Z} \exp\left(-\beta H\right) \ , \tag{2.1.2}$$

where the partition function Z is given by

$$Z = \mathrm{tr}\left(\exp\left(-\beta H\right)\right). \tag{2.1.3}$$

The similarity between the time evolution operator $\exp\left(-i\left(t-t_0\right)H\right)$ and the operator $\exp\left(-\beta H\right)$ suggests the definition of a new operator which includes the former two operators as special cases. We set

$$U\left(\tau\right) = \exp\left(-\tau H\right)$$

and allow τ to take complex values. It is obvious that $U\left(\tau\right)$ can be interpreted as evolution operator for complex-valued times. In order to evaluate the trace in Eq. (2.1.3) we can use the complete set of right- and left-eigenstates of the Heisenberg operators $\Phi\left(\boldsymbol{x},t\right)$ and $\Psi\left(\boldsymbol{x},t\right)$ for $t=0$:

$$\begin{aligned}
\Phi\left(\boldsymbol{x},t\right)\left|\varphi\left(t\right),\psi\left(t\right)\right\rangle &= \varphi\left(\boldsymbol{x}\right)\left|\varphi\left(t\right),\psi\left(t\right)\right\rangle, &(2.1.4)\\
\Psi\left(\boldsymbol{x},t\right)\left|\varphi\left(t\right),\psi\left(t\right)\right\rangle &= \psi\left(\boldsymbol{x}\right)\left|\varphi\left(t\right),\psi\left(t\right)\right\rangle, &(2.1.5)
\end{aligned}$$

and

$$\begin{aligned}
\left\langle\varphi\left(t\right),\psi\left(t\right)\right|\Phi\left(\boldsymbol{x},t\right) &= \left\langle\varphi\left(t\right),\psi\left(t\right)\right|\varphi\left(\boldsymbol{x}\right), &(2.1.6)\\
\left\langle\varphi\left(t\right),\psi\left(t\right)\right|\Psi\left(\boldsymbol{x},t\right) &= \left\langle\varphi\left(t\right),\psi\left(t\right)\right|\psi\left(\boldsymbol{x}\right). &(2.1.7)
\end{aligned}$$

The partition function is then given by

$$Z = \int\prod_{\boldsymbol{x}}\left[d\varphi\left(\boldsymbol{x}\right)d\psi\left(\boldsymbol{x}\right)\right]\ \left\langle\varphi\left(0\right),\psi\left(0\right)\right|U\left(\beta\right)\left|\varphi\left(0\right),\psi\left(0\right)\right\rangle.$$

As indicated above, by interpreting $U\left(\tau\right)$ as an evolution operator for complex-valued times, we obtain the following path integral representation for the matrix element:

$$\begin{aligned}
&\left\langle\varphi\left(0\right),\psi\left(0\right)\right|U\left(\beta\right)\left|\varphi\left(0\right),\psi\left(0\right)\right\rangle\\
&= \int_{\substack{\varphi(\boldsymbol{x},0)=\varphi(\boldsymbol{x},\beta)=\varphi(\boldsymbol{x})\\ \psi(\boldsymbol{x},0)=\psi(\boldsymbol{x},\beta)=\psi(\boldsymbol{x})}} \mathscr{D}\varphi\left(x\right)\mathscr{D}\psi\left(x\right)\mathscr{D}\bar{\psi}\left(x\right)\ \exp\left(-I_E\left[\varphi,\psi,\bar{\psi}\right]\right),
\end{aligned}$$

where we use the notation

$$\mathscr{D}\varphi\left(x\right)\mathscr{D}\psi\left(x\right)\mathscr{D}\bar{\psi}\left(x\right) = \prod_{\boldsymbol{x},t}\left[d\varphi\left(\boldsymbol{x},t\right)d\psi\left(\boldsymbol{x},t\right)d\bar{\psi}\left(\boldsymbol{x},t\right)\right].$$

I_E denotes the Euclidean action which we obtain from the classical action by substituting $\tau = ix^0$.

$$\begin{aligned} iI\left[\varphi,\psi,\bar{\psi}\right] &= i\int d^3x \int_0^{-i\beta} dx^0 \left[-\bar{\psi}\ \partial\!\!\!/\psi - \frac{1}{2}\left(\partial_\mu\varphi\right)\left(\partial^\mu\varphi\right) - \frac{1}{2}m^2\varphi^2 + \ldots\right] \\ &= -\int d^3x \int_0^{\beta} d\tau \left[\bar{\psi}\ \partial\!\!\!/_E\psi + \frac{1}{2}\delta^{\mu\nu}\left(\partial_\mu\varphi\right)\left(\partial_\nu\varphi\right) + \frac{1}{2}m^2\varphi^2 + \ldots\right] \\ &= -I_E\left[\varphi,\psi,\bar{\psi}\right] \end{aligned}$$

After all, we arrive at the following path integral representation for the partition function:

$$Z = \int\limits_{\substack{\varphi(\boldsymbol{x},0)=\varphi(\boldsymbol{x},\beta)\\ \psi(\boldsymbol{x},0)=\psi(\boldsymbol{x},\beta)}} \mathscr{D}\varphi\left(x\right)\mathscr{D}\psi\left(x\right)\mathscr{D}\bar{\psi}\left(x\right)\ \exp\left(-I_E\left[\varphi,\psi,\bar{\psi}\right]\right)\ .$$

Adding external source terms to the Euclidean action, we turn the partition function into a generating functional:

$$\begin{aligned} Z\left[J,\theta,\bar{\theta}\right] &= \int\limits_{\substack{\varphi(\boldsymbol{x},0)=\varphi(\boldsymbol{x},\beta)\\ \psi(\boldsymbol{x},0)=\psi(\boldsymbol{x},\beta)}} \mathscr{D}\varphi\left(x\right)\mathscr{D}\psi\left(x\right)\mathscr{D}\bar{\psi}\left(x\right)\ \exp\Big(-I_E\left[\varphi,\psi,\bar{\psi}\right] \\ &\qquad + \int d^3x \int_0^{\beta} d\tau \left[J\varphi + \bar{\psi}\theta + \bar{\theta}\psi\right]\Big)\ . \end{aligned}$$

As usual, the first derivative of the generating functional with respect to a source gives the expectation value of the corresponding quantum field. Using the standard procedure [44] one can identify higher functional derivatives with expectation values of "time ordered" products of quantum fields. For example, we obtain for the scalar two-point Green's function:

$$\begin{aligned} G\left(x,y\right) &= \frac{1}{Z}\left(\frac{\delta^2 Z\left[J,\theta,\bar{\theta}\right]}{\delta J\left(x\right)\delta J\left(y\right)}\right)_{J=\theta=\bar{\theta}=0} \\ &= \frac{1}{Z}\int\limits_{\substack{\varphi(\boldsymbol{z},0)=\varphi(\boldsymbol{z},\beta)\\ \psi(\boldsymbol{z},0)=\psi(\boldsymbol{z},\beta)}} \mathscr{D}\varphi\left(z\right)\mathscr{D}\psi\left(z\right)\mathscr{D}\bar{\psi}\left(z\right)\ \varphi\left(x\right)\varphi\left(y\right)\exp\left(-I_E\left[\varphi,\psi,\bar{\psi}\right]\right) \\ &= \left\langle T_{\mathcal{I}}\left\{\Phi\left(x\right)\Phi\left(y\right)\right\}\right\rangle \\ &= \frac{1}{Z}\mathrm{tr}\Big(\exp\left(-\beta H\right)T_{\mathcal{I}}\left\{\Phi\left(x\right)\Phi\left(y\right)\right\}\Big)\ . \end{aligned}$$

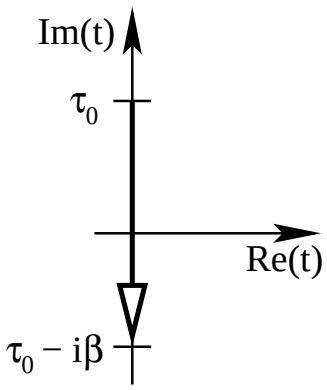

Figure 2.1: The imaginary time path $\mathcal{I}$ was introduced by Matsubara [49]. A similar time path, which partly follows the real axis, has later been proposed by Niemi and Semenoff [50, 51]

The subscript $\mathcal{I}$ indicates that the "time ordering" corresponds to the imaginary time path shown in Fig. 2.1. Similarly, the fermionic propagator is given by

$$\begin{aligned} S^{\alpha\beta}(x,y) &= \frac{1}{Z}\left(\frac{\delta}{\delta\theta^{\beta}(y)}\,\frac{\delta}{\delta\bar{\theta}^{\alpha}(x)}\,Z\left[J,\theta,\bar{\theta}\right]\right)_{J=\theta=\bar{\theta}=0} \\ &= \frac{1}{Z}\int\limits_{\substack{\varphi(\boldsymbol{z},0)=\varphi(\boldsymbol{z},\beta)\\ \psi(\boldsymbol{z},0)=\psi(\boldsymbol{z},\beta)}} \mathscr{D}\varphi(z)\,\mathscr{D}\psi(z)\,\mathscr{D}\bar{\psi}(z)\;\psi^{\alpha}(x)\,\bar{\psi}^{\beta}(y)\exp\left(-I_E\left[\varphi,\psi,\bar{\psi}\right]\right) \\ &= \left\langle T_{\mathcal{I}}\left\{\Psi^{\alpha}(x)\,\bar{\Psi}^{\beta}(y)\right\}\right\rangle \\ &= \frac{1}{Z}\mathrm{tr}\Big(\exp(-\beta H)\,T_{\mathcal{I}}\left\{\Psi^{\alpha}(x)\,\bar{\Psi}^{\beta}(y)\right\}\Big)\,. \end{aligned}$$

Because of the cyclic invariance of the trace we find for $0 \le \tau \le \beta$

$$\begin{aligned} &\Big\langle T_{\mathcal{I}}\left\{\Phi(\boldsymbol{x},\tau)\,\Phi(\boldsymbol{y},0)\right\}\Big\rangle \\ &\quad= \frac{1}{Z}\mathrm{tr}\Big(\exp(-\beta H)\exp(\tau H)\,\Phi(\boldsymbol{x},0)\exp(-\tau H)\,\Phi(\boldsymbol{y},0)\Big) \\ &\quad= \frac{1}{Z}\mathrm{tr}\Big(\exp(-\beta H)\,\Phi(\boldsymbol{y},0)\,\Phi(\boldsymbol{x},\tau-\beta)\Big) \\ &\quad= \left\langle T_{\mathcal{I}}\left\{\Phi(\boldsymbol{x},\tau-\beta)\,\Phi(\boldsymbol{y},0)\right\}\right\rangle\,. \end{aligned} \tag{2.1.8}$$

Hence, the thermal scalar propagator satisfies the periodicity condition

$$G(\boldsymbol{x},\tau,\boldsymbol{y},0) = G(\boldsymbol{x},\tau-\beta,\boldsymbol{y},0)\,. \tag{2.1.9}$$

When repeating the steps (2.1.8) for fermionic fields, we have to recall that the time ordering of fermionic fields implies an additional minus sign. Therefore, in contrast to the scalar propagator, the thermal fermion propagator satisfies an anti-periodicity condition:

$$S\left(\boldsymbol{x},\tau,\boldsymbol{y},0\right)=-S\left(\boldsymbol{x},\tau-\beta,\boldsymbol{y},0\right)\ . \tag{2.1.10}$$

Due to the (anti-)periodicity conditions (2.1.9) and (2.1.10) the thermal propagators can be expanded into Fourier series over so-called Matsubara frequencies [46, 49]. However, we will not pursue this road here. Instead, we note that traces of operators need not necessarily be evaluated using the left- and right-eigenstates of the Heisenberg quantum fields $\Phi\left(\boldsymbol{x},t\right)$ and $\Psi\left(\boldsymbol{x},t\right)$. Alternatively, one can also use a complete set of eigenstates of the Hamiltonian:

$$H\left|n\right\rangle=E_n\left|n\right\rangle\ .$$

With their aid we obtain

$$\begin{aligned}
G_{>}\left(x,y\right)&=G_{<}\left(y,x\right)=\left\langle\Phi\left(x\right)\Phi\left(y\right)\right\rangle\\
&=\sum_{l,m,n}\left\langle l\left|\mathcal{D}\right|n\right\rangle\left\langle n\left|\Phi\left(x\right)\right|m\right\rangle\left\langle m\left|\Phi\left(y\right)\right|l\right\rangle\\
&=\frac{1}{Z}\sum_{m,n}\left\langle n\left|\Phi\left(\boldsymbol{x},0\right)\right|m\right\rangle\left\langle m\left|\Phi\left(\boldsymbol{y},0\right)\right|n\right\rangle\\
&\quad\times\exp\left(-i\left(x^0-y^0\right)E_m\right)\exp\left(-\left(\beta-i\left(x^0-y^0\right)\right)E_n\right)
\end{aligned} \tag{2.1.11}$$

and similar expressions for

$$S_{>}^{\alpha\beta}\left(x,y\right)=\left\langle\Psi^{\alpha}\left(x\right)\bar{\Psi}^{\beta}\left(y\right)\right\rangle$$

and

$$S_{<}^{\alpha\beta}\left(x,y\right)=\left\langle\bar{\Psi}^{\beta}\left(y\right)\Psi^{\alpha}\left(x\right)\right\rangle\ .$$

Eq. (2.1.11) shows that the time dependence of the thermal propagators only takes the relative time x^0-y^0 into account. There is no dependence on the center time, and we can conclude that the thermal propagators are invariant under time translations. Additionally, the thermal propagators are expected to be invariant under space translations, such that we finally arrive at space-time translation invariant thermal propagators. Space-time translation invariance is characteristic for thermal quantum field theory and implies that the thermal propagators only depend on the relative coordinates $x-y$. Out of thermal equilibrium one would at least observe an additional dependence on the center time $\frac{x^0+y^0}{2}$. Furthermore, provided the matrix elements behave well enough, the convergence of the sum in Eq. (2.1.11) is controlled by the exponential functions, and we find that $G_{>}\left(x,y\right)$ is an analytic function of its time arguments in the domain

$$\left\{x^0-y^0\in\mathbb{C}\,\middle|\,-\beta<\mathrm{Im}\left(x^0-y^0\right)<0\right\}\ . \tag{2.1.12}$$

Analogously, by interchanging x and y in Eq. (2.1.11) $G_<(x,y)$ is found to be an analytic function of its time arguments in the domain

$$\left\{x^0 - y^0 \in \mathbb{C} \middle| 0 < \mathrm{Im}\left(x^0 - y^0\right) < \beta\right\} \ . \tag{2.1.13}$$

Using the correlation functions $G_>$ and $G_<$ we can resolve the imaginary-time ordering in the scalar propagator. As mentioned above, exploiting the invariance of the thermal propagator under space-time translations, we can parametrize the propagator in terms of relative coordinates $\boldsymbol{x} - \boldsymbol{y} = \boldsymbol{s}$ and $x^0 - y^0 = s^0 - i\tau$, where s^0 is the real part of the relative time. Thus, according to Eqs. (2.1.12) and (2.1.13) for $0 < \tau < \beta$ we find

$$G\left(\boldsymbol{s}, s^0 - i\tau\right) = G_>\left(\boldsymbol{s}, s^0 - i\tau\right) \tag{2.1.14}$$

and

$$G\left(\boldsymbol{s}, s^0 - i\left(\tau - \beta\right)\right) = G_<\left(\boldsymbol{s}, s^0 - i\left(\tau - \beta\right)\right) \ . \tag{2.1.15}$$

Taking the periodicity relation (2.1.9) into account, we obtain the Kubo-Martin-Schwinger condition [52, 53] for the scalar propagator

$$G_>\left(\boldsymbol{s}, s^0 - i\tau\right) = G_<\left(\boldsymbol{s}, s^0 - i\left(\tau - \beta\right)\right) \ . \tag{2.1.16}$$

Fourier transforming the Kubo-Martin-Schwinger condition (2.1.16) with respect to s yields for $\tau = 0$:

$$G_>(k) = \int d^4s \ \exp\left(-iks\right) G_>(s) = \exp\left(\beta k^0\right) G_<(k) \ .$$

Using the spectral function

$$G_\varrho(k) = G_>(k) - G_<(k)$$

and the statistical propagator

$$G_F(k) = \frac{1}{2}\left(G_>(k) + G_<(k)\right)$$

for the scalars we eventually find the so-called fluctuation-dissipation theorem

$$G_F(k) = \left(\frac{1}{2} + n_{BE}\left(k^0\right)\right) G_\varrho(k) \ , \tag{2.1.17}$$

where

$$n_{BE}(\omega) = \frac{1}{\exp\left(\beta\omega\right) - 1}$$

is the Bose-Einstein distribution function. Along the same lines we also obtain the Kubo-Martin-Schwinger condition for the fermions

$$S_>\left(\boldsymbol{s}, s^0 - i\tau\right) = S_<\left(\boldsymbol{s}, s^0 - i\left(\tau - \beta\right)\right) \ . \tag{2.1.18}$$

The fermionic spectral function and statistical propagator are defined by

$$S_\varrho(k) = S_>(k) + S_<(k)$$

and

$$S_F(k) = \frac{1}{2}\left(S_>(k) - S_<(k)\right) .$$

Thus, for the fermions the fluctuation-dissipation theorem reads

$$S_F(k) = \left(\frac{1}{2} - n_{FD}\left(k^0\right)\right) S_\varrho(k) \ , \tag{2.1.19}$$

where

$$n_{FD}(\omega) = \frac{1}{\exp(\beta\omega) + 1}$$

is the Fermi-Dirac distribution function. Summarizing, the main results of this section are the space-time translation invariance of thermal propagators and the fluctuation-dissipation theorems (2.1.17) and (2.1.19).

2.2 Quantum Fields out of Thermal Equilibrium

In this section we consider a closed system out of thermal equilibrium which at some initial time $t = t_{init} \equiv 0$ can be described by a density operator $\mathcal{D}$. As in the previous section, the Hamiltonian of the system is given by Eq. (2.1.1). In order to be able to describe general nonequilibrium initial conditions as well as initial thermal equilibrium, we allow the density operator to include mixed states, such that

$$\mathrm{tr}\left(\mathcal{D}^2\right) < 1 \ .$$

Thus, although we use the same symbol, in this section the density operator $\mathcal{D}$ may deviate significantly from the canonical density operator (2.1.2). We would like to stress, that $\mathcal{D}$ now may describe a system, which is initially arbitrarily far from equilibrium, and that there will be no assumptions which are only justifiable if our system were sufficiently close to thermal equilibrium. We are interested in the computation of expectation values of arbitrary products of Heisenberg quantum fields, which are given by

$$\langle \Phi(x_1) \ldots \Phi(x_n) \rangle = \mathrm{tr}\Big(\mathcal{D}\Phi(x_1) \ldots \Phi(x_n)\Big) \ . \tag{2.2.1}$$

In order to evaluate the trace (2.2.1), we have to take the evolution of each Heisenberg field with respect to the initial time. For example, the two-point correlation function is given by

$$\begin{aligned}
\langle \Phi(x)\Phi(y) \rangle &= \mathrm{tr}\Big(\mathcal{D}\exp\left(ix^0 H\right)\Phi(\boldsymbol{x},0)\exp\left(i\left(y^0 - x^0\right)H\right) \\
&\qquad \times \Phi(\boldsymbol{y},0)\exp\left(-iy^0 H\right)\Big) \\
&= \mathrm{tr}\Big(\mathcal{D}U\left(0,x^0\right)\Phi^I(x)\,U\left(x^0,y^0\right)\Phi^I(y)\,U\left(y^0,0\right)\Big) \ .
\end{aligned} \tag{2.2.2}$$

In the second line we have used the interaction picture evolution operator

$$U\left(x^0, y^0\right) = \exp\left(ix^0 H_0\right) \exp\left(-i\left(x^0 - y^0\right) H\right) \exp\left(-iy^0 H_0\right) \tag{2.2.3}$$

and the interaction picture quantum field

$$\Phi^I(x) = \exp\left(ix^0 H_0\right) \Phi(\boldsymbol{x}, 0) \exp\left(-ix^0 H_0\right) \ ,$$

where we have separated the full Hamiltonian H into its free part H_0 and the interaction V:

$$H = H_0 + V \ .$$

Differentiating Eq. (2.2.3) with respect to x^0 gives the differential equation

$$i\frac{d}{dx^0} U\left(x^0, y^0\right) = V^I\left(x^0\right) U\left(x^0, y^0\right) \ , \tag{2.2.4}$$

where

$$V^I\left(x^0\right) = \exp\left(ix^0 H_0\right) V \exp\left(-ix^0 H_0\right) \ .$$

The interaction picture evolution operator (2.2.3) is determined as the unique solution of the differential equation (2.2.4) by the initial condition

$$U\left(y^0, y^0\right) = 1 \ . \tag{2.2.5}$$

The crucial point of this observation is the fact that the differential equation (2.2.4) together with the initial condition (2.2.5) is equivalent to the integral equation

$$U\left(x^0, y^0\right) = 1 - i \int_{y^0}^{x^0} dt \, V^I(t) \, U\left(t, y^0\right) \ .$$

By iteration of this integral equation, we obtain an expansion for $U(x^0, y^0)$ in powers of V^I:

$$\begin{aligned} U\left(x^0, y^0\right) &= 1 - i \int_{y^0}^{x^0} dt \left[V^I(t)\right] \\ &\quad + (-i)^2 \int_{y^0}^{x^0} dt_1 \int_{y^0}^{t_1} dt_2 \left[V^I(t_1) \, V^I(t_2)\right] + \dots \ . \end{aligned}$$

For $x^0 > y^0$ this expansion can be written in the form

$$\begin{aligned} U\left(x^0, y^0\right) &= 1 - i \int_{y^0}^{x^0} dt \left[V^I(t)\right] \\ &\quad + \frac{(-i)^2}{2} \int_{y^0}^{x^0} dt_1 \int_{y^0}^{x^0} dt_2 \left[T\left\{V^I(t_1) V^I(t_2)\right\}\right] + \dots \\ &= T \exp\left(-i \int_{y^0}^{x^0} dt\, V^I(t) \right) , \end{aligned}$$

where T denotes the usual time ordering operator along the real axis. On the other hand, we obtain for $x^0 < y^0$

$$\begin{aligned} U\left(x^0, y^0\right) &= 1 + i \int_{x^0}^{y^0} dt \left[V^I(t)\right] \\ &\quad + \frac{i^2}{2} \int_{x^0}^{y^0} dt_1 \int_{x^0}^{y^0} dt_2 \left[\tilde{T}\left\{V^I(t_1) V^I(t_2)\right\}\right] + \dots \\ &= \tilde{T} \exp\left(i \int_{x^0}^{y^0} dt\, V^I(t) \right) . \end{aligned}$$

Here $\tilde{T}$ denotes the anti-temporal ordering along the real axis, i.e. the interaction with the latest time argument is placed rightmost. Now we return to the trace (2.2.2) and find that all operators are sorted according to the order in which their time arguments appear on the time contour shown in Fig. 2.2 [15, 54–62] with

$$t_{max} = \max\left(x^0, y^0\right) .$$

As a consequence we have to define the n-point Green's functions on this time contour. For example the scalar Schwinger-Keldysh propagator is given by

$$G(x, y) = \langle T_{\mathcal{C}} \left\{\Phi(x)\, \Phi(y)\right\}\rangle . \tag{2.2.6}$$

With the aid of the density operator $\mathcal{D}$, we can define a generating functional for these Schwinger-Keldysh Green's functions:

$$Z_{\mathcal{D}}\left[J, \theta, \bar{\theta}\right] = \mathrm{tr}\left(\mathcal{D}\, T_{\mathcal{C}} \Big\{ \exp\Big(i \int_{\mathcal{C}} d^4x \left[J\varphi + \bar{\psi}\theta + \bar{\theta}\psi\right] \Big) \Big\} \right) \tag{2.2.7}$$

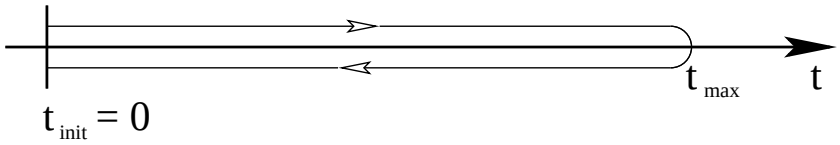

Figure 2.2: Closed real-time path $\mathcal{C}$. This time path was invented by Schwinger [54] (see also [56–61]) and applied to nonequilibrium problems by Keldysh [55]. In order to avoid the doubling of the degrees of freedom, we use the form presented in Ref. [15].

Exactly as in the previous section, we evaluate the trace using the complete set of left- and right-eigenstates (2.1.4) – (2.1.7) of the Heisenberg quantum fields $\Phi(x)$ and $\Psi(x)$ for $x^0 = 0$:

$$
\begin{aligned}
Z_{\mathcal{D}}\left[J,\theta,\bar{\theta}\right] &= \int \prod_{\boldsymbol{x}} d\varphi^{(1)}(\boldsymbol{x})\, d\psi^{(1)}(\boldsymbol{x}) \int \prod_{\boldsymbol{y}} d\varphi^{(2)}(\boldsymbol{y})\, d\psi^{(2)}(\boldsymbol{y}) \\
&\times \Bigg[\left\langle \varphi^{(1)}(0), \psi^{(1)}(0) \left| \mathcal{D} \right| \varphi^{(2)}(0), \psi^{(2)}(0) \right\rangle \\
&\times \left\langle \varphi^{(2)}(0), \psi^{(2)}(0) \right| T_{\mathcal{C}} \Big\{ \exp\left(i \int_{\mathcal{C}} d^4x \left[J\varphi + \bar{\psi}\theta + \bar{\theta}\psi \right] \right) \Big\} \left| \varphi^{(1)}(0), \psi^{(1)}(0) \right\rangle \Bigg] .
\end{aligned}
$$

The second matrix element is given by the following path integral:

$$
\int_{\substack{\varphi\left(\boldsymbol{x},\overrightarrow{0}\right)=\varphi^{(1)}(\boldsymbol{x}) \\ \varphi\left(\boldsymbol{x},\overleftarrow{0}\right)=\varphi^{(2)}(\boldsymbol{x}) \\ \psi\left(\boldsymbol{x},\overrightarrow{0}\right)=\psi^{(1)}(\boldsymbol{x}) \\ \psi\left(\boldsymbol{x},\overleftarrow{0}\right)=\psi^{(2)}(\boldsymbol{x})}} \mathscr{D}\varphi(x)\, \mathscr{D}\psi(x)\, \mathscr{D}\bar{\psi}(x)\, \exp\left(i \int_{\mathcal{C}} d^4x \left[\mathscr{L} + J\varphi + \bar{\psi}\theta + \bar{\theta}\psi \right] \right) .
$$

The matrix element of the density operator can be written in the form [41]

$$
\left\langle \varphi^{(1)}(0), \psi^{(1)}(0) \left| \mathcal{D} \right| \varphi^{(2)}(0), \psi^{(2)}(0) \right\rangle = \int \prod_{\boldsymbol{x}} d\bar{\psi}(\boldsymbol{x})\, \exp\left(iF\left[\varphi,\psi,\bar{\psi}\right] \right) ,
$$

where F can be expanded in the functional sense according to

$$\begin{aligned} F\left[\varphi,\psi,\bar{\psi}\right] &= \alpha_0 + \int\limits_{\mathcal{C}} d^4x \left[\alpha_1(x)\,\varphi(x) + \bar{\beta}_1(x)\,\psi(x) + \bar{\psi}(x)\,\beta_1(x)\right] \\ &+ \frac{1}{2}\int\limits_{\mathcal{C}} d^4x \int\limits_{\mathcal{C}} d^4y \left[\varphi(x)\,\alpha_2(x,y)\,\varphi(y) + \bar{\psi}(x)\,\beta_2(x,y)\,\psi(y)\right] \\ &+ \frac{1}{3!}\int\limits_{\mathcal{C}} d^4x \int\limits_{\mathcal{C}} d^4y \int\limits_{\mathcal{C}} d^4z \ldots \end{aligned} \tag{2.2.8}$$

The values of $\varphi(x)$ and $\psi(x)$ at the beginning and the end of the time contour are given by $\varphi^{(1)}(\boldsymbol{x})$ and $\varphi^{(2)}(\boldsymbol{x})$, and $\psi^{(1)}(\boldsymbol{x})$ and $\psi^{(2)}(\boldsymbol{x})$, respectively. Of course, the sequence of the coefficients α_j and β_j contains as much information as the original density matrix. Therefore, in general we can rewrite the trace (2.2.7) as a functional of infinitely many sources. For simplicity, however, throughout this work we will restrict our considerations to Gaussian initial conditions. This means for the sources α_j and β_j that

$$\alpha_j(x_1,\ldots,x_j) = \beta_j(x_1,\ldots,x_j) = 0 \qquad (\forall j \geq 3)\ .$$

The only purpose of the source α_j and β_j is to prepare the system under consideration in a state out of thermal equilibrium. Consequently, they are non-vanishing only at the initial time $t_{init} = 0$. Anyway, we can only compute ratios of path integrals. In such a ratio the constant factor caused by $\alpha^{(0)}$ cancels, and therefore, we can cancel $\alpha^{(0)}$ from the functional (2.2.8). Furthermore, we can absorb the sources α_1, β_1 and $\bar{\beta}_1$ into the sources J, θ and $\bar{\theta}$. Thus, the generating functional for Schwinger-Keldysh Green's functions is given by the path integral

$$\begin{aligned} Z_{\mathcal{D}}\left[J,\theta,\bar{\theta}\right] = \int \mathscr{D}\varphi(x)\,\mathscr{D}\psi(x)\,\mathscr{D}\bar{\psi}(x)\ \exp\Bigg(i\int\limits_{\mathcal{C}} d^4x \left[\mathscr{L} + J\varphi + \bar{\psi}\theta + \bar{\theta}\psi\right] \\ + \frac{i}{2}\int\limits_{\mathcal{C}} d^4x \int\limits_{\mathcal{C}} d^4y \left[\varphi(x)\,\alpha_2(x,y)\,\varphi(y) + \bar{\psi}(x)\,\beta_2(x,y)\,\psi(y)\right]\Bigg)\ . \end{aligned} \tag{2.2.9}$$

The complete Schwinger-Keldysh propagator (2.2.6) is then given by

$$G(x,y) = \left(\frac{(-i)^2}{Z_{\mathcal{D}}\left[J,\theta,\bar{\theta}\right]}\,\frac{\delta^2 Z_{\mathcal{D}}\left[J,\theta,\bar{\theta}\right]}{\delta J(x)\,\delta J(y)}\right)_{J=\alpha_1,\,\theta=0,\,\bar{\theta}=\alpha_2}\ .$$

Similarly, one also obtains the complete Schwinger-Keldysh propagator for fermionic quantum fields:

$$S^{\alpha\beta}(x,y) = \left(\frac{(-i)^2}{Z_{\mathcal{D}}\left[J,\theta,\bar{\theta}\right]}\,\frac{\delta}{\delta\theta^{\beta}(y)}\,\frac{\delta}{\delta\bar{\theta}^{\alpha}(x)}\,Z_{\mathcal{D}}\left[J,\theta,\bar{\theta}\right]\right)_{J=\alpha_1,\,\theta=0,\,\bar{\theta}=\alpha_2}\ .$$

For given initial conditions the evolution of the complete Schwinger-Keldysh propagators is determined by the so-called Kadanoff-Baym equations. These are self-consistent integro-differential equations which can be obtained by requiring that the 2PI effective action, defined on the closed real-time path Fig. 2.2, be stationary with respect to variations of the complete connected propagators. The 2PI effective action will be introduced in the next section.

2.3 Quantum Effective Action

In this section we will review the derivation of a convenient parametrization of the 2PI effective action. For notational convenience we will not specify any time contour. As they stand, the formulas are immediately applicable for considerations in vacuum. On the other hand, according to the first section of this chapter, in thermal equilibrium one would have to perform time integrations along the imaginary time path. In this case the 2PI effective action corresponds to the thermodynamic potential. In contrast to this, in subsequent chapters, when describing the evolution of quantum fields out of thermal equilibrium, we will start from the 2PI effective action defined on the closed Schwinger-Keldysh real-time contour. We show the derivation in the framework of the Yukawa-type quantum field theory considered in chapter 4, and note that one can trivially obtain the 2PI effective action for the purely scalar case by omitting the fermionic parts. For notational convenience, however, we suppress $SU(2)_L$ and $SU(2)_R$ flavor indices and use a compressed vector-matrix notation for integrals:

$$J\phi = \int d^4x \; J(x)\,\phi(x) \;\; ,$$

$$\phi G^{-1}\phi = \int d^4x \; \phi(x)\,G^{-1}(x,y)\,\phi(x) \;\; ,$$

$$\mathrm{tr}\,[KG] = \int d^4x \int d^4y \; K(x,y)\,G(y,x) \;\; .$$

1PI Effective Action

We start from the generating functional for Green's functions

$$Z\left[J,\theta,\bar{\theta}\right] = \int \mathscr{D}\varphi(x)\,\mathscr{D}\psi(x)\,\mathscr{D}\bar{\psi}(x) \;\exp\left[i\left(I\left[\varphi,\psi,\bar{\psi}\right] + \varphi J + \bar{\psi}\theta + \bar{\theta}\psi\right)\right] \;\; .$$

The generating functional for connected Green's functions is then given by

$$W\left[J,\theta,\bar{\theta}\right] = -i\log\left(Z\left[J,\theta,\bar{\theta}\right]\right) \;\; .$$

The functional derivative of W with respect to a source gives the expectation value of the corresponding quantum field in the presence of the source[1]:

$$\frac{\delta W}{\delta J(x)} = \phi(x) \quad , \quad \frac{\delta W}{\delta \theta^\alpha(x)} = -\bar{\Psi}^\alpha(x) \quad , \quad \frac{\delta W}{\delta \bar{\theta}^\alpha(x)} = \Psi^\alpha(x) \ . \tag{2.3.1}$$

Of course, a non-vanishing expectation value of a Dirac field would break Lorentz invariance. Thus physical situations imply the vanishing of these expectation values. Nevertheless, they are needed for the purpose of parametrization. The effective action is the Legendre transform of the generating functional for connected Green's functions:

$$\Gamma\left[\phi, \Psi, \bar{\Psi}\right] = W\left[J, \theta, \bar{\theta}\right] - J\phi - \bar{\Psi}\theta - \bar{\theta}\Psi \ .$$

From this we can deduce that a functional derivative of the effective action with respect to the expectation value of a quantum field reproduces the corresponding source:

$$\frac{\delta \Gamma}{\delta \phi(x)} = -J(x) \quad , \quad \frac{\delta \Gamma}{\delta \Psi^\alpha(x)} = \bar{\theta}^\alpha(x) \quad , \quad \frac{\delta \Gamma}{\delta \bar{\Psi}^\alpha(x)} = -\theta^\alpha(x) \ . \tag{2.3.2}$$

In order to find a convenient parametrization for the effective action we translate the quantum fields by their expectation values

$$\begin{aligned} \varphi(x) &\rightarrow \phi(x) + \varphi(x) \ , \\ \psi(x) &\rightarrow \Psi(x) + \psi(x) \ , \\ \bar{\psi}(x) &\rightarrow \bar{\Psi}(x) + \bar{\psi}(x) \ , \end{aligned}$$

and exploit the translational invariance of path integrals, such that we can write the generating functional for connected Green's functions in the form

$$W\left[J, \theta, \bar{\theta}\right] = I\left[\phi, \Psi, \bar{\Psi}\right] + \phi J + \bar{\Psi}\theta + \bar{\theta}\Psi + W_1\left[J, \theta, \bar{\theta}\right] \ ,$$

where

$$\begin{aligned} W_1\left[J, \theta, \bar{\theta}\right] &= -i \log \int \mathscr{D}\varphi(x)\, \mathscr{D}\psi(x)\, \mathscr{D}\bar{\psi}(x)\ \exp\Big[i\Big(I\left[\phi+\varphi, \Psi+\psi, \bar{\Psi}+\bar{\psi}\right] \\ &\quad - I\left[\phi, \Psi, \bar{\Psi}\right] + \varphi J + \bar{\psi}\theta + \bar{\theta}\psi\Big)\Big] \ . \end{aligned} \tag{2.3.3}$$

Consequently, the effective action is given by

$$\Gamma\left[\phi, \Psi, \bar{\Psi}\right] = I\left[\phi, \Psi, \bar{\Psi}\right] + \Gamma_1\left[\phi, \Psi, \bar{\Psi}\right] \ , \tag{2.3.4}$$

[1]The author apologizes for the ambiguity in the symbol Ψ, but he also promises to avoid any confusion on whether Ψ is a quantum field or its expectation value.

where

$$\Gamma_1\left[\phi,\Psi,\bar{\Psi}\right]=W_1\left[J,\theta,\bar{\theta}\right]$$

in principle could be obtained from the one-to-one correspondence (2.3.1) and (2.3.2) between the external sources and the expectation values of the quantum fields. Replacing the external sources in Eq. (2.3.3) by the functional derivatives (2.3.2) and using Eq. (2.3.4) yields the following functional integro-differential equation for Γ_1 [39]:

$$\begin{aligned}\Gamma_1\left[\phi,\Psi,\bar{\Psi}\right]=-i\log\int\mathscr{D}\varphi\left(x\right)\mathscr{D}\psi\left(x\right)\mathscr{D}\bar{\psi}\left(x\right)\,\exp\Big[i\Big(&\bar{\psi}S_0^{-1}\psi\\&-\frac{1}{2}\varphi\mathscr{G}_0^{-1}\varphi+I_{int}\left[\phi,\Psi,\bar{\Psi},\varphi,\psi,\bar{\psi}\right]-\varphi\frac{\delta\Gamma_1}{\delta\phi}-\bar{\psi}\frac{\delta\Gamma_1}{\delta\bar{\Psi}}+\frac{\delta\Gamma_1}{\delta\psi}\psi\Big)\Big]\,,\end{aligned}$$

where S_0^{-1} and G_0^{-1} are the inverse free propagators for the fermions and the scalars, respectively,

$$\mathscr{G}_0^{-1}\left(x,y\right)=G_0^{-1}\left(x,y\right)-6\lambda\phi\left(x\right)\phi\left(y\right)\delta\left(x-y\right)$$

is the inverse classical propagator, and

$$\begin{aligned}I_{int}\left[\phi,\Psi,\bar{\Psi},\varphi,\psi,\bar{\psi}\right]&=-\lambda\int d^4x\left[4\phi\varphi^3+\varphi^4\right]\\&\quad-H\int d^4x\left[\bar{\Psi}\varphi\psi+\bar{\psi}\varphi\Psi+\bar{\psi}\left(\phi+\varphi\right)\psi\right]\,.\end{aligned}$$

The 1PI parametrization (2.3.4) of the effective action will be needed in the derivation of the 2PI parametrization, which we will review in the following subsection.

2PI Effective Action

In order to derive the 2PI parametrization of the effective action [40,41,63,64], we extend the generating functional for connected Green's functions by two bi-local source terms:

$$\begin{aligned}W\left[J,\theta,\bar{\theta},K,L\right]&=-i\log\int\mathscr{D}\varphi\left(x\right)\mathscr{D}\psi\left(x\right)\mathscr{D}\bar{\psi}\left(x\right)\,\exp\Big[i\Big(I\left[\varphi,\psi,\bar{\psi}\right]\\&\quad+\varphi J+\bar{\psi}\theta+\bar{\theta}\psi+\varphi K\varphi+\bar{\psi}L\psi\Big)\Big]\,.\end{aligned}\tag{2.3.5}$$

The relations (2.3.1) are not changed by the additional non-local sources, but are supplemented by the following two relations:

$$\frac{\delta W}{\delta K\left(y,x\right)}=\left\langle T\left\{\Phi\left(x\right)\Phi\left(y\right)\right\}\right\rangle=G\left(x,y\right)+\phi\left(x\right)\phi\left(y\right)$$

and

$$\frac{\delta W}{\delta L^{\beta\alpha}(y,x)} = \left\langle T\left\{\bar{\Psi}^{\beta}(y)\,\Psi^{\alpha}(x)\right\}\right\rangle = -S^{\alpha\beta}(x,y) + \Psi^{\alpha}(x)\,\bar{\Psi}^{\beta}(y)\ .$$

Thus, a functional derivative of W with respect to a non-local external source gives the corresponding full two-point function including disconnected parts. In contrast to this, differentiating W twice with respect to corresponding local external sources gives the connected propagators G and S. The 2PI effective action is then given as Legendre transform of W:

$$\begin{aligned}\Gamma\left[\phi,\Psi,\bar{\Psi},G,S\right] &= W\left[J,\theta,\bar{\theta},K,L\right] - J\phi - \bar{\Psi}\theta - \bar{\theta}\Psi \\ &\quad -\mathrm{tr}\left[KG\right] - \phi K\phi + \mathrm{tr}\left[LS\right] - \bar{\Psi}L\Psi\ .\end{aligned}$$

From this, we obtain for the functional derivatives of the 2PI effective action with respect to the above expectation values:

$$\frac{\delta\Gamma}{\delta\phi(x)} = -J(x) - 2\int d^4y\ K(x,y)\,\phi(y)\ , \tag{2.3.6}$$

$$\frac{\delta\Gamma}{\delta\Psi^{\alpha}(x)} = \bar{\theta}^{\alpha}(x) + \int d^4y\ \bar{\Psi}^{\beta}(y)\,L^{\beta\alpha}(y,x)\ , \tag{2.3.7}$$

$$\frac{\delta\Gamma}{\delta\bar{\Psi}^{\alpha}(x)} = -\theta^{\alpha}(x) - \int d^4y\ L^{\alpha\beta}(x,y)\,\Psi^{\beta}(y)\ , \tag{2.3.8}$$

$$\frac{\delta\Gamma}{\delta G(x,y)} = -K(y,x) \tag{2.3.9}$$

$$\frac{\delta\Gamma}{\delta S^{\alpha\beta}(x,y)} = L^{\beta\alpha}(y,x)\ . \tag{2.3.10}$$

It is important to note that $\Gamma\left[\phi,\Psi,\bar{\Psi},G,S\right]$ is the generating functional of 2PI Green's functions. Consequently, $i\Gamma\left[G,S\right] = i\Gamma\left[\phi=0,\Psi=0,\bar{\Psi}=0,G,S\right]$ is the sum of all 2PI vacuum diagrams[2]. $\Gamma\left[G,S\right]$ satisfies the following functional integro-differential equation:

$$\begin{aligned}\Gamma\left[G,S\right] &= W\left[J_0,\theta_0,\bar{\theta}_0,K,L\right] - \mathrm{tr}\left[KG\right] + \mathrm{tr}\left[LS\right] \\ &= \mathrm{tr}\left[\frac{\delta\Gamma}{\delta G}G\right] + \mathrm{tr}\left[\frac{\delta\Gamma}{\delta S}S\right] - i\log\int\mathscr{D}\varphi(x)\,\mathscr{D}\psi(x)\,\mathscr{D}\bar{\psi}(x)\ \exp\left[i\Big(I\left[\varphi,\psi,\bar{\psi}\right]\right. \\ &\quad \left. + \varphi J_0 + \bar{\psi}\theta_0 + \bar{\theta}_0\psi - \varphi\frac{\delta\Gamma}{\delta G}\varphi + \bar{\psi}\frac{\delta\Gamma}{\delta S}\psi\Big)\right] \\ &\quad + i\log\int\mathscr{D}\varphi(x)\,\mathscr{D}\psi(x)\,\mathscr{D}\bar{\psi}(x)\ \exp\left[i\Big(\bar{\psi}S_0^{-1}\psi - \frac{1}{2}\varphi G_0^{-1}\varphi\Big)\right]\end{aligned} \tag{2.3.11}$$

[2] A Feynman diagram is called nPI (n-particle-irreducible), if it cannot be disconnected by cutting through any n internal lines. Vacuum here means without external legs, not perturbation theory.

The external sources J_0, θ_0 and $\bar{\theta}_0$ correspond to vanishing expectation values of the quantum fields. After we have absorbed the bi-local source terms into the free part of the classical action,

$$I^{K,L}\left[\varphi,\psi,\bar{\psi}\right]=\bar{\psi}\left(S_0^{-1}+L\right)\psi-\frac{1}{2}\varphi\left(G_0^{-1}-2K\right)\varphi+I_{int}\left[\varphi,\psi,\bar{\psi}\right]\ ,$$

we can express the 2PI effective action in terms of the 1PI effective action:

$$\begin{aligned}\Gamma^{K,L}\left[\phi,\Psi,\bar{\Psi},G,S\right] &= I^{K,L}\left[\phi,\Psi,\bar{\Psi}\right]+\Gamma_1^{K,L}\left[\phi,\Psi,\bar{\Psi}\right]\\ &\quad -\mathrm{tr}\left[KG\right]-\phi K\phi+\mathrm{tr}\left[LS\right]-\bar{\Psi}L\Psi\ ,\end{aligned}$$

where

$$\begin{aligned}\Gamma_1^{K,L}\left[\phi,\Psi,\bar{\Psi}\right] &= -i\log\int\mathscr{D}\varphi\left(x\right)\mathscr{D}\psi\left(x\right)\mathscr{D}\bar{\psi}\left(x\right)\ \exp\Big[i\Big(\bar{\psi}\left(S_0^{-1}+L\right)\psi\\ &\quad -\frac{1}{2}\varphi\left(\mathscr{G}_0^{-1}-2K\right)\varphi+I_{int}\left[\phi,\Psi,\bar{\Psi},\varphi,\psi,\bar{\psi}\right]\\ &\quad -\varphi\frac{\delta\Gamma_1}{\delta\phi}-\bar{\psi}\frac{\delta\Gamma_1}{\delta\bar{\Psi}}+\frac{\delta\Gamma_1}{\delta\Psi}\psi\Big)\Big]\ .\end{aligned}$$

Thus we get

$$\Gamma\left[\phi,\Psi,\bar{\Psi},G,S\right]=I\left[\phi,\Psi,\bar{\Psi}\right]-\mathrm{tr}\left[KG\right]+\mathrm{tr}\left[LS\right]+\Gamma_1^{K,L}\left[\phi,\Psi,\bar{\Psi}\right]\ . \quad (2.3.12)$$

Now, we tentatively write the 2PI effective action in the form

$$\begin{aligned}\Gamma\left[\phi,\Psi,\bar{\Psi},G,S\right] &= I\left[\phi,\Psi,\bar{\Psi}\right]-\frac{1}{2}\mathrm{tr}\left[\mathscr{G}_0^{-1}G\right]+\frac{i}{2}\mathrm{tr}\log\left[G^{-1}\right]\\ &\quad -\mathrm{tr}\left[S_0^{-1}S\right]-i\mathrm{tr}\log\left[S^{-1}\right]+\Gamma_2\left[\phi,\Psi,\bar{\Psi},G,S\right]+const\ , \quad (2.3.13)\end{aligned}$$

thereby defining the functional Γ_2. Inserting the parametrization (2.3.13) into Eqs. (2.3.9) and (2.3.10) we find that

$$\mathscr{G}_0^{-1}\left(x,y\right)-2K\left(x,y\right)=-iG^{-1}\left(x,y\right)+2\frac{\delta\Gamma_2}{\delta G\left(y,x\right)}$$

and

$$\left(S_0^{-1}\right)^{\alpha\beta}\left(x,y\right)+L^{\alpha\beta}\left(x,y\right)=-i\left(S^{-1}\right)^{\alpha\beta}\left(x,y\right)-\frac{\delta\Gamma_2}{\delta S^{\beta\alpha}\left(y,x\right)}\ .$$

Thus, in Eq. (2.3.12) we can eliminate the bi-local sources K and L in favor of the propagators G and S and the functional Γ_2. Additionally, we use the identities

$$\int\mathscr{D}\varphi\left(x\right)\ \exp\left[-\frac{1}{2}\varphi G^{-1}\varphi\right]=\left(\det\left[\frac{G^{-1}}{2\pi}\right]\right)^{-\frac{1}{2}}$$

and

$$\int \mathscr{D}\psi\,(x)\,\mathscr{D}\bar{\psi}\,(x)\;\exp\left[\bar{\psi}S^{-1}\psi\right]=\det\left[S^{-1}\right]\;.$$

The 2PI effective action then takes the form

$$\begin{aligned}\Gamma\left[\phi,\Psi,\bar{\Psi},G,S\right]&=I\left[\phi,\Psi,\bar{\Psi}\right]-i\log\left(\det\left[G^{-1}\right]\right)^{-\frac{1}{2}}-\frac{1}{2}\mathrm{tr}\left[\mathscr{G}_0^{-1}G\right]\\&-i\log\det\left[S^{-1}\right]+\mathrm{tr}\left[S_0^{-1}S\right]+\mathrm{tr}\left[\frac{\delta\Gamma_2}{\delta G}G\right]+\mathrm{tr}\left[\frac{\delta\Gamma_2}{\delta S}S\right]\\&-i\log\int\mathscr{D}\varphi\,(x)\,\mathscr{D}\psi\,(x)\,\mathscr{D}\bar{\psi}\,(x)\;\exp\Big[i\Big(\bar{\psi}\left(-iS^{-1}\right)\psi-\frac{1}{2}\varphi\left(-iG^{-1}\right)\varphi\\&+I_{int}\left[\phi,\Psi,\bar{\Psi},\varphi,\psi,\bar{\psi}\right]+\varphi J_0+\bar{\psi}\theta_0+\bar{\theta}_0\psi-\bar{\psi}\frac{\delta\Gamma_2}{\delta S}\psi-\varphi\frac{\delta\Gamma_2}{\delta G}\varphi\Big)\Big]\\&+i\log\int\mathscr{D}\varphi\,(x)\,\mathscr{D}\psi\,(x)\,\mathscr{D}\bar{\psi}\,(x)\;\exp\Big[i\Big(\bar{\psi}\left(-iS^{-1}\right)\psi-\frac{1}{2}\varphi\left(-iG^{-1}\right)\varphi\Big)\Big]\;.\end{aligned}\tag{2.3.14}$$

Equating the right hand sides of Eqs. (2.3.14) and (2.3.13) we find that Γ_2 must satisfy the functional integro-differential equation (2.3.11) for a theory with classical action

$$I\left[\varphi,\psi,\bar{\psi}\right]=\bar{\psi}\left(-iS^{-1}\right)\psi-\frac{1}{2}\varphi\left(-iG^{-1}\right)\varphi+I_{int}\left[\phi,\Psi,\bar{\Psi},\varphi,\psi,\bar{\psi}\right]\;.$$

Consequently, $i\Gamma_2$ is the sum of all 2PI vacuum diagrams with vertices as given by I_{int} and internal lines representing the complete connected propagators G and S.

Equations of Motion

Physical situations imply the vanishing of the external sources and Eqs. (2.3.9) and (2.3.10) turn into the equations of motion

$$\frac{\delta\Gamma}{\delta G\,(y,x)}=0\qquad\text{and}\qquad\frac{\delta\Gamma}{\delta S^{\beta\alpha}\,(y,x)}=0\;.\tag{2.3.15}$$

From the identity

$$\frac{\delta}{\delta G\,(y,x)}\int d^4w\;G^{-1}\,(u,w)\,G\,(w,v)=0$$

we can infer that

$$\frac{\delta G^{-1}\,(u,v)}{\delta G\,(y,x)}=-G^{-1}\,(u,y)\,G^{-1}\,(x,v)\;.$$

Accordingly, we find

$$\frac{\delta}{\delta G\,(y,x)}\mathrm{tr}\log\left[G^{-1}\right]=-G^{-1}\,(x,y)\;.$$

Therefore, the equations of motion (2.3.15) are equivalent to the Schwinger-Dyson equations

$$G^{-1}(x,y) = iG_0^{-1}(x,y) - \Pi(x,y) \tag{2.3.16}$$

and

$$S^{-1}(x,y) = -iS_0^{-1}(x,y) - \Sigma(x,y) \ , \tag{2.3.17}$$

where the self energies Π and Σ are self-consistently given by

$$\Pi(x,y) = 2i\frac{\delta\Gamma_2}{\delta G(y,x)} \tag{2.3.18}$$

and

$$\Sigma^{\alpha\beta}(x,y) = -i\frac{\delta\Gamma_2}{\delta S^{\beta\alpha}(y,x)} \ . \tag{2.3.19}$$

Of course, for an interacting theory one cannot compute the effective action, i.e. the functional Γ_2, completely. Instead, one has to resort to truncations of the functional Γ_2. A given truncation of Γ_2 determines so-called skeleton diagrams for the self-energies (2.3.18) and (2.3.19). Due to their self consistency, the Schwinger-Dyson equations (2.3.16) and (2.3.17) re-sum an infinite series of perturbative Feynman diagrams corresponding to the topology imposed by the self-energy skeletons [65–67]. For simplicity, we illustrate how this works in detail in the framework of the real scalar Φ^4 theory discussed in chapter 3. Suppose, we truncate the functional Γ_2 according to Fig. 3.1. The corresponding self-energy skeletons are then shown in Fig. 3.2. The perturbative diagrams which are re-summed by the Schwinger-Dyson equation can be constructed with the following recursion: We start the recursion with the free propagator

$$G^{(0)}(x,y) = -iG_0(x,y) \ .$$

At each step of the recursion the self energy is given by the skeleton diagrams where internal lines represent the propagator at the current step of the recursion. According to Eq. (3.1.3) we have

$$\Pi^{(n)}(x,y) = -\frac{i\lambda}{2}\delta_{\mathcal{C}}(x-y)\,G^{(n)}(x,x) - \frac{\lambda^2}{6}G^{(n)}(x,y)\,G^{(n)}(x,y)\,G^{(n)}(y,x) \ . \tag{2.3.20}$$

The propagator at the next step of the recursion is then given by the geometric series which is encoded in the Schwinger-Dyson equation:

$$\begin{aligned} G^{(n+1)}(x,y) \;=\; & -iG_0(x,y) \\ & + (-i)^2 \int d^4u_1\, d^4u_2\; G_0(x,u_1)\,\Pi^{(n)}(u_1,u_2)\,G_0(u_2,y) \\ & + (-i)^3 \int d^4u_1\, d^4u_2\, d^4u_3\, d^4u_4\; G_0(x,u_1) \\ & \qquad \times \Pi^{(n)}(u_1,u_2)\,G_0(u_2,u_3)\,\Pi^{(n)}(u_3,u_4)\,G_0(u_4,y) \\ & + \dots \ . \end{aligned} \tag{2.3.21}$$

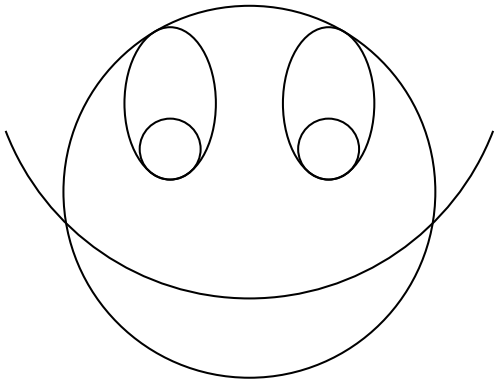

Figure 2.3: This perturbative smiley contributes to the self energy (2.3.20) at the second step of the iteration. The eye balls stem from the tadpole in $\Pi^{(0)}$ and the complete eyes are two-storied tadpole towers, emerging in $\Pi^{(1)}$. After all, the complete diagram can be constructed from the setting-sun self-energy skeleton and appropriate parts of the complete propagator at the second step of the iteration.

From this we see, that $\Pi^{(0)}$ consists exactly of the two skeleton diagrams where internal lines correspond to the free propagator. In contrast to this, due to the geometric series (2.3.21) $\Pi^{(1)}$ already includes infinitely many perturbative diagrams up to arbitrary order in the coupling. More generally, with each step of the iteration infinitely many new perturbative diagrams come into play. Note, however, that all these diagrams comply with the topology imposed by the skeletons. For example, iterating only the tadpole skeleton, one may build tadpole towers and even complete cities of tadpole towers. But topological reasons prohibit to connect the top floors of two adjacent towers.

Addressing the question of renormalization in this highly non-perturbative business is a non-trivial task. In particular, the standard proof that a certain quantum field theory be renormalizable up to infinite order of perturbation theory cannot be applied. After all this proof requires that all diagrams contributing to the self-energy at any given order of perturbation theory are taken into account. Due to the topological restrictions described above, this requirement is not fulfilled by the self-consistent Schwinger-Dyson equations (2.3.16) and (2.3.17): Only a subset of all diagrams available at a given order is taken into account. Therefore, new methods are needed to prove the renormalizability of the Schwinger-Dyson equations (2.3.16) and (2.3.17). Indeed, in vacuum and thermal equilibrium these methods have been established recently [67–74]. However, out of thermal equilibrium the renormalization of self-consistent Schwinger-Dyson equations is still an open question. Therefore, in subsequent chapters we will be

content to use an approximate perturbative renormalization procedure, which is sufficient to guarantee reliable numerical solutions of Kadanoff-Baym equations.

Chapter 3

Thermalization of Scalars

In this chapter we compare the Boltzmann and Kadanoff-Baym equations in the framework of a real scalar Φ^4 quantum field theory in $3+1$ space-time dimensions. In the first section we derive the Kadanoff-Baym equations from the 2PI effective action. The second and third section are devoted to the quantum kinetic and Boltzmann equations, respectively. In the last section we present numerical solutions of the Boltzmann and Kadanoff-Baym equations. We verify that the Kadanoff-Baym equations respect full universality, include chemical equilibration and strongly separate the time scales between kinetic and chemical equilibration. In contrast to this, the corresponding Boltzmann equation respects only a restricted universality, is incapable of describing the process of chemical equilibration and does not separate any time-scales.

3.1 Quantum Dynamics

2PI Effective Action

In this chapter we consider a real scalar quantum field, whose dynamics is determined by the Lagrangian density

$$\mathscr{L} = -\frac{1}{2}\Big(\partial_\mu \Phi\Big)\Big(\partial^\mu \Phi\Big) - \frac{1}{2} m_B^2 \Phi^2 - \frac{\lambda}{4!}\Phi^4 \, .$$

As we will compute the evolution of the two-point Green's function for a nonequilibrium many body system, we have to work with the closed real-time contour $\mathcal{C}$ as shown in Fig. 2.2. We consider a system without symmetry breaking, i.e. $\langle \Phi(x) \rangle = 0$. In this case the full connected Schwinger-Keldysh propagator is given by

$$G(x,y) = \langle T_{\mathcal{C}} \{ \Phi(x) \Phi(y) \} \rangle \, .$$

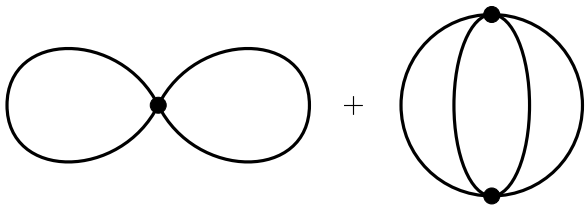

Figure 3.1: Two- and three-loop contribution to $\Gamma_2[G]$. The lines represent the complete connected Schwinger-Keldysh propagator.

According to Eq. (2.3.13), for Gaussian initial conditions the 2PI effective action for this theory then reads

$$\Gamma[G] = \frac{i}{2}\mathrm{tr}_{\mathcal{C}} \log_{\mathcal{C}}\left[G^{-1}\right] - \frac{1}{2}\mathrm{tr}_{\mathcal{C}}\left[G_0^{-1}G\right] + \Gamma_2[G] + const\ .$$

G_0^{-1} is the inverse free propagator

$$G_0^{-1}(x,y) = \left(\partial_{x^\mu}\partial_{y_\mu} + m_B^2\right)\delta_{\mathcal{C}}(x-y) \tag{3.1.1}$$

and $i\Gamma_2[G]$ is the sum of all two-particle-irreducible vacuum diagrams with classical four-point vertices and internal lines representing the complete connected propagator $G(x,y)$. In this work we apply the loop expansion of the 2PI effective action up to three-loop order. The diagrams contributing to $\Gamma_2[G]$ in this approximation are shown in Fig. 3.1. We find [23]:

$$\begin{aligned}\Gamma_2[G] &= -\frac{\lambda}{8}\int_{\mathcal{C}} d^4x\,[G(x,x)\,G(x,x)] \\ &\quad + \frac{i\lambda^2}{48}\int_{\mathcal{C}} d^4x \int_{\mathcal{C}} d^4y\,[G(x,y)\,G(x,y)\,G(y,x)\,G(y,x)]\ .\end{aligned}$$

Kadanoff-Baym equations

As described in the previous chapter [39, 40], the equation of motion for the complete propagator

$$\frac{\delta\Gamma[G]}{\delta G(y,x)} = 0$$

is equivalent to the self-consistent Schwinger-Dyson equation

$$G^{-1}(x,y) = iG_0^{-1}(x,y) - \Pi(x,y)\ , \tag{3.1.2}$$

where the proper self energy is given by

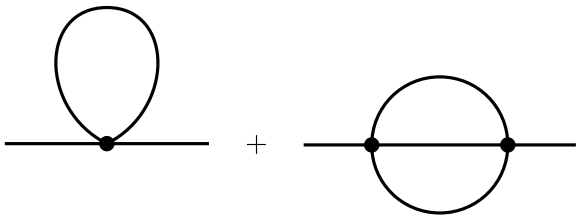

Figure 3.2: One- and two-loop contribution to the proper self-energy Π. Again, internal lines represent the complete connected Schwinger-Keldysh propagator. The tadpole represents the local part which causes a mass shift only. The setting-sun diagram represents the non-local part and leads to thermalization.

$$\begin{aligned}\Pi(x,y) &= 2i\frac{\delta\Gamma_2[G]}{\delta G(y,x)} \\ &= -\frac{i\lambda}{2}\delta_{\mathcal{C}}(x-y)\,G(x,x) - \frac{\lambda^2}{6}G(x,y)\,G(x,y)\,G(y,x)\ . \end{aligned} \tag{3.1.3}$$

After we have inserted the inverse free propagator (3.1.1), we convolve the Schwinger-Dyson equation (3.1.2) with G from the right:

$$i\left(-\partial_{x^\mu}\partial_{x_\mu} + m_B^2\right)G(x,y) = \delta_{\mathcal{C}}(x-y) + \int_{\mathcal{C}} d^4z\,[\Pi(x,z)\,G(z,y)] \tag{3.1.4}$$

Next, we define the spectral function[1]

$$G_\varrho(x,y) = i\left\langle[\Phi(x),\Phi(y)]_-\right\rangle$$

and the statistical propagator[2]

$$G_F(x,y) = \frac{1}{2}\left\langle[\Phi(x),\Phi(y)]_+\right\rangle\ ,$$

such that we can write the complete propagator as

$$G(x,y) = G_F(x,y) - \frac{i}{2}\mathrm{sign}_{\mathcal{C}}\left(x^0-y^0\right)G_\varrho(x,y)\ . \tag{3.1.5}$$

[1]From the definition of the spectral function we see that it is antisymmetric in the sense that $G_\varrho(x,y) = -G_\varrho(y,x)$. Furthermore, the canonical equal-time commutation relations give $(G_\varrho(x,y))_{x^0=y^0} = 0$ and $\left(\partial_{y^0}G_\varrho(x,y)\right)_{x^0=y^0} = -\delta^3(\boldsymbol{x}-\boldsymbol{y})$.

[2]In contrast to the spectral function, the statistical propagator is symmetric in the sense that $G_F(x,y) = G_F(y,x)$.

Note that for real scalar quantum fields both the statistical propagator and the spectral function are real-valued quantities [22]. The spectral function describes the particle spectrum of our theory. From its Wigner transform we can obtain the thermal mass and the decay width of the particles in our system. On the other hand we will define an effective particle number density given by the statistical propagator and its time derivatives evaluated at equal times. From Eq. (3.1.3) (and Fig. 3.2) we see that the self energy contains a local and a non-local part:

$$\Pi\left(x,y\right)=-i\delta_{\mathcal{C}}\left(x-y\right)\Pi^{(local)}\left(x\right)+\Pi^{(non-local)}\left(x,y\right)\ .$$

The local part of the self energy only causes a mass shift, which can be absorbed in an effective mass:

$$M^{2}\left(x\right)=m_{B}^{2}+\Pi^{(local)}\left(x\right)=m_{B}^{2}+\frac{\lambda}{2}G_{F}\left(x,x\right)\ . \tag{3.1.6}$$

After inserting Eq. (3.1.5) into Eq. (3.1.3), we can decompose the non-local part of the self energy in exactly the same way as the propagator:

$$\Pi^{(non-local)}\left(x,y\right)=\Pi_{F}\left(x,y\right)-\frac{i}{2}\mathrm{sign}_{\mathcal{C}}\left(x^{0}-y^{0}\right)\Pi_{\varrho}\left(x,y\right)\ .$$

We find

$$\begin{aligned}\Pi_{F}\left(x,y\right) &= -\frac{\lambda^{2}}{6}\Big(G_{F}\left(x,y\right)G_{F}\left(x,y\right)G_{F}\left(x,y\right)\\ &\quad -\frac{3}{4}G_{\varrho}\left(x,y\right)G_{\varrho}\left(x,y\right)G_{F}\left(x,y\right)\Big)\end{aligned} \tag{3.1.7}$$

and

$$\begin{aligned}\Pi_{\varrho}\left(x,y\right) &= -\frac{\lambda^{2}}{6}\Big(3G_{F}\left(x,y\right)G_{F}\left(x,y\right)G_{\varrho}\left(x,y\right)\\ &\quad -\frac{1}{4}G_{\varrho}\left(x,y\right)G_{\varrho}\left(x,y\right)G_{\varrho}\left(x,y\right)\Big)\ .\end{aligned} \tag{3.1.8}$$

When we insert all these definitions into Eq. (3.1.4), we observe that it splits into two complementary real-valued evolution equations for the statistical propagator and the spectral function, respectively [22]. These are the so-called Kadanoff-Baym equations:

$$\begin{aligned}&\left(-\partial_{x^{\mu}}\partial_{x_{\mu}}+M^{2}\left(x\right)\right)G_{F}\left(x,y\right) \\ &=\int_{0}^{y^{0}}d^{4}z\,\Pi_{F}\left(x,z\right)G_{\varrho}\left(z,y\right)-\int_{0}^{x^{0}}d^{4}z\,\Pi_{\varrho}\left(x,z\right)G_{F}\left(z,y\right)\end{aligned} \tag{3.1.9}$$

and

$$\left(-\partial_{x^{\mu}}\partial_{x_{\mu}}+M^{2}\left(x\right)\right)G_{\varrho}\left(x,y\right)=-\int_{y^{0}}^{x^{0}}d^{4}z\,\Pi_{\varrho}\left(x,z\right)G_{\varrho}\left(z,y\right)\ . \tag{3.1.10}$$

For a spatially homogeneous system, one can Fourier transform these equations with respect to the spatial relative coordinate. Furthermore, in an isotropic system the propagator will depend only on the absolute value of the momentum. More information on symmetries and how they can be exploited to simplify Kadanoff-Baym equations can be found in Section 4.2. In order to make contact with Boltzmann equations one has to introduce some kind of particle number density. It is important to note that there is no unique definition for such a particle number density. For our purposes the most suitable definition relies on a free field ansatz. An indispensable feature, that a particle number density in our context must possess, is that it allows for thermalization, meaning that for late times it approaches the form of a Bose-Einstein distribution function. Indeed the effective particle number density which we use possesses this feature. Additional intriguing properties of the free-field ansatz are that it does not involve a quasi-particle approximation and that it incorporates conserved charges if present in the considered theory. As explained in more detail in Refs. [22, 35], the effective kinetic energy and particle number densities $\omega(t, \boldsymbol{p})$ and $n(t, \boldsymbol{p})$ are given by

$$\omega^2(t, \boldsymbol{p}) = \left(\frac{\partial_{x^0} \partial_{y^0} G_F(x^0, y^0, \boldsymbol{p})}{G_F(x^0, y^0, \boldsymbol{p})} \right)_{x^0 = y^0 = t} \tag{3.1.11}$$

and

$$n(t, \boldsymbol{p}) = \omega(t, \boldsymbol{p}) G_F(t, t, \boldsymbol{p}) - \frac{1}{2} . \tag{3.1.12}$$

We would like to emphasize that the Kadanoff-Baym equations are self-consistent evolution equations for the complete propagator of our system. It is important to note that, due to the memory integrals on the right hand side of Eqs. (3.1.9) and (3.1.10), a numerical solution of the Kadanoff-Baym equations requires tracing the evolution of the propagator throughout the complete x^0-y^0-plane (of course, constrained to the part with $x^0 \geq 0$ and $y^0 \geq 0$). One can then follow the evolution of the effective particle number density (3.1.12) along the bisecting line of this plane. The details of our computational algorithm to solve the Kadanoff-Baym equations numerically can be found in the appendix.

Energy Conservation

As we will see in subsequent sections, Boltzmann equations include an explicit energy conserving δ function. A similar manifest ingredient enforcing the conservation of energy is missing in the Kadanoff-Baym equations. Nevertheless, the Kadanoff-Baym equations (3.1.9) and (3.1.10), together with the self energies (3.1.7) and (3.1.8), conserve the average energy density. Originally, it was found that the conservation of energy is guaranteed once a so-called Φ-derivable approximation is used [36, 37]. This means that the Kadanoff-Baym equations are more or less written down from scratch and that the self energy is obtained

by functional derivation of the so-called Φ functional. Identifying the functional Φ with Γ_2 we immediately see that the 2PI effective action furnishes such a Φ-derivable approximation. Actually, the proof that the Kadanoff-Baym equations conserve energy can be drastically simplified, once we take into account that the Kadanoff-Baym equations themselves can be derived from the equation of motion (2.3.15). In the same way, as one can derive an energy-momentum tensor from the classical action, one can also derive an energy-momentum tensor from the 2PI effective action. We consider an infinitesimal space-time translation

$$\begin{aligned} G(x,y) &\rightarrow G(x+\epsilon(x), y+\epsilon(y)) \\ &= G(x,y) + \underbrace{\epsilon^{\mu}(x)\,\partial_{x^{\mu}} G(x,y) + \epsilon^{\mu}(y)\,\partial_{y^{\mu}} G(x,y)}_{\Delta G(x,y)} . \end{aligned}$$

In general, the variation of the 2PI effective action under this translation will have to be of the form

$$\Delta\Gamma[G] = -\int_{\mathcal{C}} d^4x\; \Theta^{\mu\nu}(x)\,\partial_{x^{\mu}}\epsilon_{\nu}(x) \; . \tag{3.1.13}$$

On the other hand the variation of the 2PI effective action is also given by

$$\Delta\Gamma[G] = \int_{\mathcal{C}} d^4x\; d^4y\; \frac{\delta\Gamma[G]}{\delta G(x,y)} \Delta G(x,y) \; . \tag{3.1.14}$$

As the physical propagator satisfies the equation of motion (2.3.15), $\Delta\Gamma[G]$ vanishes. Integrating Eq. (3.1.13) by parts, we find that $\Theta^{\mu\nu}$ satisfies a conservation law:

$$\partial_{x^{\mu}} \Theta^{\mu\nu}(x) = 0 \; .$$

Analogous to the classical case we can identify $\Theta^{\mu\nu}(x)$ with the energy-momentum tensor. Converting Eq. (3.1.14) into Eq. (3.1.13) yields [75]

$$\begin{aligned} \Theta^{\mu\nu}(x) &= \left[\left(\partial_{x_{\mu}}\partial_{y_{\nu}} - \frac{1}{2}\eta^{\mu\nu}\partial_{x^{\kappa}}\partial_{y_{\kappa}} - \frac{m_B^2}{2}\eta^{\mu\nu}\right) G_F(x,y)\right]_{y=x} - \eta^{\mu\nu}\frac{\lambda}{8} G_F^2(x,x) \\ &\quad + \frac{1}{4}\eta^{\mu\nu}\int_0^{x^0} d^4z \Big[\Pi_F(x,z)\, G_{\varrho}(z,x) - \Pi_{\varrho}(x,z)\, G_F(z,x)\Big] \; . \end{aligned}$$

The average energy density is then given by the time-time component of the energy-momentum tensor. For a spatially homogeneous and isotropic system we obtain

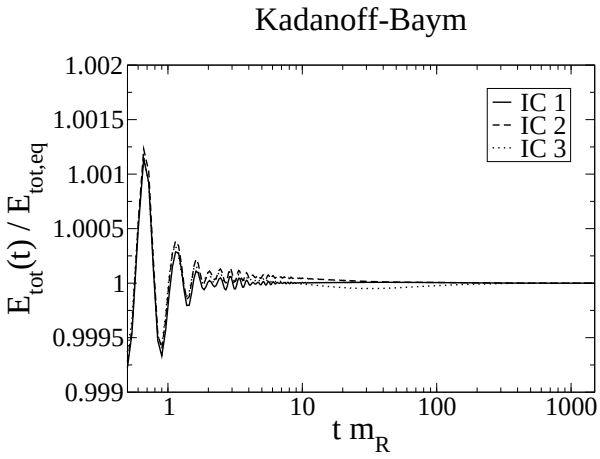

Figure 3.3: Time evolution of the average energy density for various initial conditions, cf. Fig. 3.8. Our numerical solutions of the Kadanoff-Baym equations conserve the average energy density up to numerical errors $< 0.2\%$.

$$
\begin{aligned}
E_{tot}(t) = \int \frac{d^3p}{(2\pi)^3} \Bigg[& \left(\frac{1}{2} \left(\partial_{x^0} \partial_{y^0} + p^2 + m_B^2 \right) G_F \left(x^0, y^0, p \right) \right)_{x^0 = y^0 = t} \\
& + \frac{\lambda}{8} G_F(t,t,p) \int \frac{d^3q}{(2\pi)^3} \left[G_F(t,t,q) \right] \\
& - \frac{1}{4} \int_0^t dz^0 \left[\Pi_F \left(t, z^0, p \right) G_\varrho \left(z^0, t, p \right) - \Pi_\varrho \left(t, z^0, p \right) G_F \left(z^0, t, p \right) \right] \Bigg] .
\end{aligned}
$$

Fig. 3.3 shows that our numerical solutions, which we discuss in Section 3.4, indeed conserve the average energy density up to numerical errors $< 0.2\%$.

3.2 Quantum Kinetics

Employing a first order gradient expansion and a Wigner transformation, one can derive quantum kinetic equations from the Kadanoff-Baym equations. As we will see, these quantum kinetic equations should be a good approximation to the full quantum dynamics already after moderate times. Compared to the full Kadanoff-Baym equations, these quantum kinetic equations have the advantage of being local in time, which extraordinarily reduces the computational resources needed for their numerical solution. In this section we review the derivation of

these quantum kinetic equations. We start from the Kadanoff-Baym equation for the statistical propagator (3.1.9). Using the retarded and advanced propagators

$$G_R(x,y) = \theta\left(x^0 - y^0\right) G_\varrho(x,y) \tag{3.2.1}$$

and

$$G_A(x,y) = -\theta\left(y^0 - x^0\right) G_\varrho(x,y) \tag{3.2.2}$$

and corresponding definitions for the self energies we can send the upper limits of the memory integrals to $+\infty$:

$$\begin{aligned}&\left(-\partial_{x^\mu}\partial_{x_\mu} + M^2(x)\right) G_F(x,y)\\ &\quad = -\int d^4z\, \theta\left(z^0\right)\left[\Pi_F(x,z)\, G_A(z,y) + \Pi_R(x,z)\, G_F(z,y)\right] .\end{aligned} \tag{3.2.3}$$

Obviously the retarded and advanced propagators satisfy

$$G_R(y,x) = G_A(x,y) \ .$$

The same relation also holds for the self energies. Furthermore, we have already seen that the statistical propagator and the statistical component of the self energy are invariant under a transposition of their arguments. Thus, interchanging x and y on both sides of Eq. (3.2.3) yields

$$\begin{aligned}&\left(-\partial_{y^\mu}\partial_{y_\mu} + M^2(y)\right) G_F(x,y)\\ &\quad = -\int d^4z\, \theta\left(z^0\right)\left[G_R(x,z)\, \Pi_F(z,y) + G_F(x,z)\, \Pi_A(z,y)\right] .\end{aligned} \tag{3.2.4}$$

Next, we switch to center and relative coordinates, i.e. we re-parametrize the propagator according to

$$G(u,v) = \tilde{G}\left(\frac{u+v}{2}, u-v\right) \ .$$

The coordinates x and y in Eqs. (3.2.3) and (3.2.4) are particularly important:

$$X = \frac{x+y}{2} \qquad \text{and} \qquad s = x - y \ . \tag{3.2.5}$$

Subtracting Eq. (3.2.4) from Eq. (3.2.3) gives the difference equation

$$\begin{aligned}&\left(-\partial_{x^\mu}\partial_{x_\mu} + \partial_{y^\mu}\partial_{y_\mu} + M^2(x) - M^2(y)\right) G_F(x,y)\\ &\quad = -\int d^4z\, \theta\left(z^0\right)\Big[\Pi_F(x,z)\, G_A(z,y) + \Pi_R(x,z)\, G_F(z,y)\\ &\qquad - G_R(x,z)\, \Pi_F(z,y) - G_F(x,z)\, \Pi_A(z,y)\Big] .\end{aligned} \tag{3.2.6}$$

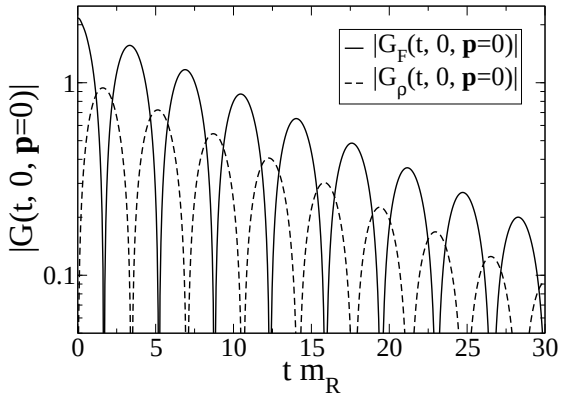

Figure 3.4: The modulus of the unequal-time propagator as function of time for fixed momentum mode $\boldsymbol{p} = 0$. Correlations between earlier and later times are exponentially damped.

On the left hand side of this difference equation we observe that

$$-\partial_{x^\mu}\partial_{x_\mu} + \partial_{y^\mu}\partial_{y_\mu} = -2\partial_{s_\mu}\partial_{X^\mu} \ .$$

is automatically of first order in ∂_X. Furthermore we Taylor expand the effective masses on the left hand side, and the propagators and self energies on the right hand side of the difference equation to first order in ∂_X around the center coordinate X:

$$M^2(x) - M^2(y) = s^\mu \partial_{X^\mu} M^2(X) \ .$$

According to Fig. 3.4 correlations between earlier and later times are suppressed exponentially. This suppression leads to a gradual loss of the dependence on the details of the initial conditions. Exploiting this memory loss, for late enough times we can drop the θ function from the memory integral in the difference equation (3.2.6), which corresponds to sending the initial time to $-\infty$. This allows us to Fourier transform the difference equation with respect to the relative coordinate s. The Wigner transformed statistical propagator is given by

$$\tilde{G}_F(X,k) = \int d^4 s \exp(-iks)\, \tilde{G}_F(X,s) \ .$$

As the spectral function is anti-symmetric with respect to the interchange of its time arguments, we introduce a factor of $-i$ into its Wigner transform, such that

$$\tilde{G}_\varrho(X,k) = -i \int d^4 s \exp(-iks)\, \tilde{G}_\varrho(X,s)$$

is again a real-valued quantity. Due to the first order gradient expansion and the Wigner transformation the memory integrals become

$$\int d^4z\; f\left(x,z\right) g\left(z,y\right) \rightarrow \tilde{f}\left(X,k\right) \tilde{g}\left(X,k\right) + \frac{i}{2}\left\{\tilde{f}\left(X,k\right);\; \tilde{g}\left(X,k\right)\right\}_{PB} \;,$$

where the Poisson brackets are defined by

$$\left\{\tilde{f};\; \tilde{g}\right\}_{PB} = \left[\partial_{X^\mu}\tilde{f}\right]\left[\partial_{k_\mu}\tilde{g}\right] - \left[\partial_{k_\mu}\tilde{f}\right]\left[\partial_{X^\mu}\tilde{g}\right] \;.$$

In order to calculate the Wigner transform of the retarded and advanced propagators, we have to recall that the Fourier transform of a θ function in one dimension is given by

$$\int ds^0\; \exp\left(i\omega s^0\right)\theta\left(\pm s^0\right) = \lim_{\varepsilon\rightarrow 0}\frac{\pm i}{\omega \pm i\varepsilon} \;.$$

Consequently, we find

$$\tilde{G}_R\left(X,k\right) = -\int \frac{d\omega}{2\pi}\; \frac{G_\varrho\left(X,\omega,\boldsymbol{k}\right)}{k^0-\omega+i\varepsilon} \tag{3.2.7}$$

and

$$\tilde{G}_A\left(X,k\right) = -\int \frac{d\omega}{2\pi}\; \frac{G_\varrho\left(X,\omega,\boldsymbol{k}\right)}{k^0-\omega-i\varepsilon} \;. \tag{3.2.8}$$

As $\tilde{G}_\varrho\left(X,k\right)$ is a real-valued quantity, the Wigner transformed retarded and advanced propagators satisfy

$$\tilde{G}_A\left(X,k\right) = \tilde{G}_R^*\left(X,k\right)$$

$$\Longleftrightarrow \qquad \left\{\begin{array}{rcl} \tilde{G}_R\left(X,k\right) + \tilde{G}_A\left(X,k\right) &=& 2\mathrm{Re}\left(\tilde{G}_R\left(X,k\right)\right) \\ \tilde{G}_R\left(X,k\right) - \tilde{G}_A\left(X,k\right) &=& 2i\mathrm{Im}\left(\tilde{G}_R\left(X,k\right)\right) \end{array}\right. \;. \tag{3.2.9}$$

Recalling that the δ function can be approximated by

$$\delta_\varepsilon\left(\omega\right) = \frac{\varepsilon}{\pi\left(\omega^2+\varepsilon^2\right)}$$

we also find

$$\tilde{G}_R\left(X,k\right) - \tilde{G}_A\left(X,k\right) = i\tilde{G}_\varrho\left(X,k\right) \;. \tag{3.2.10}$$

Using the quantity

$$\tilde{\Omega}\left(X,k\right) = k^\mu k_\mu + M^2\left(X\right) + \mathrm{Re}\left(\tilde{\Pi}_R\left(X,k\right)\right) \;, \tag{3.2.11}$$

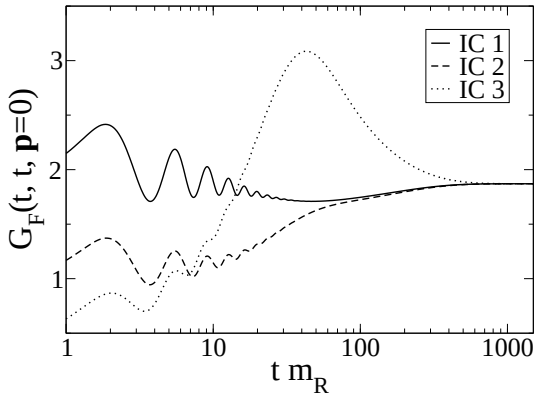

Figure 3.5: The equal-time propagator as a function of time for three different initial conditions (cf. Fig. 3.8). The system shows rapid oscillations which die out after moderate times and are followed by a monotonous drifting regime.

eventually, the kinetic equation for the statistical propagator can be written in the form [76]

$$\begin{aligned} &-\left\{\tilde{\Omega}\,(X,k)\,;\;\tilde{G}_F\,(X,k)\right\}_{PB} \\ &\quad = \;\tilde{\Pi}_\varrho\,(X,k)\,\tilde{G}_F\,(X,k) - \tilde{\Pi}_F\,(X,k)\,\tilde{G}_\varrho\,(X,k) \\ &\qquad + \left\{\tilde{\Pi}_F\,(X,k)\,;\;\mathrm{Re}\left(\tilde{G}_R\,(X,k)\right)\right\}_{PB} . \end{aligned} \tag{3.2.12}$$

In very much the same way we also can derive a kinetic equation for the spectral function:

$$-\left\{\tilde{\Omega}\,(X,k)\,;\;\tilde{G}_\varrho\,(X,k)\right\}_{PB} = \left\{\tilde{\Pi}_\varrho\,(X,k)\,;\;\mathrm{Re}\left(\tilde{G}_R\,(X,k)\right)\right\}_{PB} . \tag{3.2.13}$$

What is the expected range of validity of these quantum kinetic equations? Employing the first-order gradient expansion is clearly not justifiable for early times when the equal-time propagator is rapidly oscillating, as can be seen in Fig. 3.5. But this is obvious, since employing the first-order gradient expansion is clearly motivated by equilibrium considerations. As we saw in Section 2.1, in equilibrium the propagator depends on the relative coordinates only. There is no dependence on the center coordinates, and one may hope that there are situations where the propagator depends only moderately on the center coordinates. This is certainly the case for late times when our system is sufficiently close to equilibrium.

However, as is shown in Fig. 3.5, already after moderate times the rapid oscillations mentioned above have died out and are followed by a monotonous drifting regime [22]. Due to the monotonous character, in this drifting regime the second derivative with respect to X should be negligible as compared to the first order derivative and a consistent Taylor expansion to first order in ∂_X can be justified even though the system may still be far from equilibrium. However, it is crucial that the Taylor expansion is performed consistently for two reasons: First, this guarantees that the quantum kinetic equations satisfy exactly the same conservation laws as the full Kadanoff-Baym equations [17]. Second, it has been shown that neglecting the Poisson brackets on the right hand side of the quantum kinetic equations (3.2.12) and (3.2.13), as well as the X-dependence of $\tilde{\Omega}$ on the left hand side, leads to equations whose range of validity is quite restricted [77, 78].

The convolution of the Wigner transformed θ function with the Wigner transformed spectral function in Eq. (3.2.7) leads to a principal value integral, which cannot be evaluated in general. Therefore, we cannot use Eq. (3.2.7) to compute the real part of the Wigner transform of the retarded propagator. We circumvent this difficulty by deriving an extra kinetic equation for the retarded propagator. In order to do so, we first note that

$$-\partial_{x^\mu}\partial_{x_\mu} G_R(x,y) = \delta(x-y) - \theta\left(x^0-y^0\right)\partial_{x^\mu}\partial_{x_\mu} G_\varrho(x,y)$$

and

$$-\partial_{x^\mu}\partial_{x_\mu} G_A(x,y) = \delta(x-y) + \theta\left(y^0-x^0\right)\partial_{x^\mu}\partial_{x_\mu} G_\varrho(x,y) \ .$$

Thus, multiplying the Kadanoff-Baym equation (3.1.10) for the spectral function with $\theta(x^0-y^0)$ and $-\theta(y^0-x^0)$, respectively, yields

$$\left(-\partial_{x^\mu}\partial_{x_\mu} + M^2(x)\right) G_R(x,y) = \delta(x-y) - \int d^4z\, \Pi_R(x,z)\, G_R(z,y) \quad (3.2.14)$$

and

$$\left(-\partial_{x^\mu}\partial_{x_\mu} + M^2(x)\right) G_A(x,y) = \delta(x-y) - \int d^4z\, \Pi_A(x,z)\, G_A(z,y) \ . \quad (3.2.15)$$

Next, we add Eq. (3.2.15), with x and y interchanged, to Eq. (3.2.14). Having switched to center and relative coordinates, we observe on the left hand side of the sum equation, that to first order in ∂_X

$$-\partial_{x^\mu}\partial_{x_\mu} - \partial_{y^\mu}\partial_{y_\mu} = -2\partial_{s^\mu}\partial_{s_\mu} \ .$$

As in the derivation of the kinetic equation for the statistical propagator, we Taylor expand the effective masses on the left hand side of the sum equation and the propagators and self energies on the right hand side to first order in ∂_X. For the effective masses we find

$$M^2(x) + M^2(y) = 2M^2(X) \ .$$

Eventually, we Fourier transform the sum equation with respect to the relative coordinate s. In contrast to the kinetic equations for the statistical propagator and the spectral function, the kinetic equation for the retarded propagator is not a differential equation, but an algebraic equation:

$$\tilde{G}_R(X,k) = \frac{1}{k^\mu k_\mu + M^2(X) + \tilde{\Pi}_R(X,k)} . \tag{3.2.16}$$

Consequently, we obtain for the real part of the retarded propagator

$$\mathrm{Re}\left(\tilde{G}_R(X,k)\right) = \frac{\tilde{\Omega}(X,k)}{\tilde{\Omega}^2(X,k) + \frac{1}{4}\tilde{\Pi}_\varrho^2(X,k)} . \tag{3.2.17}$$

Furthermore, due to Eqs. (3.2.9) and (3.2.10) the kinetic equation for the retarded propagator also gives us a solution to the kinetic equation for the spectral function (3.2.13):

$$\tilde{G}_\varrho(X,k) = \frac{-\tilde{\Pi}_\varrho(X,k)}{\tilde{\Omega}^2(X,k) + \frac{1}{4}\tilde{\Pi}_\varrho^2(X,k)} .$$

After all, it remains to work out the self energies. Wigner transforming Eqs. (3.1.7) and (3.1.8) yields:

$$\begin{aligned}\Pi_F(X,k) &= -\frac{\lambda^2}{6}\int \frac{d^4p}{(2\pi)^4}\,\frac{d^4q}{(2\pi)^4}\Big[G_F(X,k-p-q)\,G_F(X,p)\,G_F(X,q) \\ &\quad -\frac{3}{4}G_\varrho(X,k-p-q)\,G_\varrho(X,p)\,G_F(X,q)\Big]\end{aligned} \tag{3.2.18}$$

and

$$\begin{aligned}\Pi_\varrho(X,k) &= -\frac{\lambda^2}{6}\int \frac{d^4p}{(2\pi)^4}\,\frac{d^4q}{(2\pi)^4}\Big[3G_F(X,k-p-q)\,G_F(X,p)\,G_\varrho(X,q) \\ &\quad -\frac{1}{4}G_\varrho(X,k-p-q)\,G_\varrho(X,p)\,G_\varrho(X,q)\Big] .\end{aligned} \tag{3.2.19}$$

On the other hand, multiplying Eq. (3.1.8) with $\theta(x^0-y^0)$ yields an equation for the retarded self-energy

$$\begin{aligned}\Pi_R(x,y) &= -\frac{\lambda^2}{6}\Big(3G_F(x,y)\,G_F(x,y)\,G_R(x,y) \\ &\quad -\frac{1}{4}G_\varrho(x,y)\,G_\varrho(x,y)\,G_R(x,y)\Big) .\end{aligned}$$

Accordingly, the Wigner transformed retarded self-energy is given by

$$\begin{aligned}\Pi_R(X,k) &= -\frac{\lambda^2}{6}\int \frac{d^4p}{(2\pi)^4}\,\frac{d^4q}{(2\pi)^4}\Big[3G_F(X,k-p-q)\,G_F(X,p)\,G_R(X,q) \\ &\quad -\frac{1}{4}G_\varrho(X,k-p-q)\,G_\varrho(X,p)\,G_R(X,q)\Big] .\end{aligned} \tag{3.2.20}$$

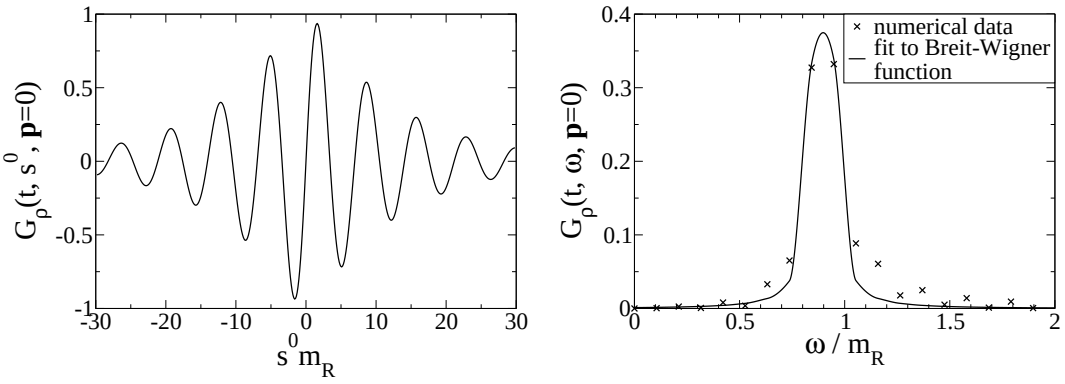

Figure 3.6: The left plot shows the spectral function for fixed center time $tm_R = 1485$ and spatial momentum $\boldsymbol{p} = 0$ as function of the relative time $s^0 = x^0 - y^0$. On the right hand side we see its Fourier transform as function of the energy and a fit of the numerical data to a Breit-Wigner function.

Similarly as for the propagator, the imaginary part of the retarded self-energy is given by the spectral self-energy. On the other hand, taking the real part of Eq. (3.2.20) and inserting Eqs. (3.2.17) and (3.2.11) yields an integral equation for the real part of the retarded self-energy.

3.3 Boltzmann Kinetics

Boltzmann Equation

In order to derive a Boltzmann equation from the quantum kinetic equation (3.2.12), first we have to discard the Poisson brackets on the right hand side, thereby sacrificing the consistency of the gradient expansion. On the left hand side we replace $\tilde{\Omega}(X,k)$ by

$$\tilde{\Omega}(k) = k^\mu k_\mu + m_{th}^2 \,,$$

where m_{th} is the time-independent thermal mass of the particles in our system. After that, we generalize the fluctuation-dissipation theorem (2.1.17) to the so-called Kadanoff-Baym ansatz

$$\tilde{G}_F(X,k) = \tilde{G}_\varrho(X,k)\left(\tilde{n}(X,k) + \frac{1}{2}\right) \,. \tag{3.3.1}$$

In Ref. [79] a generalized Kadanoff-Baym ansatz has been proposed. For simplicity, however, in this work we will be content with the standard form (3.3.1). Furthermore, we employ the quasi-particle (or on-shell) approximation:

$$\tilde{G}_{\varrho}(X,k) = \tilde{G}_{\varrho}(k) = \frac{\pi}{E(\boldsymbol{k})}\Big(\delta\left(k^0 - E(\boldsymbol{k})\right) - \delta\left(k^0 + E(\boldsymbol{k})\right)\Big)\,, \tag{3.3.2}$$

where the quasi-particle energy is given by

$$E(\boldsymbol{k}) = \sqrt{m_{th}^2 + \boldsymbol{k}^2}\,.$$

After all, Eq. (3.2.12) has become

$$\begin{aligned} & 2k^{\mu}\partial_{X^{\mu}}\left(\tilde{n}(X,k) + \frac{1}{2}\right)\frac{\pi}{E(\boldsymbol{k})}\left(\delta\left(k^0 - E(\boldsymbol{k})\right) - \delta\left(k^0 + E(\boldsymbol{k})\right)\right) \\ = \;& \left(\tilde{\Pi}_{\varrho}(X,k)\left(\tilde{n}(X,k) + \frac{1}{2}\right) - \tilde{\Pi}_{F}(X,k)\right) \\ & \times \frac{\pi}{E(\boldsymbol{k})}\left(\delta\left(k^0 - E(\boldsymbol{k})\right) - \delta\left(k^0 + E(\boldsymbol{k})\right)\right) \end{aligned} \tag{3.3.3}$$

Once more, we would like to stress that the exact time evolution of the spectral function is determined by the Kadanoff-Baym equations. As one can see in the right plot of Fig. 3.6 the Wigner transform of the spectral function can be parametrized by a Breit-Wigner function with a non-vanishing width [23, 30]. Reducing the width of this Breit-Wigner curve to zero is certainly not a controllable approximation and causes significant discrepancies for solutions of Kadanoff-Baym and Boltzmann equations, already on a qualitative level. In fact the on-shell approximation implies the assumption that our system consist of stable quasi-particles. In contrast to this, however, in a relativistic quantum field theory the interactions of particles are described by their creation and annihilation, which amount to decay and recombination processes.

As already indicated at the end of the previous section, a completely self-consistent determination of the thermal mass in the framework of the Boltzmann equation would require solving an integral equation for the energy density. This would drastically increase the complexity of the computational algorithm which we use to solve the Boltzmann equation numerically. As none of our physical results depend on the exact value of the thermal mass, for convenience, we set m_{th} to the equilibrium value of the thermal mass as determined by the Kadanoff-Baym equations. Eventually, we define the quasi-particle number density by

$$n(X,\boldsymbol{k}) = \tilde{n}(X,\boldsymbol{k},E(\boldsymbol{k}))\;.$$

After equating the positive energy components in Eq. (3.3.3) and integrating over k^0 we arrive at the Boltzmann equation. For a spatially homogeneous system

there is no dependence on the spatial center coordinates and the Boltzmann equation reads[3]:

$$\begin{aligned}\partial_t n\left(t,\boldsymbol{k}\right) = \frac{\lambda^2\pi}{48}\int\frac{d^3p}{\left(2\pi\right)^3}\int\frac{d^3q}{\left(2\pi\right)^3}\int d^3r\Bigg[&\frac{1}{E_kE_pE_qE_r}\\ &\times\delta\left(\boldsymbol{k}+\boldsymbol{p}-\boldsymbol{q}-\boldsymbol{r}\right)\delta\left(E_k+E_p-E_q-E_r\right)\\ &\times\Big(\left(1+n_{\boldsymbol{k}}\right)\left(1+n_{\boldsymbol{p}}\right)n_{\boldsymbol{q}}n_{\boldsymbol{r}}-n_{\boldsymbol{k}}n_{\boldsymbol{p}}\left(1+n_{\boldsymbol{q}}\right)\left(1+n_{\boldsymbol{r}}\right)\Big)\Bigg]\,.\end{aligned}\tag{3.3.4}$$

It is pleasant to observe that the Kadanoff-Baym ansatz entails the Nordheim-Uehling-Uhlenbeck corrections to the classical Boltzmann equation [19–21,80–84], which are necessary to guarantee that the stationary solution of the Boltzmann equation takes the form of a Bose-Einstein distribution function. We would like to emphasize that the Boltzmann equation (3.3.4) comprises only the scattering of two particles, which leaves the total particle number unchanged. As was detailed in Ref. [85], due to the quasi-particle approximation, for the present truncation of the 2PI effective action decay and recombination processes are kinematically forbidden. In this context we would like to note that the inclusion of further diagrams in the 2PI effective action could lead to terms in the Boltzmann collision integral which describe collisions of more than two particles [86–88].

Simplifying the Boltzmann Collision Integral

As it stands, the numerical solution of Eq. (3.3.4) requires an enormous amount of (parallel) computing power, because the evaluation of the six-dimensional collision integral in Eq. (3.3.4) is extraordinarily expensive. However, as we consider a spatially homogeneous and isotropic system, we can dramatically simplify the collision integral, which allows us to reduce the complexity of our numerical algorithm significantly. The simplification of the Boltzmann collision integral relies on the Fourier representation of the momentum conservation delta function [89]:

$$\delta^3\left(\boldsymbol{m}\right) = \int\frac{d^3\xi}{\left(2\pi\right)^3}\,\exp\left(-i\boldsymbol{m}\boldsymbol{\xi}\right)\,.$$

Using spherical coordinates, we find

$$\boldsymbol{m}\boldsymbol{\xi} = m\xi\Big(\sin\vartheta_m\,\sin\vartheta_\xi\,\cos\left(\varphi_m-\varphi_\xi\right)+\cos\vartheta_m\,\cos\vartheta_\xi\Big)\,.$$

Now, we consider just the integration over the solid angle. As we integrate over the complete solid angle Ω_ξ, it does not matter in which direction $\boldsymbol{m}$ is pointing. The result will always be the same:

$$\int d\Omega_\xi\exp\left(-i\boldsymbol{m}\boldsymbol{\xi}\right) = \int d\Omega_\xi\exp\left(-i\boldsymbol{m}_0\boldsymbol{\xi}\right)\,,$$

[3]Here, we use the abbreviations $E_k=\sqrt{m_{th}^2+\boldsymbol{k}^2}$ and $n_{\boldsymbol{k}}=n\left(t,\boldsymbol{k}\right)$.

where we can choose $\boldsymbol{m}_0 = (0, 0, m)$, such that $\varphi_m = \vartheta_m = 0$. Now, we can evaluate the integral quite easily:

$$\int d\Omega_\xi \exp\left(-i\boldsymbol{m}\boldsymbol{\xi}\right) = \int d\Omega_\xi \exp\left(-im\xi\cos\vartheta_\xi\right) = \frac{4\pi}{m\xi}\sin\left(m\xi\right) \ . \tag{3.3.5}$$

After we have rewritten Eq. (3.3.4) using spherical coordinates and inserted the Fourier representation for the momentum conservation delta function, we can use Eq. (3.3.5) to perform the integrations over the solid angles. Here it is crucial to evaluate the integrals over Ω_p, Ω_q and Ω_r first, and to do the integral over Ω_ξ last. We find:

$$\begin{aligned}\partial_t n\left(t,k\right) = \frac{\lambda^2}{96\pi^4}\int\limits_0^\infty dp\int\limits_0^\infty dq\int\limits_0^\infty dr\int\limits_0^\infty d\xi\Bigg[pqr\frac{\delta\left(E_k+E_p-E_q-E_r\right)}{E_kE_pE_q}\\ \times\frac{1}{k\xi^2}\sin\left(k\xi\right)\ \sin\left(p\xi\right)\ \sin\left(q\xi\right)\ \sin\left(r\xi\right)\\ \times\Big(\left(1+n_k\right)\left(1+n_p\right)n_qn_r-n_kn_p\left(1+n_q\right)\left(1+n_r\right)\Big)\Bigg] \ ,\end{aligned}$$

Next, it is important to observe that the function

$$D\left(k,p,q,r\right) = \int\limits_0^\infty d\xi\frac{1}{k\xi^2}\sin\left(k\xi\right)\ \sin\left(p\xi\right)\ \sin\left(q\xi\right)\ \sin\left(r\xi\right) \ .$$

can easily be evaluated using a computer algebra program. For $k > 0$ we find

$$\begin{aligned}D\left(k,p,q,r\right) \ &= \ \frac{\pi}{16k}\Big(\left|k-p-q-r\right|-\left|k+p-q-r\right|\\ &\quad -\left|k-p+q-r\right|+\left|k+p+q-r\right|\\ &\quad -\left|k-p-q+r\right|+\left|k+p-q+r\right|\\ &\quad +\left|k-p+q+r\right|-\left|k+p+q+r\right|\Big) \ ,\end{aligned}$$

and for $k = 0$ we obtain

$$\begin{aligned}D\left(0,p,q,r\right) \ &= \ \frac{\pi}{8}\Big(\mathrm{sign}\left(p+q-r\right)-\mathrm{sign}\left(p-q-r\right)\\ &\quad +\mathrm{sign}\left(p-q+r\right)-\mathrm{sign}\left(p+q+r\right)\Big).\end{aligned}$$

Eventually, we use the energy conservation δ function to evaluate the integral over r, using the well-known formula

$$\delta\left(f\left(r\right)\right) = \sum_{\{r_0|f(r_0)=0\}}\frac{\delta\left(r-r_0\right)}{\left|\left(\frac{df}{dr}\right)_{r=r_0}\right|} \ .$$

r_0 is determined by the condition that the argument of the energy conservation δ function is zero:

$$E_k + E_p - E_q - E_{r_0} = 0 \; . \tag{3.3.6}$$

If this condition can be satisfied, r_0 is given by

$$r_0 = r_0 \left(t, k, p, q\right) = \sqrt{\left(E_k + E_p - E_q\right)^2 - M^2 \left(t\right)} \; .$$

If k, p and q are such that condition (3.3.6) cannot be satisfied, the above square root yields a purely imaginary result and $r_0^2 < 0$. Using a θ function we can prevent the corresponding term from contributing to the collision integral. After these final steps the Boltzmann equation takes the form[4]:

$$\begin{aligned} \partial_t n \left(t, k\right) = \frac{\lambda^2}{96\pi^4} \int\limits_0^\infty dp \int\limits_0^\infty dq \Bigg[\theta \left(r_0^2\right) \frac{pqD \left(k, p, q, r_0\right)}{E_k E_p E_q} \\ \times \Big(\left(1 + n_k\right) \left(1 + n_p\right) n_q n_{r_0} - n_k n_p \left(1 + n_q\right) \left(1 + n_{r_0}\right) \Big) \Bigg] \; . \end{aligned} \tag{3.3.7}$$

The form (3.3.7) of the Boltzmann equation underlies our numerical algorithm. More information on the details of this algorithm can be found in the appendix.

Energy Conservation

As indicated already in the first section of this chapter, the conservation of the average energy density

$$E_{tot} \left(t\right) = \int \frac{d^3 p}{\left(2\pi\right)^3} E \left(p\right) n \left(t, p\right) \; .$$

is guaranteed by the explicit energy-conserving δ function in the Boltzmann equation (3.3.4). Fig. 3.7 shows that our numerical algorithm indeed conserves the average energy density up to numerical errors $< 0.3\%$.

In this and the previous section we have shown that, using a gradient expansion and a quasi-particle (or on-shell) approximation, one can derive Boltzmann equations from Kadanoff-Baym equations. In this sense Kadanoff-Baym equations can be considered as quantum Boltzmann equations re-summing the gradient expansion up to infinite order and including off-shell and memory effects.

3.4 Comparison of Numerical Solutions

Initial Conditions

We consider three different initial conditions denoted with IC1, IC2 and IC3, which correspond to the same average energy density. Above that, the initial

[4] Now, $k = |\boldsymbol{k}|$ and $n_k = n \left(t, |\boldsymbol{k}|\right)$

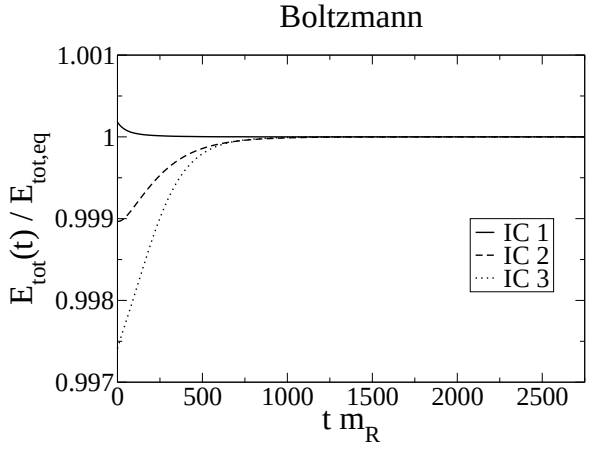

Figure 3.7: Time evolution of the average energy density for various initial conditions, cf. Fig. 3.8. Our numerical solutions of the Boltzmann equation conserve the average energy density up to numerical errors $< 0.3\%$.

conditions IC1 and IC2 also correspond to the same initial average particle number density. The corresponding initial particle number distributions are shown in Fig. 3.8. These particle number distributions can immediately be fed into the numerics for the Boltzmann equation. In order to obtain the initial conditions for the Kadanoff-Baym equations, we follow Refs. [22, 35]: The initial values for the spectral function are determined from the canonical commutation relations. On the other hand, for a given initial particle number distribution, the initial values for the statistical propagator and its derivatives are determined according to:

$$G_F\left(x^0, y^0, \boldsymbol{p}\right)_{x^0=y^0=0} = \left[\frac{n\left(t, \boldsymbol{p}\right) + \frac{1}{2}}{\omega\left(t, \boldsymbol{p}\right)}\right]_{t=0}, \tag{3.4.1}$$

$$\left[\partial_{x^0} G_F\left(x^0, y^0, \boldsymbol{p}\right)\right]_{x^0=y^0=0} = 0\,, \tag{3.4.2}$$

$$\left[\partial_{x^0}\partial_{y^0} G_F\left(x^0, y^0, \boldsymbol{p}\right)\right]_{x^0=y^0=0} = \left[\omega\left(t, \boldsymbol{p}\right)\left(n\left(t, \boldsymbol{p}\right) + \frac{1}{2}\right)\right]_{t=0}, \tag{3.4.3}$$

where the initial effective energy density is given by

$$\omega\left(t = 0, \boldsymbol{p}\right) = \sqrt{m_R^2 + \boldsymbol{p}^2}\,.$$

m_R denotes the renormalized vacuum mass. The corresponding bare mass m_B is obtained through a perturbative renormalization at one-loop order of the self energy (tadpole) [75]. $\omega\left(t, \boldsymbol{p} = 0\right)$ plays the role of a time-dependent thermal mass.

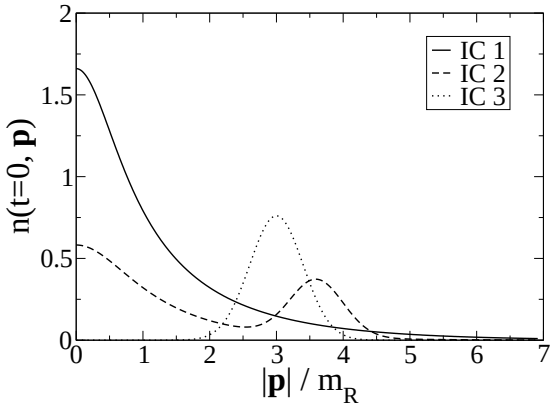

Figure 3.8: Initial particle number distributions against absolute momenta. Shown are the three different initial conditions (IC) discussed in the text, for which we numerically solved the Boltzmann and the Kadanoff-Baym equations, respectively. All initial conditions correspond to the same (conserved) average energy density. Above that, the initial conditions IC1 and IC2 also correspond to the same initial average particle number density.

After equilibrium has effectively been reached, we denote the time-independent thermal mass by $m_{th} = \omega_{eq}(\boldsymbol{p} = 0)$, which is used to set the scale in some of the plots shown in the following subsections. The computational algorithms employed to solve the Kadanoff-Baym and Boltzmann equations numerically are described in detail in the appendix. For the Kadanoff-Baym equations we used a standard lattice discretization with $N_t = 500$ and $N_s = 32$. The lattice spacings were $a_s m_R = 0.5$ and $a_t m_R = 0.06$. The coupling has been set to $\lambda = 18$. For the Boltzmann equation we used 500 momentum bins and the same momentum cut-off and coupling as for the Kadanoff-Baym equations.

Universality

Figs. 3.9 and 3.10 show the evolution of the particle number distributions for two momentum modes and the corresponding equilibrium particle number distributions, respectively, for all initial conditions. In the left plots we can see, that the Kadanoff-Baym equations lead to a universal equilibrium particle number density. The left plot in Fig. 3.9 shows that the particle number distributions may evolve

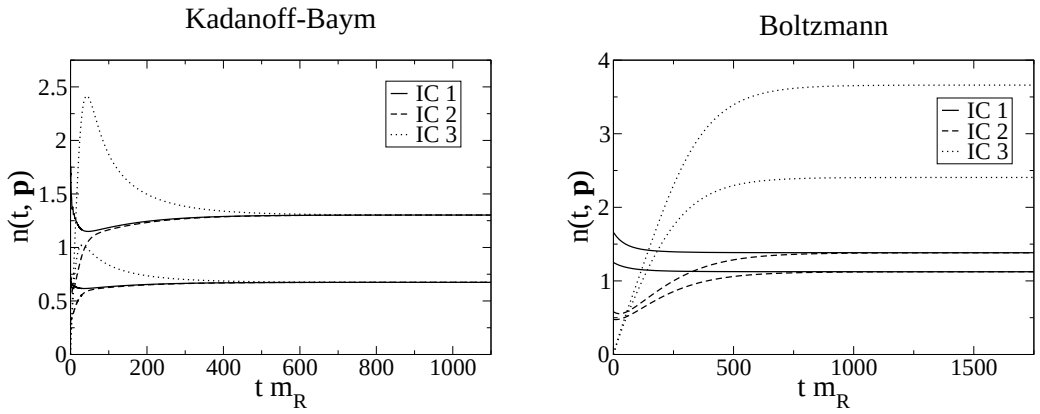

Figure 3.9: These plots show the time evolution of the particle number distributions for two different momentum modes and all initial conditions (cf. Fig. 3.8) as determined by the Boltzmann and the Kadanoff-Baym equations, respectively. We see that the Kadanoff-Baym equations respect full universality, whereas in the case of the Boltzmann equation only a restricted universality is maintained, cf. Fig. 3.10.

quite differently for early times[5]. However, respecting universality, for any given momentum mode all distributions approach the same late-time value. This plot is supplemented by the left plot in Fig. 3.10. There, one can see that the various particle number densities, after equilibrium has effectively been reached, indeed completely agree. Hence, this plot proves that we could have shown plots similar to the left one in Fig. 3.9 for all momentum modes. In particular the predicted temperature, given by the inverse slope of the line, is the same for all initial conditions. In contrast to this, the right plots reveal that the Boltzmann equation respects only a restricted universality. In general, e.g. for the initial conditions IC1 and IC3, for any given momentum mode the particle number densities will not approach the same late-time value. For both momentum modes shown in Fig. 3.9 a considerable discrepancy is revealed. However, for the special case of the initial conditions IC1 and IC2, which, as mentioned above, correspond to the same initial average particle number density, the late-time results do agree[6].

[5]As we will see, the steep over-shooting of the particle number distribution leads to a quick kinetic equilibration, whereas the rather long tail accounts for chemical equilibration.

[6]In Fig. 3.10 one can see that in the case of the Boltzmann equation there is only one momentum mode for which the late-time values of all particle number densities agree, namely the intersection point of the lines. However, we could easily have chosen a fourth initial condition for which the late-time result would intersect the lines in Fig. 3.10 in different points. Then there would not be a single momentum mode for which the late-time values of all particle

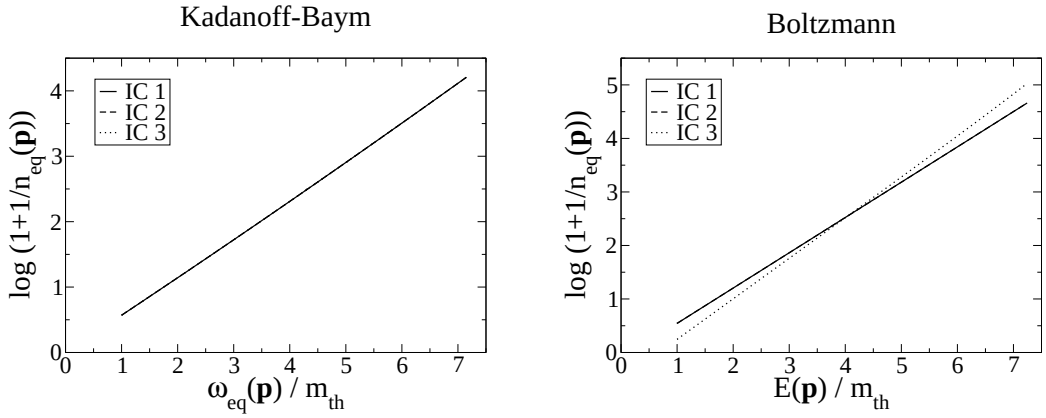

Figure 3.10: Here, we plotted the particle number distributions obtained for times when thermal equilibrium has effectively been reached, against the corresponding thermal energy densities. The thermal mass is given by the zero mode of the effective kinetic equilibrium energy density as determined by the Kadanoff-Baym equations: $m_{th} = \omega_{eq}(\boldsymbol{p} = 0)$. The temperature is given by the inverse slope of the line and the chemical potential is obtained from the y-axis intercept divided by $-\beta$. Supplementing Fig. 3.9 we observe full (restricted) universality in the case of the Kadanoff-Baym (Boltzmann) equations. In particular, the Kadanoff-Baym equations lead to a universal temperature $T = 1.68\ m_{th}$ and a universally vanishing chemical potential. In contrast to this, the Boltzmann equation gives $T = 1.52\ m_{th}$ and $\mu = 0.18\ m_{th}$ for the initial conditions IC1 and IC2, and $T = 1.32 m_{th}$ and $\mu = 0.68\ m_{th}$ for IC3.

The reason for the observed restriction of universality can be extracted from Fig. 3.11. There we show the time evolution of the total particle number per volume

$$N_{tot}(t) = \int \frac{d^3p}{(2\pi)^3}\, n(t, \boldsymbol{p}) \ .$$

In general the Kadanoff-Baym equations conserve the average energy density and global charges [36–38]. However, as there is no conserved charge in our theory, the total particle number need not be conserved. Indeed, the Kadanoff-Baym equations include off-shell particle creation and annihilation [23]. Consequently, the total particle number may change, and in fact approaches a universal equilibrium value. In contrast to this, due to the quasi-particle (or on-shell) approximation particle number changing processes are kinematically forbidden in the Boltzmann

number densities agreed.

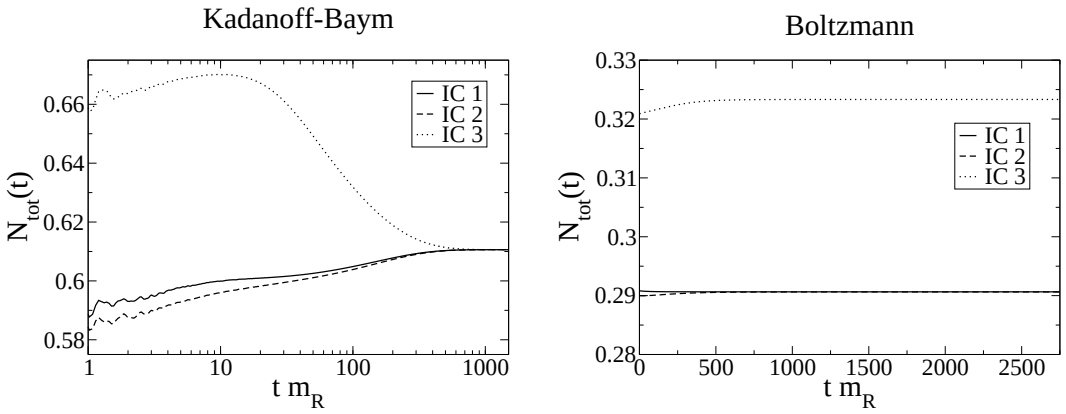

Figure 3.11: Time evolution of the total particle number. As expected from Fig. 3.6, the Kadanoff-Baym equations include off-shell particle creation and annihilation. As a result the total particle number may change with time. In contrast to this, up to numerical errors $< 0.8\%$, the total particle number is strictly conserved in the case of the Boltzmann equation. The quantitative disagreement of the total particle numbers in both plots can be attributed to the substantial discrepancies in the discretization schemes underlying our Boltzmann and Kadanoff-Baym numerics and are of no relevance for the purposes of the present work.

equation. The Boltzmann equation only includes two-particle scattering, which leaves the total particle number constant. Of course, this additional constant of motion severely restricts the evolution of the particle number density. Therefore the Boltzmann equation cannot lead to a universal quantum thermal equilibrium. Only initial conditions for which the average energy density and the total particle number agree from the very beginning, lead to the same equilibrium results.

Chemical Equilibration

The artificial conservation of the total particle number does not only lead to a severe restriction of universality, but in addition prohibits thermodynamical equilibration in the strict sense. Here, it is again important to recall that we consider in this chapter real (neutral) scalar quantum fields with a quartic self-interaction. In such a system, which allows for creation and annihilation of particles, the total particle number is not restricted by any conserved quantity. Consequently, the chemical potential must vanish in thermodynamical equilibrium. The chemical potential predicted by the Boltzmann and Kadanoff-Baym equations, respec-

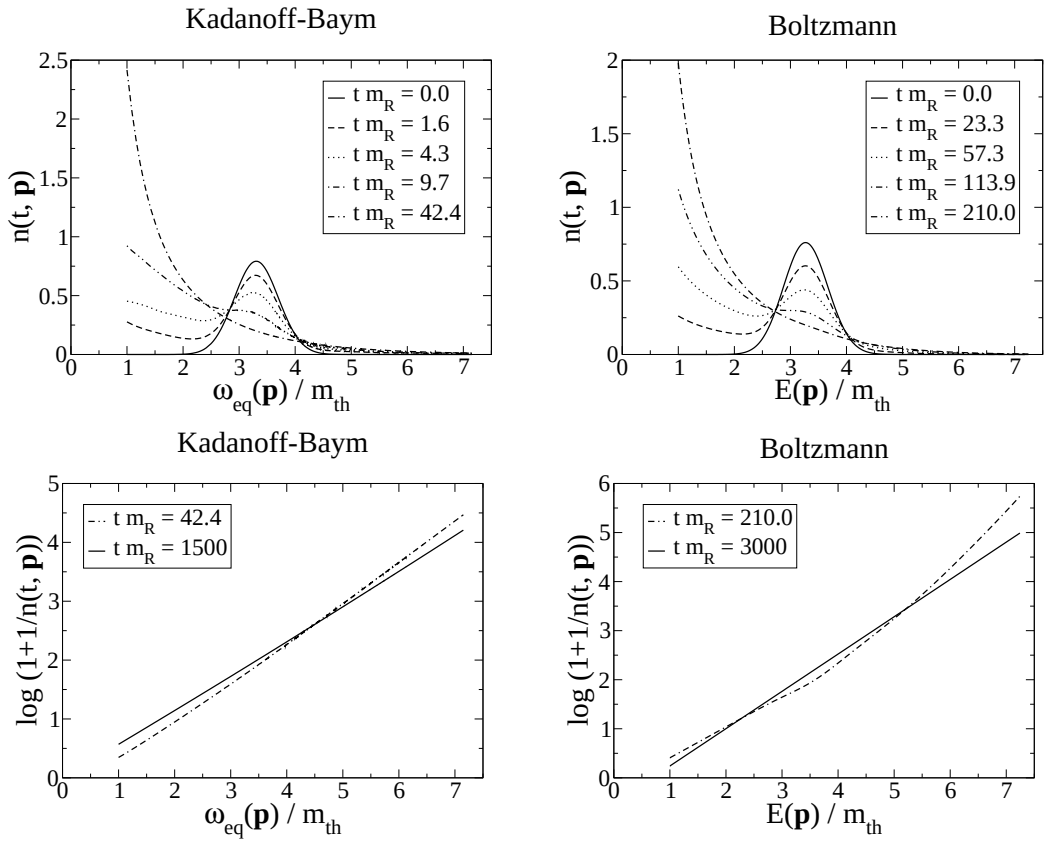

Figure 3.12: (Missing) separation of time scales. The particle number distribution is shown against the equilibrium energy density at various times for initial condition IC3.

tively, is given by the y-axis intercept, extracted from Fig. 3.10, divided by $-\beta$. Using a ruler the reader might convince himself that (up to numerical errors) the Kadanoff-Baym equations indeed lead to a universally vanishing chemical potential. In contrast to this, even without a ruler one can see that the Boltzmann equation, in general, will lead to a non-vanishing chemical potential. For the initial conditions considered in this work, the Boltzmann equation predicted even a positive chemical potential. However, already on very general grounds, one can deduce that the chemical potential of bosons has to be negative [90]!

Separation of Time Scales

In the upper left plot of Fig. 3.12 one can see that the Kadanoff-Baym equations rapidly wash out our tsunami-type initial condition IC3. In both plots

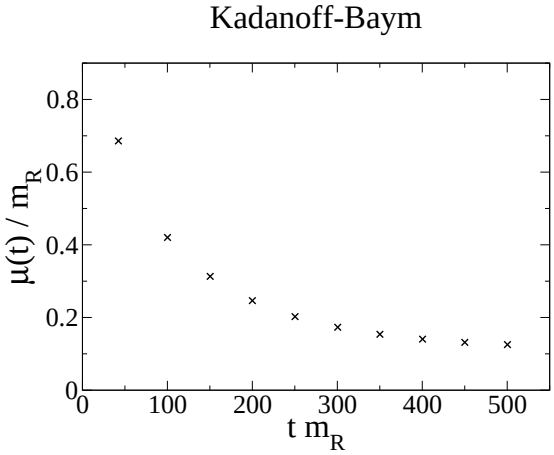

Figure 3.13: This plot shows the relaxation of the chemical potential obtained by fitting the particle number distribution to the Bose-Einstein distribution function for various times. We see that chemical equilibration is a long-term process.

on the left hand side the double-dashed-dotted lines correspond to the particle number distribution at the same time $tm_R = 42.4$. The fact that we obtain an approximate straight line in the lower left plot already after a relatively short period of time indicates a swift approach to kinetic equilibrium. Subsequently, this straight line is tilted until it intersects the origin of our coordinate system (full line), corresponding to a vanishing chemical potential. The relaxation of the chemical potential is displayed in Fig. 3.13. Starting at the time $tm_R = 42.4$, for several times t we fitted the particle number distribution to the Bose-Einstein distribution function

$$n_{BE}(\omega) = \frac{1}{\exp\left(\frac{\omega-\mu}{T}\right) - 1}$$

and extracted the chemical potential μ from these fits. Fig. 3.13 then shows the time evolution of the chemical potential. We observe that full thermodynamical (including chemical) equilibration takes a very long time [11]. In this way, Fig. 3.13 and the left plots in Fig. 3.12 reveal two distinct time scales: a fast kinetic equilibration, and a very slow chemical equilibration. These two time scales can also be identified in the left plot of Fig. 3.9 and in Fig. 3.5. The over-shooting of the particle number density (equal-time propagator) for early times leads to the kinetic equilibration. In fact, the double-dashed-dotted lines correspond to the time, when the particle number distribution (equal-time propagator) reaches its maximum value in Fig. 3.9 (Fig. 3.5). Interestingly, although the initial conditions IC1 and IC2 do not show this excessive over-shooting, the corresponding

particle number distributions (equal-time propagators) approach each other on the same time scale, from which on they show an almost identical evolution. The following rather long tail, again indicates that full thermalization takes place on much larger time scales.

The right plot in Fig. 3.9 shows that the steep initial evolution, which is characteristic for the Kadanoff-Baym equations, is absent in the case of the Boltzmann equation and that the Boltzmann equation leads only to a gently inclined evolution for the particle number distribution. One might be tempted to conclude that the evolution of the particle number distribution is strictly monotonous in the Boltzmann case [30]. However, the small dip for the particle number distribution IC2 in Fig. 3.9 shows that this is not necessarily the case. In summary, the plots on the right hand side of Fig. 3.12 show that it takes a considerably longer time for the Boltzmann equation to reach kinetic equilibrium. As already mentioned above, in contrast to the Kadanoff-Baym equations, the Boltzmann equation cannot describe the process of chemical equilibration. Consequently, the separation of time scales furnished by the Kadanoff-Baym equations is absent in the Boltzmann case.

Summary

In this chapter we reviewed the derivation of Kadanoff-Baym equations from the 2PI effective action in the framework of a real scalar Φ^4 quantum field theory. We also reviewed how Boltzmann equations arise as approximations to Kadanoff-Baym equations.

We have verified that Kadanoff-Baym equations respect full universality, including the process of chemical equilibration, and strongly separate the time scales between kinetic and chemical equilibration.

In contrast to this, the corresponding Boltzmann equation respects only a restricted universality, fails to describe the process of chemical equilibration and does not separate any time scales.

In the next chapter we will generalize these results to a chirally Yukawa-type quantum field theory including fermions.

Chapter 4

Thermalization of Fermions

In this chapter we generalize our considerations of the previous chapter to the case of a chirally invariant Yukawa-type quantum field theory including scalars and fermions. This chapter is structured similar to the previous one. In the first section we derive the Kadanoff-Baym equations from the 2PI effective action. When fermions are involved, it is crucial to exploit all available symmetries in order to reduce the complexity of the Kadanoff-Baym equations, such that a numerical solution becomes feasible. The simplification of the Kadanoff-Baym equations due to symmetries is detailed in section 2. The third and fourth sections are devoted to the quantum kinetic and Boltzmann equations, respectively. In the last section we present numerical solutions of the Boltzmann and Kadanoff-Baym equations. Once more, we find that Kadanoff-Baym equations respect full universality, include chemical equilibration and strongly separate the time scales between kinetic and chemical equilibration. Again, in contrast to this, the corresponding Boltzmann equations respect only a restricted universality, fail to describe the process of chemical equilibration and do not separate any time-scales.

4.1 Quantum Dynamics

2PI Effective Action

We consider a globally $SU(2)_L \times SU(2)_R \times U(1)_{B-L}$ symmetric quantum field theory with one generation of Dirac leptons and a Higgs bi-doublet. The Dirac fields are denoted with $\Psi_l^\alpha(x)$, where α is a Dirac index and $l \in \{\nu, e\}$ denotes the flavor of the leptons. According to Ref. [91] the most general $SU(2)_L \times SU(2)_R \times U(1)_{B-L}$ symmetric Yukawa coupling of a Higgs bi-doublet Φ with left- and right-handed fermion doublets Ψ_L and Ψ_R reads

$$\left(f_{jk}\bar{\Psi}_L^j \Phi \Psi_R^k + g_{jk}\bar{\Psi}_L^j \sigma_2 \Phi^* \sigma_2 \Psi_R^k\right) + h.c. \,.$$

j and k are generation indices. In the case of just one generation f and g can be chosen to be real. For simplification,we go even further, and take

$$f = g = \eta \, .$$

In this case the above Yukawa coupling takes the form

$$\eta \bar{\Psi}_L \left(\Phi + \sigma_2 \Phi^* \sigma_2 \right) \Psi_R + h.c. \, . \tag{4.1.1}$$

Using the Pauli matrices σ_1, σ_2, σ_3 and the matrix $\sigma_0 = i\mathbb{1}$, we can parametrize the Higgs bi-doublet in terms of four real scalar fields Φ_a:

$$\Phi + \sigma_2 \Phi^* \sigma_2 = i \sigma_a \Phi_a \, .$$

Exploiting that

$$\left(i \bar{\Psi}_L \sigma_a \Phi_a \Psi_R \right)^\dagger = -i \bar{\Psi}_R \sigma_a^\dagger \Phi_a \Psi_L$$

and using the left-handed and right-handed chiral projection operators

$$P_L = \frac{1}{2} \left(\mathbb{1} + \gamma_5 \right) \qquad \text{and} \qquad P_R = \frac{1}{2} \left(\mathbb{1} - \gamma_5 \right) \, ,$$

the Yukawa coupling (4.1.1) can be cast in the form

$$\begin{aligned} \eta \bar{\Psi}_L \left(\Phi + \sigma_2 \Phi^* \sigma_2 \right) \Psi_R + h.c. &= i \eta \bar{\Psi} \Phi_a \left(\sigma_a P_R - \sigma_a^\dagger P_L \right) \Psi \\ &= -\eta \bar{\Psi} \left(\Phi_0 + i \Phi_j \sigma_j \gamma_5 \right) \Psi \, . \end{aligned} \tag{4.1.2}$$

After all, in this chapter we consider a system whose dynamics is determined by the Lagrangian density[1]

$$\begin{aligned} \mathscr{L} &= -\bar{\Psi} \, \partial\!\!\!/ \Psi - \frac{1}{2} \Big(\partial_\mu \Phi_a \Big) \Big(\partial^\mu \Phi_a \Big) - \frac{1}{2} m^2 \Phi_a \Phi_a \\ &\quad - \lambda \left(\Phi_a \Phi_a \right)^2 - i \eta \bar{\Psi} \Phi_a \left(\sigma_a P_R - \sigma_a^\dagger P_L \right) \Psi \, . \end{aligned}$$

Although we refer to the scalar (fermion) fields as Higgs (lepton) fields, we would like to note that according to Eq. (4.1.2) this theory is equivalent to the linear σ-model [92–94], which can be used to describe low-energy quark-meson dynamics in two-flavor QCD. This and a closely related model have been considered in a similar context in Refs. [11,35]. As we will compute the evolution of the two-point Green's functions for nonequilibrium initial conditions, already the classical action has to be defined on the closed Schwinger-Keldysh real-time contour, shown

[1] Unless otherwise indicated, we adopt the following convention for the various indices: Dirac (Lorentz) indices will be denoted by letters from the beginning (middle) of the Greek alphabet. Letters from the beginning (middle) of the Latin alphabet will denote Higgs fields (lepton flavor).

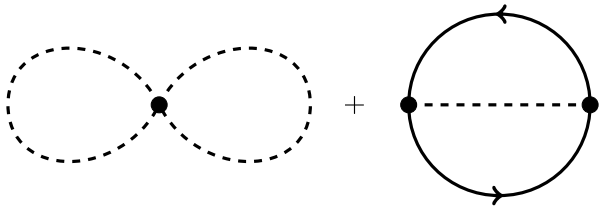

Figure 4.1: Two-loop contribution to $\Gamma_2[G,S]$. Full (dashed) lines represent the complete connected lepton (Higgs) propagator S (G).

in Fig. 2.2. The inverse free propagators can then be read off the free part of the classical action:

$$I_0 = \int\limits_{\mathcal{C}} d^4x\, d^4y \left[\bar{\Psi}_l(x)\, S^{-1}_{0,lm}(x,y)\, \Psi_m(y) - \frac{1}{2}\Phi_a(x)\, G^{-1}_{0,ab}(x,y)\, \Phi_b(y) \right],$$

where the inverse free propagators are given by

$$G^{-1}_{0,ab}(x,y) = \left(\partial_{x^\mu}\partial_{y_\mu} + m_B^2\right) \delta_{\mathcal{C}}(x-y)\, \delta_{ab} \tag{4.1.3}$$

and

$$S^{-1}_{0,lm}(x,y) = -\not{\partial}_x \delta_{\mathcal{C}}(x-y)\, \delta_{lm}\,. \tag{4.1.4}$$

As in the previous chapter, we consider a system without symmetry breaking, i.e. $\langle \Phi_a(x) \rangle = 0$. In this case the complete connected Schwinger-Keldysh propagators are given by

$$G_{ab}(x,y) = \langle T_{\mathcal{C}} \{ \Phi_a(x)\, \Phi_b(y) \} \rangle \tag{4.1.5}$$

and

$$S^{\alpha\beta}_{lm}(x,y) = \left\langle T_{\mathcal{C}} \left\{ \Psi^\alpha_l(x)\, \bar{\Psi}^\beta_m(y) \right\} \right\rangle\,. \tag{4.1.6}$$

According to Eq. (2.3.13), for Gaussian initial conditions the 2PI effective action for this theory is then given by

$$\begin{aligned} \Gamma[G,S] &= \frac{i}{2}\mathrm{tr}_{\mathcal{C}} \log_{\mathcal{C}}\left[G^{-1}\right] - \frac{1}{2}\mathrm{tr}_{\mathcal{C}}\left[G_0^{-1}G\right] \\ &\quad -i\mathrm{tr}_{\mathcal{C}} \log_{\mathcal{C}}\left[S^{-1}\right] - \mathrm{tr}_{\mathcal{C}}\left[S_0^{-1}S\right] + \Gamma_2[G,S] + const\,. \end{aligned}$$

$i\Gamma_2[G,S]$ is the sum of all two-particle irreducible vacuum diagrams with classical vertices and internal lines representing the complete connected propagators S and G. In this work we apply the loop expansion of the 2PI effective action up to two-loop order. The diagrams contributing to Γ_2 in this approximation are shown in Fig. 4.1. Using the abbreviation

$$H^{\alpha\beta}_{a,lm} = i\eta \left[(\sigma_a)_{lm} P_R^{\alpha\beta} - \left(\sigma_a^\dagger\right)_{lm} P_L^{\alpha\beta} \right]$$

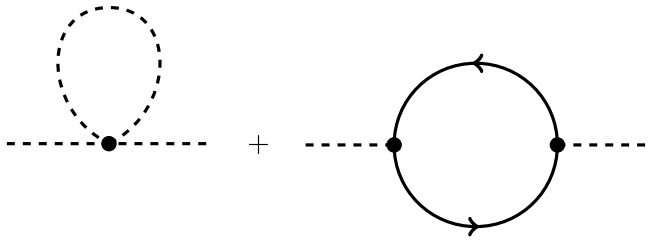

Figure 4.2: One-loop contribution to the Higgs self-energy.

we find

$$\begin{aligned}\Gamma_2[G,S] &= -\lambda\int_{\mathcal{C}} d^4x\Big[G_{aa}(x,x)\,G_{bb}(x,x)+2G_{ab}(x,x)\,G_{ab}(x,x)\Big]\\ &\quad -\frac{i}{2}\int_{\mathcal{C}} d^4x\,d^4y\,G_{ab}(x,y)\,\mathrm{tr}\Big(H_aS(x,y)\,H_bS(y,x)\Big)\,,\end{aligned}$$

where the trace runs over Dirac and lepton flavor indices.

Kadanoff-Baym Equations

The equations of motion for the complete propagators

$$\frac{\delta\Gamma[G,S]}{\delta G_{ba}(y,x)}=0 \qquad \text{and} \qquad \frac{\delta\Gamma[G,S]}{\delta S^{\beta\alpha}_{ml}(y,x)}=0$$

are equivalent to the corresponding self-consistent Schwinger-Dyson equations

$$G^{-1}_{ab}(x,y)=iG^{-1}_{0,ab}(x,y)-\Pi_{ab}(x,y) \tag{4.1.7}$$

and

$$S^{-1}_{lm}(x,y)=-iS^{-1}_{0,lm}(x,y)-\Sigma_{lm}(x,y)\ , \tag{4.1.8}$$

where the proper self-energies are given by

$$\begin{aligned}\Pi_{ab}(x,y) &= 2i\frac{\delta\Gamma_2[G,S]}{\delta G_{ba}(y,x)}\\ &= -4\lambda i\delta_{\mathcal{C}}(x-y)\Big(G_{dd}(x,x)\,\delta_{ab}+2G_{ab}(x,x)\Big)\\ &\quad +\mathrm{tr}\Big(H_aS(x,y)\,H_bS(y,x)\Big)\end{aligned} \tag{4.1.9}$$

and

$$\Sigma^{\alpha\beta}_{lm}(x,y)=-i\frac{\delta\Gamma_2[G,S]}{\delta S^{\beta\alpha}_{ml}(y,x)}=-H^{\alpha\gamma}_{a,lk}H^{\delta\beta}_{b,nm}S^{\gamma\delta}_{kn}(x,y)\,G_{ab}(x,y)\ . \tag{4.1.10}$$

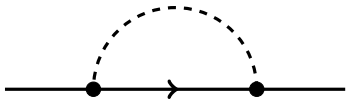

Figure 4.3: One-loop contribution to the lepton self-energy.

As one can see from Eq. (4.1.9) (and Fig. 4.2), the Higgs self-energy contains a local and a non-local part:

$$\Pi_{ab}(x,y) = -i\delta_{\mathcal{C}}(x-y)\,\Pi_{ab}^{(local)}(x) + \Pi_{ab}^{(non-local)}(x,y) \ . \tag{4.1.11}$$

Analogous to the previous chapter, we absorb the local part of the scalar self-energy into an effective mass:

$$\begin{aligned} M_{ab}^2(x) &= m_B^2\delta_{ab} + \Pi_{ab}^{(local)}(x) \\ &= m_B^2\delta_{ab} + 4\lambda\Big(G_{dd}(x,x)\,\delta_{ab} + 2G_{ab}(x,x)\Big) \ . \end{aligned} \tag{4.1.12}$$

Next, we define the spectral function[2]

$$G_{\varrho,ab}(x,y) = i\left\langle\left[\Phi_a(x),\Phi_b(y)\right]_-\right\rangle$$

and statistical propagator[3]

$$G_{F,ab}(x,y) = \frac{1}{2}\left\langle\left[\Phi_a(x),\Phi_b(y)\right]_+\right\rangle$$

for the Higgs bosons, such that we can write the Higgs propagator as

$$G_{ab}(x,y) = G_{F,ab}(x,y) - \frac{i}{2}\mathrm{sign}_{\mathcal{C}}\left(x^0-y^0\right)G_{\varrho,ab}(x,y) \ . \tag{4.1.13}$$

In very much the same way, we also define the spectral function[4]

$$S_{\varrho,lm}^{\alpha\beta}(x,y) = i\left\langle\left[\Psi_l^{\alpha}(x),\Psi_m^{\beta\,*}(y)\right]_+\right\rangle$$

[2]From the definition of the Higgs spectral-function we see that it is anti-symmetric in the sense that $G_{\varrho,ba}(y,x) = -G_{\varrho,ab}(x,y)$. Furthermore, the canonical equal-time commutation relations give $\left(G_{\varrho,ab}(x,y)\right)_{x^0=y^0} = 0$ and $\left(\partial_{y^0}G_{\varrho,ab}(x,y)\right)_{x^0=y^0} = -\delta_{ab}\delta^3(\boldsymbol{x}-\boldsymbol{y})$.

[3]In contrast to the spectral function, the statistical Higgs-propagator is symmetric in the sense that $G_{F,ba}(y,x) = G_{F,ab}(x,y)$.

[4]The adjoint of the lepton spectral-function is given by $S_{\varrho,lm}^{\dagger}(x,y) = -\beta S_{\varrho,ml}(y,x)\,\beta$. Furthermore, the canonical anti-commutation relations give $\left(S_{\varrho,lm}(x,y)\right)_{x^0=y^0} = i\beta\delta(\boldsymbol{x}-\boldsymbol{y})\,\delta_{lm}$.

and the statistical propagator[5]

$$S^{\alpha\beta}_{F,lm}(x,y) = \frac{1}{2}\left\langle \left[\Psi^{\alpha}_{l}(x), \Psi^{\beta\,*}_{m}(y)\right]_{-}\right\rangle$$

for the leptons, such that we can decompose the complete lepton propagator according to

$$S_{lm}(x,y) = S_{F,lm}(x,y) - \frac{i}{2}\mathrm{sign}_{\mathcal{C}}\left(x^0 - y^0\right) S_{\varrho,lm}(x,y) \ . \tag{4.1.14}$$

Whereas the spectral function and the statistical propagator for real scalars are real-valued quantities [22], in general they may be complex-valued in the case of fermions [35]. Using Eqs. (4.1.13) and (4.1.14), we can decompose the non-local part of the Higgs self-energy as well as the lepton self-energy into statistical and spectral parts:

$$\Pi^{(non-local)}_{ab}(x,y) = \Pi_{F,ab}(x,y) - \frac{i}{2}\mathrm{sign}_{\mathcal{C}}\left(x^0 - y^0\right)\Pi_{\varrho,ab}(x,y) \tag{4.1.15}$$

and

$$\Sigma_{lm}(x,y) = \Sigma_{F,lm}(x,y) - \frac{i}{2}\mathrm{sign}_{\mathcal{C}}\left(x^0 - y^0\right)\Sigma_{\varrho,lm}(x,y) \ . \tag{4.1.16}$$

After convolving Eqs. (4.1.7) and (4.1.8) from the right with the corresponding complete propagators and inserting the decompositions (4.1.13), (4.1.14), (4.1.15) and (4.1.16) we arrive at the Kadanoff-Baym equations [35]:

$$\begin{aligned}&\left(-\partial_{x^\mu}\partial_{x_\mu}\delta_{ac} + M^2_{ac}(x)\right) G_{F,cb}(x,y) \\ &= \int_0^{y^0} d^4z\, \Pi_{F,ac}(x,z)\, G_{\varrho,cb}(z,y) - \int_0^{x^0} d^4z\, \Pi_{\varrho,ac}(x,z)\, G_{F,cb}(z,y) \ ,\end{aligned} \tag{4.1.17}$$

$$\left(-\partial_{x^\mu}\partial_{x_\mu}\delta_{ac} + M^2_{ac}(x)\right) G_{\varrho,cb}(x,y) = -\int_{y^0}^{x^0} d^4z\, \Pi_{\varrho,ac}(x,z)\, G_{\varrho,cb}(z,y) \ , \tag{4.1.18}$$

$$-\not{\partial}_x S_{F,lm}(x,y) = \int_0^{x^0} d^4z\, \Sigma_{\varrho,lk}(x,z)\, S_{F,km}(z,y) - \int_0^{y^0} d^4z\, \Sigma_{F,lk}(x,z)\, S_{\varrho,km}(z,y) \tag{4.1.19}$$

and

$$-\not{\partial}_x S_{\varrho,lm}(x,y) = \int_{y^0}^{x^0} d^4z\, \Sigma_{\varrho,lk}(x,z)\, S_{\varrho,km}(z,y) \ . \tag{4.1.20}$$

[5]The adjoint of the statistical lepton-propagator is given by $S^{\dagger}_{F,lm}(x,y) = \beta S_{F,ml}(y,x)\,\beta$.

Of course, it is (at least, in 2006 it was ;-) practically impossible to solve the Kadanoff-Baym equations (4.1.17) – (4.1.20) numerically in this general form. Therefore, in the next section we will show how one can exploit symmetries to reduce the complexity of the Kadanoff-Baym equations, such that their numerical solution becomes feasible [35].

4.2 Symmetries

Let the initial density matrix $\mathcal{D}$ be invariant under a symmetry U. Then we have

$$\mathcal{D} = U^{-1}\mathcal{D}U \ .$$

Accordingly, the expectation value of some operator Ω satisfies

$$\langle\Omega\rangle = \mathrm{tr}\left(\mathcal{D}\Omega\right) = \mathrm{tr}\left(\mathcal{D}U\Omega U^{-1}\right) = \left\langle U\Omega U^{-1}\right\rangle \ . \tag{4.2.1}$$

If U is a continuous symmetry, generated by some set of generators G^a, an infinitesimal transformation can be written in the form

$$U = 1 + i\varepsilon_a G^a \ .$$

In this case Eq. (4.2.1) is equivalent to

$$0 = \langle[G^a, \Omega]\rangle \ . \tag{4.2.2}$$

In the following subsections we will exploit spatial homogeneity, isotropy, parity, chiral symmetry and CP invariance in order to find helpful relations which have to be satisfied by the Higgs and lepton propagators. We will use these relations in order to simplify the Kadanoff-Baym equations in such a way that they can be solved numerically.

Spatial Homogeneity

Spatial translations are generated by the spatial components of the four-momentum operator

$$[P_j, \Phi_a(x)] = i\partial_{x^j}\Phi_a(x) \ .$$

According to Eq. (4.2.2) for a spatially homogeneous system we have

$$0 = \langle[P_j, T_\mathcal{C}\{\Phi_a(x)\,\Phi_b(y)\}]\rangle \ .$$

Consequently, the Higgs propagator does not depend on the spatial center coordinates,

$$G_{ab}(x,y) = G_{ab}\left(x^0, y^0, \boldsymbol{x}-\boldsymbol{y}\right) \ ,$$

and we can perform a Fourier transformation with respect to the spatial relative coordinates:

$$G_{ab}(x,y) = \int d^3k \ \exp\left(i\boldsymbol{k}\left(\boldsymbol{x}-\boldsymbol{y}\right)\right) G_{ab}\left(x^0,y^0,\boldsymbol{k}\right) \ . \tag{4.2.3}$$

The same relations also holds for the fermion propagator:

$$S_{lm}(x,y) = \int d^3k \ \exp\left(i\boldsymbol{k}\left(\boldsymbol{x}-\boldsymbol{y}\right)\right) S_{lm}\left(x^0,y^0,\boldsymbol{k}\right) \ . \tag{4.2.4}$$

Isotropy and Parity

In this context, it will be convenient to employ the Lorentz decomposition of the lepton propagator. Using the standard basis $\{\mathbb{1}, \gamma_5, \gamma_\mu, \gamma_5\gamma_\mu, \mathscr{J}_{\mu\nu}\}$[6] we can expand the lepton propagator according to

$$S = S_S\mathbb{1} - iS_P\gamma_5 - iS_V^\mu\gamma_\mu - iS_A^\mu\gamma_5\gamma_\mu + \frac{1}{2}S_T^{\mu\nu}\,\mathscr{J}_{\mu\nu} \ . \tag{4.2.5}$$

The indices indicate that under a Lorentz transformation S_S, S_P, S_V, S_A and S_T would transform as scalar, pseudo-scalar, vector, axial-vector and tensor, respectively. For the scalar component of the lepton propagator invariance under a spatial rotation R and parity imply

$$S_S\left(x^0,y^0,\boldsymbol{k}\right) = S_S\left(x^0,y^0,R\boldsymbol{k}\right) \tag{4.2.6}$$

and

$$S_S\left(x^0,y^0,\boldsymbol{k}\right) = S_S\left(x^0,y^0,-\boldsymbol{k}\right) \ , \tag{4.2.7}$$

respectively. Both requirements (4.2.6) and (4.2.7) can be satisfied if

$$S_S\left(x^0,y^0,\boldsymbol{k}\right) = S_S\left(x^0,y^0,|\boldsymbol{k}|\right) \ . \tag{4.2.8}$$

The same also holds for the Higgs propagator and the time-like vector component of the lepton propagator:

$$G\left(x^0,y^0,\boldsymbol{k}\right) = G\left(x^0,y^0,|\boldsymbol{k}|\right) \ , \tag{4.2.9}$$

$$S_V^0\left(x^0,y^0,\boldsymbol{k}\right) = S_V^0\left(x^0,y^0,|\boldsymbol{k}|\right) \ . \tag{4.2.10}$$

On the other hand, for the pseudo-scalar component isotropy and parity imply

$$S_P\left(x^0,y^0,\boldsymbol{k}\right) = S_P\left(x^0,y^0,|\boldsymbol{k}|\right)$$

and

$$S_P\left(x^0,y^0,\boldsymbol{k}\right) = -S_P\left(x^0,y^0,-\boldsymbol{k}\right) \ .$$

[6] We take $\gamma_5 = -i\gamma^0\gamma^1\gamma^2\gamma^3$ and $\mathscr{J}^{\mu\nu} = -\frac{i}{4}\left[\gamma^\mu,\gamma^\nu\right]_-$.

Consequently, for a system which is invariant under spatial rotations and parity, the pseudo scalar component must vanish. For the spatial vector components isotropy and parity imply

$$\boldsymbol{S}_V\left(x^0, y^0, \boldsymbol{k}\right) = R^{-1}\boldsymbol{S}_V\left(x^0, y^0, R\boldsymbol{k}\right) \tag{4.2.11}$$

and

$$\boldsymbol{S}_V\left(x^0, y^0, \boldsymbol{k}\right) = -\boldsymbol{S}_V\left(x^0, y^0, -\boldsymbol{k}\right) \ . \tag{4.2.12}$$

Both requirements (4.2.11) and (4.2.12) can be satisfied if

$$\boldsymbol{S}_V\left(x^0, y^0, \boldsymbol{k}\right) = \frac{\boldsymbol{k}}{|\boldsymbol{k}|} S_V\left(x^0, y^0, |\boldsymbol{k}|\right) \ . \tag{4.2.13}$$

Similarly as for the pseudo-scalar component, the axial-vector component also must vanish. Since the matrices $\mathscr{J}^{\mu\nu}$ are anti-symmetric with respect to the interchange of the indices μ and ν, we can also take the tensor components $S_T^{\mu\nu}$ to be anti-symmetric. However, a tensor which is invariant under rotations has to be diagonal. Consequently for an isotropic system the spatial tensor components must vanish, too.

Chiral $SU(2)_L \times SU(2)_R$ Symmetry

The $SU(2)_L$ and $SU(2)_R$ symmetries are generated by unitary operators L_j and R_j, respectively, where $j \in \{1, 2, 3\}$. For the scalar fields this means

$$\left[L_j, \Phi_a\left(x\right)\right] = \left(\Sigma_j^L\right)_{ab} \Phi_b\left(x\right)$$

and

$$\left[R_j, \Phi_a\left(x\right)\right] = \left(\Sigma_j^R\right)_{ab} \Phi_b\left(x\right) \ .$$

Here, the matrices Σ_j^L and Σ_j^R are given by[7]

$$\left(\Sigma_j^L\right)_{ab} = -\frac{i}{2}\left(\delta_{a0}\delta_{jb} + \delta_{b0}\delta_{ja} + \varepsilon_{jab}\right)$$

and

$$\left(\Sigma_j^R\right)_{ab} = \frac{i}{2}\left(\delta_{a0}\delta_{jb} + \delta_{b0}\delta_{ja} - \varepsilon_{jab}\right) \ .$$

For $SU(2)_L \times SU(2)_R$ symmetric initial conditions the Higgs propagator must commute with the matrices Σ_j^L and Σ_j^R. Consequently, in flavor space the Higgs propagator is proportional to the unit matrix:

$$G_{ab}\left(x, y\right) = G\left(x, y\right)\delta_{ab} \ . \tag{4.2.14}$$

[7]For $a, b \in \{1, 2, 3\}$, ε_{jab} is the usual totally anti-symmetric Levi-Civita symbol. However, ε_{jab} vanishes if either a or b is zero.

The fermion fields transform under chiral symmetry according to

$$[L_j, \Psi_l^\alpha(x)] = \frac{1}{2}(\sigma_j)_{lm} P_L^{\alpha\beta} \Psi_m^\beta(x) \ ,$$

$$[R_j, \Psi_l^\alpha(x)] = \frac{1}{2}(\sigma_j)_{lm} P_R^{\alpha\beta} \Psi_m^\beta(x) \ .$$

For $SU(2)_L \times SU(2)_R$ invariant initial conditions the lepton propagator must commute with the Pauli matrices, and hence must be proportional to the unit matrix in flavor space:

$$S_{lm}(x,y) = S(x,y)\,\delta_{lm} \ . \tag{4.2.15}$$

Additionally, in Dirac space the lepton propagator must anti-commute with γ_5. Using the Lorentz decomposition (4.2.5), we find that this is the case if and only if

$$S_S(x,y) = S_P(x,y) = S_T^{\mu\nu}(x,y) = 0 \ . \tag{4.2.16}$$

CP Symmetry

For a CP invariant system the fermion propagator must satisfy

$$S(x,y) = \mathscr{C}\beta S^T(\mathscr{P}y, \mathscr{P}x)\,\beta\mathscr{C}^{-1} \ . \tag{4.2.17}$$

The superscript T here denotes matrix transposition in Dirac and flavor space. Eq. (4.2.17) splits into two equations for the statistical propagator and the spectral function, namely

$$S_F(x,y) = \mathscr{C}\beta S_F^T(\mathscr{P}y, \mathscr{P}x)\,\beta\mathscr{C}^{-1}$$

and

$$S_\varrho(x,y) = -\mathscr{C}\beta S_\varrho^T(\mathscr{P}y, \mathscr{P}x)\,\beta\mathscr{C}^{-1} \ .$$

Hence, for a spatially homogeneous and isotropic system the vector components of the statistical lepton-propagator and the lepton spectral-function satisfy

$$\begin{array}{rcrcrl}
S^0_{V,F}(x^0,y^0,k) &=& -S^0_{V,F}(y^0,x^0,k) &=& -S^{0*}_{V,F}(x^0,y^0,k) \ , \\
S_{V,F}(x^0,y^0,k) &=& S_{V,F}(y^0,x^0,k) &=& S^*_{V,F}(x^0,y^0,k) \ , \\
S^0_{V,\varrho}(x^0,y^0,k) &=& S^0_{V,\varrho}(y^0,x^0,k) &=& -S^{0*}_{V,\varrho}(x^0,y^0,k) \ , \\
S_{V,\varrho}(x^0,y^0,k) &=& -S_{V,\varrho}(y^0,x^0,k) &=& S^*_{V,\varrho}(x^0,y^0,k) \ .
\end{array} \tag{4.2.18}$$

As a consequence

$$\mathrm{Re}\left(S^0_{V,F}\right) = \mathrm{Re}\left(S^0_{V,\varrho}\right) = \mathrm{Im}\left(S_{V,F}\right) = \mathrm{Im}\left(S_{V,\varrho}\right) = 0 \ .$$

Simplified Kadanoff-Baym Equations

Due to the previous subsections, for initial conditions which are invariant under spatial translations, spatial rotations, parity, charge conjugation and chiral transformations we can write the Higgs and lepton propagators in the form

$$G_{ab}\left(x,y\right)=\int\frac{d^{3}k}{\left(2\pi\right)^{3}}\,\exp\Big(i\boldsymbol{k}\left(\boldsymbol{x}-\boldsymbol{y}\right)\Big)\,G\left(x^{0},y^{0},k\right)\,\delta_{ab} \tag{4.2.19}$$

and

$$\begin{aligned}S_{lm}\left(x,y\right)=&\int\frac{d^{3}k}{\left(2\pi\right)^{3}}\,\exp\Big(i\boldsymbol{k}\left(\boldsymbol{x}-\boldsymbol{y}\right)\Big)\\&\times\left(S_{V}^{0}\left(x^{0},y^{0},k\right)\gamma_{0}-i\frac{k^{j}}{k}S_{V}\left(x^{0},y^{0},k\right)\gamma_{j}\right)\,\delta_{lm}\,.\end{aligned} \tag{4.2.20}$$

Note that, as compared to the previous subsections, we rearranged the factors of i in order to make all statistical and spectral Lorentz components of the lepton propagator real-valued quantities:

$$\begin{aligned}S_{V,F}^{0}\left(x^{0},y^{0},k\right)&=-S_{V,F}^{0}\left(y^{0},x^{0},k\right)&&=S_{V,F}^{0*}\left(x^{0},y^{0},k\right)\,,\\S_{V,F}\left(x^{0},y^{0},k\right)&=\;\;S_{V,F}\left(y^{0},x^{0},k\right)&&=S_{V,F}^{*}\left(x^{0},y^{0},k\right)\,,\\S_{V,\varrho}^{0}\left(x^{0},y^{0},k\right)&=\;\;S_{V,\varrho}^{0}\left(y^{0},x^{0},k\right)&&=S_{V,\varrho}^{0*}\left(x^{0},y^{0},k\right)\,,\\S_{V,\varrho}\left(x^{0},y^{0},k\right)&=-S_{V,\varrho}\left(y^{0},x^{0},k\right)&&=S_{V,\varrho}^{*}\left(x^{0},y^{0},k\right)\,.\end{aligned} \tag{4.2.21}$$

Of course, the relations (4.2.19), (4.2.20) and (4.2.21) also hold for the corresponding self energies, such that the Kadanoff-Baym equations can drastically be simplified. The simplified Kadanoff-Baym equations for the Higgs propagator read [35]

$$\begin{aligned}&\left[\partial_{x^{0}}^{2}+k^{2}+M^{2}\left(x^{0}\right)\right]G_{F}\left(x^{0},y^{0},k\right)\\&=\int_{0}^{y^{0}}dz^{0}\,\Pi_{F}\left(x^{0},z^{0},k\right)G_{\varrho}\left(z^{0},y^{0},k\right)-\int_{0}^{x^{0}}dz^{0}\,\Pi_{\varrho}\left(x^{0},z^{0},k\right)G_{F}\left(z^{0},y^{0},k\right)\end{aligned} \tag{4.2.22}$$

and

$$\left[\partial_{x^{0}}^{2}+k^{2}+M^{2}\left(x^{0}\right)\right]G_{\varrho}\left(x^{0},y^{0},k\right)=-\int_{y^{0}}^{x^{0}}dz^{0}\,\Pi_{\varrho}\left(x^{0},z^{0},k\right)G_{\varrho}\left(z^{0},y^{0},k\right)\,. \tag{4.2.23}$$

The effective mass in Eqs. (4.2.22) and (4.2.23) is given by

$$M^{2}\left(x^{0}\right)=m_{B}^{2}+24\lambda\int\frac{d^{3}p}{\left(2\pi\right)^{3}}G_{F}\left(x^{0},x^{0},p\right)\,.$$

Using the notation

$$\boldsymbol{S_V}\left(x^0,y^0,\boldsymbol{k}\right)=\frac{\boldsymbol{k}}{k}S_V\left(x^0,y^0,k\right)$$

the statistical and spectral Higgs self-energies can be written in the form

$$\begin{aligned}\Pi_F\left(x^0,y^0,k\right)&=-8\eta^2\int\frac{d^3p}{(2\pi)^3}\int d^3q\,\delta\left(\boldsymbol{k}-\boldsymbol{p}-\boldsymbol{q}\right)\\&\times\Big[-S^0_{V,F}\left(x^0,y^0,q\right)S^0_{V,F}\left(x^0,y^0,p\right)+\frac{1}{4}S^0_{V,\varrho}\left(x^0,y^0,q\right)S^0_{V,\varrho}\left(x^0,y^0,p\right)\\&+\boldsymbol{S_{V,F}}\left(x^0,y^0,\boldsymbol{q}\right)\boldsymbol{S_{V,F}}\left(x^0,y^0,\boldsymbol{p}\right)-\frac{1}{4}\boldsymbol{S_{V,\varrho}}\left(x^0,y^0,\boldsymbol{q}\right)\boldsymbol{S_{V,\varrho}}\left(x^0,y^0,\boldsymbol{p}\right)\Big]\end{aligned}$$

and

$$\begin{aligned}\Pi_\varrho\left(x^0,y^0,k\right)&=-16\eta^2\int\frac{d^3p}{(2\pi)^3}\int d^3q\,\delta\left(\boldsymbol{k}-\boldsymbol{p}-\boldsymbol{q}\right)\\&\times\Big[-S^0_{V,\varrho}\left(x^0,y^0,q\right)S^0_{V,F}\left(x^0,y^0,p\right)+\boldsymbol{S_{V,\varrho}}\left(x^0,y^0,\boldsymbol{q}\right)\boldsymbol{S_{V,F}}\left(x^0,y^0,\boldsymbol{p}\right)\Big].\end{aligned}$$

The 128 complex-valued Kadanoff-Baym equations (4.1.19) and (4.1.20) for the lepton propagator can be reduced to the following 4 real-valued equations [35]:

$$\begin{aligned}&\partial_{x^0}S^0_{V,F}\left(x^0,y^0,k\right)+kS_{V,F}\left(x^0,y^0,k\right)\qquad(4.2.24)\\&=\int_0^{x^0}dz^0\left[\Sigma^0_{V,\varrho}\left(x^0,z^0,k\right)S^0_{V,F}\left(z^0,y^0,k\right)+\Sigma_{V,\varrho}\left(x^0,z^0,k\right)S_{V,F}\left(z^0,y^0,k\right)\right]\\&\quad-\int_0^{y^0}dz^0\left[\Sigma^0_{V,F}\left(x^0,z^0,k\right)S^0_{V,\varrho}\left(z^0,y^0,k\right)+\Sigma_{V,F}\left(x^0,z^0,k\right)S_{V,\varrho}\left(z^0,y^0,k\right)\right],\end{aligned}$$

$$\begin{aligned}&\partial_{x^0}S_{V,F}\left(x^0,y^0,k\right)-kS^0_{V,F}\left(x^0,y^0,k\right)\qquad(4.2.25)\\&=\int_0^{x^0}dz^0\left[\Sigma^0_{V,\varrho}\left(x^0,z^0,k\right)S_{V,F}\left(z^0,y^0,k\right)-\Sigma_{V,\varrho}\left(x^0,z^0,k\right)S^0_{V,F}\left(z^0,y^0,k\right)\right]\\&\quad-\int_0^{y^0}dz^0\left[\Sigma^0_{V,F}\left(x^0,z^0,k\right)S_{V,\varrho}\left(z^0,y^0,k\right)-\Sigma_{V,F}\left(x^0,z^0,k\right)S^0_{V,\varrho}\left(z^0,y^0,k\right)\right],\end{aligned}$$

$$\begin{aligned}&\partial_{x^0}S^0_{V,\varrho}\left(x^0,y^0,k\right)+kS_{V,\varrho}\left(x^0,y^0,k\right)\qquad(4.2.26)\\&=\int_{y^0}^{x^0}dz^0\left[\Sigma^0_{V,\varrho}\left(x^0,z^0,k\right)S^0_{V,\varrho}\left(z^0,y^0,k\right)+\Sigma_{V,\varrho}\left(x^0,z^0,k\right)S_{V,\varrho}\left(z^0,y^0,k\right)\right]\end{aligned}$$

and

$$\partial_{x^0} S_{V,\varrho}\left(x^0,y^0,k\right) - kS^0_{V,\varrho}\left(x^0,y^0,k\right) \tag{4.2.27}$$
$$= \int\limits_{y^0}^{x^0} dz^0 \left[\Sigma^0_{V,\varrho}\left(x^0,z^0,k\right) S_{V,\varrho}\left(z^0,y^0,k\right) - \Sigma_{V,\varrho}\left(x^0,z^0,k\right) S^0_{V,\varrho}\left(z^0,y^0,k\right)\right] .$$

The simplified lepton self-energies are given by

$$\Sigma^0_{V,F}\left(x^0,y^0,k\right) = -4\eta^2 \int \frac{d^3p}{(2\pi)^3} \int d^3q\; \delta\left(\boldsymbol{k}-\boldsymbol{p}-\boldsymbol{q}\right)$$
$$\times \left[G_F\left(x^0,y^0,q\right) S^0_{V,F}\left(x^0,y^0,p\right) - \frac{1}{4} G_\varrho\left(x^0,y^0,q\right) S^0_{V,\varrho}\left(x^0,y^0,p\right)\right] ,$$

$$\Sigma^0_{V,\varrho}\left(x^0,y^0,k\right) = -4\eta^2 \int \frac{d^3p}{(2\pi)^3} \int d^3q\; \delta\left(\boldsymbol{k}-\boldsymbol{p}-\boldsymbol{q}\right)$$
$$\times \left[G_\varrho\left(x^0,y^0,q\right) S^0_{V,F}\left(x^0,y^0,p\right) + G_F\left(x^0,y^0,q\right) S^0_{V,\varrho}\left(x^0,y^0,p\right)\right] ,$$

$$\Sigma_{V,F}\left(x^0,y^0,k\right) = -4\eta^2 \frac{\boldsymbol{k}}{k} \int \frac{d^3p}{(2\pi)^3} \int d^3q\; \delta\left(\boldsymbol{k}-\boldsymbol{p}-\boldsymbol{q}\right)$$
$$\times \left[G_F\left(x^0,y^0,q\right) \boldsymbol{S_{V,F}}\left(x^0,y^0,\boldsymbol{p}\right) - \frac{1}{4} G_\varrho\left(x^0,y^0,q\right) \boldsymbol{S_{V,\varrho}}\left(x^0,y^0,\boldsymbol{p}\right)\right] ,$$

and

$$\Sigma_{V,\varrho}\left(x^0,y^0,k\right) = -4\eta^2 \frac{\boldsymbol{k}}{k} \int \frac{d^3p}{(2\pi)^3} \int d^3q\; \delta\left(\boldsymbol{k}-\boldsymbol{p}-\boldsymbol{q}\right)$$
$$\times \left[G_\varrho\left(x^0,y^0,q\right) \boldsymbol{S_{V,F}}\left(x^0,y^0,\boldsymbol{p}\right) + G_F\left(x^0,y^0,q\right) \boldsymbol{S_{V,\varrho}}\left(x^0,y^0,\boldsymbol{p}\right)\right] .$$

In order to make contact with Boltzmann equations, again we have to introduce effective particle number densities. For the scalars we use the same definition as in the previous chapter:

$$\omega^2\left(t,k\right) = \left(\frac{\partial_{x^0}\partial_{y^0} G_F\left(x^0,y^0,k\right)}{G_F\left(x^0,y^0,k\right)}\right)_{x^0=y^0=t} , \tag{4.2.28}$$

$$n_s\left(t,k\right) = \omega\left(t,k\right) G_F\left(t,t,k\right) - \frac{1}{2} . \tag{4.2.29}$$

We consider systems with vanishing net charge density, where the distribution functions for fermions and anti-fermions agree:

$$n_{\bar{f}}\left(t,k\right) = n_f\left(t,k\right) . \tag{4.2.30}$$

As explained in more detail in Ref. [35], for the fermions we define the effective particle number density by

$$n_f\left(t,k\right) = \frac{1}{2} - S_{V,F}\left(t,t,k\right) . \tag{4.2.31}$$

Conservation of Energy and Global Charges

In order to define the energy-momentum tensor we proceed along the same lines as in the previous chapter. We consider the variation of the 2PI effective action under an infinitesimal space-time translation:

$$\begin{aligned}\Delta\Gamma\left[G,S\right] &= \int\limits_{\mathcal{C}} d^4x\, d^4y\, \left[\frac{\delta\Gamma\left[G,S\right]}{\delta G\left(x,y\right)}\Delta G\left(x,y\right) + \frac{\delta\Gamma\left[G,S\right]}{\delta S^{\alpha\beta}_{lm}\left(x,y\right)}\Delta S^{\alpha\beta}_{lm}\left(x,y\right)\right] \\ &= -\int\limits_{\mathcal{C}} d^4x\, \Theta^{\mu\nu}\left(x\right)\partial_{x^\mu}\epsilon_\nu\left(x\right)\ .\end{aligned}$$

After a rather tedious calculation we find

$$\begin{aligned}\Theta^{\mu\nu}\left(x\right) = \int\limits_{\mathcal{C}} d^4y\, \delta_{\mathcal{C}}\left(x-y\right)\Bigg[&\left(\partial_{x_\mu}\partial_{y_\nu} - \frac{1}{2}\eta^{\mu\nu}\partial_{x^\kappa}\partial_{y^\kappa} - \frac{1}{2}\eta^{\mu\nu}m_B^2\right)G_{aa}\left(x,y\right) \\ &- \eta^{\mu\nu}\partial_{y^\kappa}\mathrm{tr}\Big(\gamma^\kappa S_{mm}\left(x,y\right)\Big) + \partial_{y_\nu}\mathrm{tr}\Big(\gamma^\mu S_{mm}\left(y,x\right)\Big)\Bigg] \\ &- \eta^{\mu\nu}\lambda\Big(G_{aa}\left(x,x\right)G_{bb}\left(x,x\right) + 2G_{ab}\left(x,x\right)G_{ab}\left(x,x\right)\Big) \\ &+ \eta^{\mu\nu}\int\limits_0^{x^0} d^4z\Big[\Pi_{F,ab}\left(x,z\right)G_{\varrho,ba}\left(z,x\right) - \Pi_{\varrho,ab}\left(x,z\right)G_{F,ba}\left(z,x\right)\Big]\ .\end{aligned}$$

The average energy density is then obtained from the time-time component of the energy-momentum tensor. For a system which is invariant under space-time translations, spatial rotations, parity, charge conjugation and chiral transformations the average energy density is given by

$$\begin{aligned}E_{tot}\left(t\right) = \int\frac{d^3p}{\left(2\pi\right)^3}\Bigg[&2\Big(\left(\partial_{x^0}\partial_{y^0} + p^2 + m_B^2\right)G_F\left(x^0,y^0,p\right)\Big)_{x^0=y^0=t} \\ &- 8pS_{V,F}\left(t,t,p\right) + 24\lambda G_F\left(t,t,p\right)\int\frac{d^3q}{\left(2\pi\right)^3}\left[G_F\left(t,t,q\right)\right] \\ &- 4\int\limits_0^t dz^0\Big[\Pi_F\left(t,z^0,p\right)G_\varrho\left(z^0,t,p\right) - \Pi_\varrho\left(t,z^0,p\right)G_F\left(z^0,t,p\right)\Big]\Bigg]\end{aligned}$$

Apart from the conservation of energy, the conservation of global charges also has to be guaranteed if such charges are present in the considered theory. The corresponding conservation law and an expression for the conserved global charge can be derived in very much the same way.

4.3 Quantum Kinetics

Analogous to the purely scalar theory, which we considered the previous chapter, employing a first order gradient expansion and a Wigner transformation, one can derive quantum kinetic equations from the full Kadanoff-Baym equations also in the case of the Yukawa theory considered in this chapter. Of course, the derivation of the kinetic equations for the Higgs propagator follows exactly the lines of Section 3.2. Due to the previous section, we restrict our considerations to systems which are spatially homogeneous and isotropic. Therefore, the Wigner transformed propagators depend only on the center time t, the energy ω and the absolute value of the momentum k. Consequently, in this section the Poisson brackets reduce to

$$\left\{\tilde{f};\ \tilde{g}\right\}_{PB} = -\left[\partial_t \tilde{f}\right]\left[\partial_\omega \tilde{g}\right] + \left[\partial_\omega \tilde{f}\right]\left[\partial_t \tilde{g}\right]$$

and the kinetic equations for the scalar propagator are given by

$$\begin{aligned} &-\left\{\tilde{\Omega}\left(t,\omega,k\right);\ \tilde{G}_F\left(t,\omega,k\right)\right\}_{PB} \\ &= \tilde{\Pi}_\varrho\left(t,\omega,k\right)\tilde{G}_F\left(t,\omega,k\right) - \tilde{\Pi}_F\left(t,\omega,k\right)\tilde{G}_\varrho\left(t,\omega,k\right) \\ &\quad + \left\{\tilde{\Pi}_F\left(t,\omega,k\right);\ \mathrm{Re}\left(\tilde{G}_R\left(t,\omega,k\right)\right)\right\}_{PB}, \end{aligned} \tag{4.3.1}$$

$$-\left\{\tilde{\Omega}\left(t,\omega,k\right);\ \tilde{G}_\varrho\left(t,\omega,k\right)\right\}_{PB} = \left\{\tilde{\Pi}_\varrho\left(t,\omega,k\right);\ \mathrm{Re}\left(\tilde{G}_R\left(t,\omega,k\right)\right)\right\}_{PB} \tag{4.3.2}$$

and

$$\tilde{G}_R\left(t,\omega,k\right) = \frac{1}{-\omega^2 + k^2 + M^2\left(t\right) + \tilde{\Pi}_R\left(t,\omega,k\right)}\,. \tag{4.3.3}$$

In order to derive the kinetic equations for the lepton propagator, we start from the Kadanoff-Baym equation for the time-like vector component of the statistical lepton propagator (4.2.24). Using retarded and advanced propagators and self energies defined analogously to Eqs. (3.2.1) and (3.2.2), we can send the upper limits of the memory integrals to $+\infty$:

$$\begin{aligned} &\partial_{x^0} S^0_{V,F}\left(x^0,y^0,k\right) + kS_{V,F}\left(x^0,y^0,k\right) \\ &= \int dz^0\,\theta\left(z^0\right)\Big[\Sigma^0_{V,R}\left(x^0,z^0,k\right)S^0_{V,F}\left(z^0,y^0,k\right) \\ &\quad + \Sigma_{V,R}\left(x^0,z^0,k\right)S_{V,F}\left(z^0,y^0,k\right) \\ &\quad + \Sigma^0_{V,F}\left(x^0,z^0,k\right)S^0_{V,A}\left(z^0,y^0,k\right) \\ &\quad + \Sigma_{V,F}\left(x^0,z^0,k\right)S_{V,A}\left(z^0,y^0,k\right)\Big]\,. \end{aligned} \tag{4.3.4}$$

The retarded and advanced lepton propagators satisfy

$$S^0_{V,R}\left(y^0,x^0,k\right) = -S^0_{V,A}\left(x^0,y^0,k\right) \tag{4.3.5}$$

and

$$S_{V,R}\left(y^0,x^0,k\right)=S_{V,A}\left(x^0,y^0,k\right)\ . \tag{4.3.6}$$

The same relations also hold for the retarded and advanced self energies. Interchanging x^0 and y^0 in Eq. (4.3.4) and exploiting the (anti-)symmetry properties (4.2.21), as well as relations (4.3.5) and (4.3.6) yields:

$$\begin{aligned}
&-\partial_{y^0}S^0_{V,F}\left(x^0,y^0,k\right)+kS_{V,F}\left(x^0,y^0,k\right) \\
&=\int dz^0\ \theta\left(z^0\right)\Big[S^0_{V,F}\left(x^0,z^0,k\right)\Sigma^0_{V,A}\left(z^0,y^0,k\right) \\
&\quad+S_{V,F}\left(x^0,z^0,k\right)\Sigma_{V,A}\left(z^0,y^0,k\right) \\
&\quad+S^0_{V,R}\left(x^0,z^0,k\right)\Sigma^0_{V,F}\left(z^0,y^0,k\right) \\
&\quad+S_{V,R}\left(x^0,z^0,k\right)\Sigma_{V,F}\left(z^0,y^0,k\right)\Big]\ .
\end{aligned} \tag{4.3.7}$$

Next, we subtract Eq. (4.3.7) from Eq. (4.3.4). Having switched to center and relative times, cf. Eq. (3.2.5), we observe on the left hand side of the difference equation that

$$\partial_{x^0}+\partial_{y^0}=\partial_t$$

is automatically of first order in ∂_t. Furthermore, we Taylor expand the propagators and self energies on the right hand side of the difference equation to first order in ∂_t around the center time t. Exploiting the effective memory loss, we send the initial time to $-\infty$ and Fourier transform the difference equation with respect to the relative time s^0. As already pointed out at the end of the previous section, all propagator and self-energy components appearing in the simplified Kadanoff-Baym equations (4.2.24) – (4.2.27) are real-valued quantities. Above that, $S_{V,F}\left(t,s^0,k\right)$ and $S^0_{V,\varrho}\left(t,s^0,k\right)$ are even functions of the relative time s^0. Accordingly, their Wigner transforms

$$S_{V,F}\left(t,\omega,k\right)=\int ds^0\ \exp\left(i\omega s^0\right)S_{V,F}\left(t,s^0,k\right)$$

and

$$S^0_{V,\varrho}\left(t,\omega,k\right)=\int ds^0\ \exp\left(i\omega s^0\right)S^0_{V,\varrho}\left(t,s^0,k\right)$$

are also real-valued quantities. In contrast to this $S^0_{V,F}\left(t,s^0,k\right)$ and $S_{V,\varrho}\left(t,s^0,k\right)$ are odd functions of the relative time s^0. Therefore, we introduce an extra factor of $-i$ in order to make their Wigner transforms real-valued quantities, again:

$$S^0_{V,F}\left(t,\omega,k\right)=-i\int ds^0\ \exp\left(i\omega s^0\right)S^0_{V,F}\left(t,s^0,k\right)\ ,$$

$$S_{V,\varrho}\left(t,\omega,k\right)=-i\int ds^0\ \exp\left(i\omega s^0\right)S_{V,\varrho}\left(t,s^0,k\right)\ .$$

The Wigner transformed retarded and advanced lepton propagators are given by

$$S^0_{V,R}\left(t,\omega,k\right) = i\int\frac{dE}{2\pi}\,\frac{S^0_{V,\varrho}\left(t,E,k\right)}{\omega-E+i\varepsilon}\;,$$

$$S^0_{V,A}\left(t,\omega,k\right) = i\int\frac{dE}{2\pi}\,\frac{S^0_{V,\varrho}\left(t,E,k\right)}{\omega-E-i\varepsilon}\;,$$

$$S_{V,R}\left(t,\omega,k\right) = -\int\frac{dE}{2\pi}\,\frac{S_{V,\varrho}\left(t,E,k\right)}{\omega-E+i\varepsilon}$$

and

$$S_{V,A}\left(t,\omega,k\right) = -\int\frac{dE}{2\pi}\,\frac{S_{V,\varrho}\left(t,E,k\right)}{\omega-E-i\varepsilon}\;.$$

As $S_{V,\varrho}$ and $S^0_{V,\varrho}$ are real-valued quantities, the Wigner transformed retarded and advanced lepton propagators satisfy

$$S^0_{V,R}\left(t,\omega,k\right) = -S^{0*}_{V,A}\left(t,\omega,k\right)$$

and

$$S_{V,R}\left(t,\omega,k\right) = S^*_{V,A}\left(t,\omega,k\right)\;.$$

Furthermore, analogous to the scalar case we have

$$S^0_{V,R}\left(t,\omega,k\right) - S^0_{V,A}\left(t,\omega,k\right) = S^0_{V,\varrho}\left(t,\omega,k\right)$$

and

$$S_{V,R}\left(t,\omega,k\right) - S_{V,A}\left(t,\omega,k\right) = iS_{V,\varrho}\left(t,\omega,k\right)\;.$$

After all, using the quantity

$$W\left(t,\omega,k\right) = \omega + \mathrm{Im}\left(\Sigma^0_{V,R}\left(t,\omega,k\right)\right)$$

the kinetic equation for the time-like vector component of the statistical lepton propagator can be written in the form

$$\begin{aligned}\left\{W;\;S^0_{V,F}\right\}_{PB} &= \Sigma^0_{V,\varrho}S^0_{V,F} - \Sigma^0_{V,F}S^0_{V,\varrho} + \Sigma_{V,\varrho}S_{V,F} - \Sigma_{V,F}S_{V,\varrho} \\ &- \left\{\Sigma^0_{V,F};\;\mathrm{Im}\left(S^0_{V,R}\right)\right\}_{PB} + \left\{\mathrm{Re}\left(\Sigma_{V,R}\right);\;S_{V,F}\right\}_{PB} + \left\{\Sigma_{V,F};\;\mathrm{Re}\left(S_{V,R}\right)\right\}_{PB}\;.\end{aligned} \tag{4.3.8}$$

In very much the same way, we can derive the kinetic equations for the remaining components of the lepton propagator:

$$\begin{aligned}\left\{W;\;S_{V,F}\right\}_{PB} &= \Sigma^0_{V,\varrho}S_{V,F} + \Sigma^0_{V,F}S_{V,\varrho} + \Sigma_{V,\varrho}S^0_{V,F} + \Sigma_{V,F}S^0_{V,\varrho} \\ &- \left\{\Sigma^0_{V,F};\;\mathrm{Re}\left(S_{V,R}\right)\right\}_{PB} + \left\{\mathrm{Re}\left(\Sigma_{V,R}\right);\;S^0_{V,F}\right\}_{PB} + \left\{\Sigma_{V,F};\;\mathrm{Im}\left(S^0_{V,R}\right)\right\}_{PB}\;,\end{aligned} \tag{4.3.9}$$

$$\begin{aligned}\left\{W;\;S^0_{V,\varrho}\right\}_{PB} &= -\left\{\Sigma^0_{V,\varrho};\;\mathrm{Im}\left(S^0_{V,R}\right)\right\}_{PB} - \left\{\mathrm{Re}\left(\Sigma_{V,R}\right);\;S_{V,\varrho}\right\}_{PB} \\ &- \left\{\Sigma_{V,\varrho};\;\mathrm{Re}\left(S_{V,R}\right)\right\}_{PB}\;,\end{aligned} \tag{4.3.10}$$

$$\{W;\, S_{V,\varrho}\}_{PB} = \left\{\Sigma^0_{V,\varrho};\, \mathrm{Re}\,(S_{V,R})\right\}_{PB} - \left\{\mathrm{Re}\,(\Sigma_{V,R});\, S^0_{V,\varrho}\right\}_{PB} + \left\{\Sigma_{V,\varrho};\, \mathrm{Im}\left(S^0_{V,R}\right)\right\}_{PB} . \tag{4.3.11}$$

Next, we derive the kinetic equation for the time-like vector component of the retarded lepton propagator. First, we note that

$$\theta\left(x^0 - y^0\right) \partial_{x^0} S^0_{V,\varrho}\left(x^0, y^0, k\right) = \partial_{x^0} S^0_{V,R}\left(x^0, y^0, k\right) - \delta\left(x^0 - y^0\right)$$

and

$$-\theta\left(y^0 - x^0\right) \partial_{x^0} S^0_{V,\varrho}\left(x^0, y^0, k\right) = \partial_{x^0} S^0_{V,A}\left(x^0, y^0, k\right) - \delta\left(y^0 - x^0\right) .$$

Multiplying the Kadanoff-Baym equation for the time-like vector component of the lepton spectral function once with $\theta\left(x^0 - y^0\right)$ and once with $-\theta\left(y^0 - x^0\right)$ yields equations for the time-like vector components of the retarded and advanced lepton propagators:

$$\partial_{x^0} S^0_{V,R}\left(x^0, y^0, k\right) - \delta\left(x^0 - y^0\right) + k S_{V,R}\left(x^0, y^0, k\right) = \int dz^0 \left[\Sigma^0_{V,R}\left(x^0, z^0, k\right) S^0_{V,R}\left(z^0, y^0, k\right) + \Sigma_{V,R}\left(x^0, z^0, k\right) S_{V,R}\left(z^0, y^0, k\right)\right] \tag{4.3.12}$$

and

$$\partial_{x^0} S^0_{V,A}\left(x^0, y^0, k\right) - \delta\left(y^0 - x^0\right) + k S_{V,A}\left(x^0, y^0, k\right) = \int dz^0 \left[\Sigma^0_{V,A}\left(x^0, z^0, k\right) S^0_{V,A}\left(z^0, y^0, k\right) + \Sigma_{V,A}\left(x^0, z^0, k\right) S_{V,A}\left(z^0, y^0, k\right)\right] . \tag{4.3.13}$$

Now we add Eq. (4.3.13), with x^0 and y^0 interchanged, to Eq. (4.3.12). Having switched to center and relative times, we observe on the left hand side that

$$\partial_{x^0} - \partial_{y^0} = 2\partial_{s^0} .$$

A first-order gradient expansion and a Fourier transformation with respect to the relative time s^0 then yields an algebraic equation for the time-like vector component of the retarded lepton propagator:

$$S^0_{V,R}\left(t, \omega, k\right) = i\, \frac{1 - \left(k + \Sigma_{V,R}\right) S_{V,R}}{W - i\mathrm{Re}\left(\Sigma^0_{V,R}\right)} . \tag{4.3.14}$$

In very much the same way we obtain the corresponding equation for the space-like vector component of the retarded lepton propagator:

$$S_{V,R}\left(t, \omega, k\right) = i\, \frac{\left(k - \Sigma_{V,R}\right) S^0_{V,R}}{W - i\mathrm{Re}\left(\Sigma^0_{V,R}\right)} . \tag{4.3.15}$$

The various self energies that have to be inserted in the kinetic equations for scalar and fermionic propagator components can easily be obtained by Wigner transforming the expressions given in the previous section with respect to their time arguments.

4.4 Boltzmann Kinetics

Boltzmann Equation for Scalars

As in the previous chapter, the derivation of the Boltzmann equation for the scalars starts from the kinetic equation for the statistical Higgs propagator (4.3.1). We discard the Poisson brackets on the right hand side and replace $\Omega(t,\omega,k)$ by

$$\Omega(\omega,k) = -\omega^2 + k^2 + m^2 \ ,$$

where m is the thermal mass of the scalars. Next, we generalize the fluctuation-dissipation theorem (2.1.17) to the Kadanoff-Baym ansatz

$$G_F(t,\omega,k) = G_\varrho(t,\omega,k)\left(\frac{1}{2} + n_s(t,\omega,k)\right) \tag{4.4.1}$$

and employ the quasi-particle (or on-shell) approximation:

$$G_\varrho(t,\omega,k) = G_\varrho(\omega,k) = \frac{\pi}{E(k)}\Big(\delta(\omega - E(k)) - \delta(\omega + E(k))\Big) \ , \tag{4.4.2}$$

where the quasi-particle energy is given by

$$E(k) = \sqrt{m^2 + k^2} \ .$$

On the mass shell we define

$$n_s(t,k) = \tilde{n}_s(t, E(k), k) \ .$$

Equating the positive energy components in the kinetic equation for the statistical Higgs propagator and integrating over ω yields

$$\partial_t n_s(t,k) = \frac{1}{E(k)}\left(\Pi_\varrho(t,E(k),k)\left(\frac{1}{2} + n_s(t,k)\right) - \Pi_F(t,E(k),k)\right) \ . \tag{4.4.3}$$

In order to evaluate the Higgs self-energies, we also have to employ the Kadanoff-Baym ansatz

$$S_F(t,\omega,k) = S_\varrho(t,\omega,k)\left(\frac{1}{2} - \tilde{n}_f(t,\omega,k)\right) \tag{4.4.4}$$

and the quasi-particle approximation

$$S^0_{V,\varrho}(t,\omega,k) = \pi(\delta(\omega - k) + \delta(\omega + k)) \ , \tag{4.4.5}$$

$$S_{V,\varrho}(t,\omega,k) = \pi(\delta(\omega - k) - \delta(\omega + k)) \tag{4.4.6}$$

for the fermions. Inserting the Kadanoff-Baym ansatz (4.4.4) and the quasi-particle approximation (4.4.5) and (4.4.6) into the Wigner transformed statistical Higgs self-energy, we find

$$\begin{aligned}\Pi_F\left(t,\omega,k\right) = -8\pi^2 \int \frac{d^4p}{\left(2\pi\right)^4} \int d^4q\; \delta\left(\boldsymbol{k}-\boldsymbol{p}-\boldsymbol{q}\right)\; \delta\left(\omega - p^0 - q^0\right) \\ \times \left(\frac{1}{4} - \left(\frac{1}{2} - n_f\left(t,q^0,q\right)\right)\left(\frac{1}{2} - n_f\left(t,p^0,p\right)\right)\right) \\ \times \Big[\left(\delta\left(q^0-q\right)+\delta\left(q^0+q\right)\right)\left(\delta\left(p^0-p\right)+\delta\left(p^0+p\right)\right) \\ - \frac{\boldsymbol{qp}}{qp}\left(\delta\left(q^0-q\right)-\delta\left(q^0+q\right)\right)\left(\delta\left(p^0-p\right)-\delta\left(p^0+p\right)\right)\Big] \,. \quad (4.4.7)\end{aligned}$$

Note that we have to evaluate the Higgs self-energies in Eq. (4.4.3) only for $\omega = E\left(k\right)$. Taking $\omega = E\left(k\right)$ in Eq. (4.4.7), resolving the parentheses with the δ functions and integrating over p^0 and q^0 leads to terms proportional to either $\delta\left(E\left(k\right)-p-q\right)$, $\delta\left(E\left(k\right)-p+q\right)$, $\delta\left(E\left(k\right)+p-q\right)$ or $\delta\left(E\left(k\right)+p+q\right)$. We immediately see that

$$E\left(k\right)+p+q>0\,,$$

and thus we can discard the term including the corresponding δ function from Eq. (4.4.7). Due to momentum conservation we have

$$\boldsymbol{q} = \boldsymbol{k}-\boldsymbol{p}\,.$$

The triangle inequality then gives

$$0 \leq k+p-q < E\left(k\right)+p-q$$

and after shifting $\boldsymbol{p} \to \boldsymbol{k}-\boldsymbol{p}$

$$0 \leq k+q-p < E\left(k\right)+q-p\,.$$

Consequently, only the term including $\delta\left(E\left(k\right)-p-q\right)$ in Eq. (4.4.7) gives a non-vanishing contribution. The quasi-particle number density for the fermions is defined by

$$n_f\left(t,k\right) = \tilde{n}_f\left(t,k,k\right)\;.$$

After all, at $\omega = E\left(k\right)$ the statistical Higgs self-energy reads:

$$\begin{aligned}\Pi_F\left(t,E\left(k\right),k\right) &= -4\pi\eta^2 \int \frac{d^3p}{\left(2\pi\right)^3} \int d^3q\; \delta^3\left(\boldsymbol{k}-\boldsymbol{p}-\boldsymbol{q}\right)\; \delta\left(E\left(k\right)-p-q\right) \\ &\quad \times \left(1-\frac{\boldsymbol{pq}}{pq}\right)\left(\frac{1}{4} - \left(\frac{1}{2} - n_f\left(t,q\right)\right)\left(\frac{1}{2} - n_f\left(t,p\right)\right)\right)\,.\end{aligned}$$

Along the same lines we also have to treat the spectral part of the Higgs self-energy. Eventually we find the Boltzmann equation for the scalars in the form[8]

$$\begin{aligned}\partial_t n_s(t,k) &= \frac{2\pi\eta^2}{E(k)}\int\frac{d^3p}{(2\pi)^3}\int d^3q\,\delta^3(\boldsymbol{k}-\boldsymbol{p}-\boldsymbol{q})\;\delta(E(k)-p-q)\\ &\quad\times\left(1-\frac{\boldsymbol{pq}}{pq}\right)\Big[\Big(n_s^k+1\Big)n_f^p n_f^q-n_s^k\Big(n_f^p-1\Big)\Big(n_f^q-1\Big)\Big]\,. \qquad (4.4.8)\end{aligned}$$

Simplifying the Collision Integral for Scalars

For $k=0$ the evaluation of the Boltzmann collision integral in Eq. (4.4.8) is literally trivial:

$$\begin{aligned}\partial_t n_s(t,k=0) &= -\frac{m\eta^2}{4\pi}\times\Big[\Big(n_s(t,k=0)+1\Big)n_f(t,p)\,n_f(t,q)\\ &\qquad -n_s(t,k=0)\Big(n_f(t,p)-1\Big)\Big(n_f(t,q)-1\Big)\Big]_{p=q=\frac{m}{2}}\,.\end{aligned}$$

For $k>0$ a little more work has to be done. We rewrite Eq. (4.4.8) using the Fourier representation of the momentum conservation δ function

$$\delta^3(\boldsymbol{k}-\boldsymbol{p}-\boldsymbol{q})=\int\frac{d^3\xi}{(2\pi)^3}\;\exp(-i\boldsymbol{k}\boldsymbol{\xi}+i\boldsymbol{p}\boldsymbol{\xi}+i\boldsymbol{q}\boldsymbol{\xi})$$

and spherical coordinates. The scalar product of two vectors is then given by

$$\boldsymbol{pq}=pq\Big(\sin\vartheta_p\;\sin\vartheta_q\;\cos(\varphi_p-\varphi_q)+\cos\vartheta_p\;\cos\vartheta_q\Big)\,.$$

We perform the integrals over the solid angles in the order Ω_q, Ω_p, Ω_ξ. Using the notation

$$j(x)=\frac{\sin(x)}{x}-\cos(x)$$

we find

$$\int d\Omega_q\;\exp(i\boldsymbol{q}\boldsymbol{\xi})\left(\frac{\boldsymbol{pq}}{pq}-1\right)=\frac{4\pi}{q\xi}\Big(i\cos(\vartheta_p)\,j(q\xi)-\sin(q\xi)\Big)\,,$$

$$\begin{aligned}&\int d\Omega_p\;\exp(i\boldsymbol{p}\boldsymbol{\xi})\Big(i\cos(\vartheta_p)\,j(q\xi)-\sin(q\xi)\Big)\\ &\qquad=-\frac{4\pi}{p\xi}\Big(j(p\xi)\,j(q\xi)+\sin(p\xi)\sin(q\xi)\Big)\,,\end{aligned}$$

[8] We use the notation $n_s^k=n_s(t,k)$ and $n_f^k=n_f(t,k)$.

$$\int d\Omega_\xi \exp\left(-i\boldsymbol{k}\boldsymbol{\xi}\right) = \frac{4\pi}{k\xi}\sin\left(k\xi\right) \ .$$

After defining the auxiliary function

$$\begin{aligned} J_s\left(k,p,q\right) &= pq\int\limits_0^\infty d\xi\ \frac{\sin\left(k\xi\right)}{k\xi}\Big(j\left(p\xi\right)j\left(q\xi\right)+\sin\left(p\xi\right)\sin\left(q\xi\right)\Big) \\ &= \frac{\pi}{16k}\Big(k^2-\left(p+q\right)^2\Big)\Big(\mathrm{sign}\left(k-p-q\right)-\mathrm{sign}\left(k+p-q\right) \\ &\quad -\mathrm{sign}\left(k-p+q\right)+\mathrm{sign}\left(k+p+q\right)\Big) \end{aligned}$$

and integrating over q, we eventually arrive at a form of the Boltzmann equation (4.4.8) which is suitable for an efficient numerical solution:

$$\begin{aligned} \partial_t n_s\left(t,k\right) &= \frac{2\eta^2}{\pi^2 E\left(k\right)}\int\limits_0^\infty dp\ \theta\left(q_0\right)J_s\left(k,p,q_0\right) \\ &\quad\times\left[\Big(n_s^k+1\Big)n_f^p n_f^{q_0}-n_s^k\Big(n_f^p-1\Big)\Big(n_f^{q_0}-1\Big)\right], \end{aligned} \tag{4.4.9}$$

where

$$q_0 = E\left(k\right)-p\ .$$

Boltzmann Equation for Fermions

In order to derive the Boltzmann equation for the fermions, we discard the Poisson brackets on the right hand side of the kinetic equation for the time-like vector component of the statistical lepton-propagator (4.3.8), and on the left hand side we replace $W\left(t,\omega,k\right)$ by ω. Next, we employ the Kadanoff-Baym ansatz (4.4.4) and the quasi-particle approximation (4.4.5) and (4.4.6), equate the positive energy components and integrate over ω:

$$\begin{aligned} \partial_t n_f\left(t,k\right) &= -\left(\Sigma^0_{V,\varrho}\left(t,k,k\right)+\Sigma_{V,\varrho}\left(t,k,k\right)\right)\left(\frac{1}{2}-n_f\left(t,k\right)\right) \\ &\quad +\Sigma_{V,F}\left(t,k,k\right)+\Sigma^0_{V,F}\left(t,k,k\right)\ . \end{aligned} \tag{4.4.10}$$

The time-like vector component of the spectral lepton self-energy reads

$$\begin{aligned} \Sigma^0_{V,\varrho}\left(t,\omega,k\right) &= -4\pi^2\eta^2\int\frac{d^4p}{\left(2\pi\right)^4}\int d^4q\ \delta^3\left(\boldsymbol{k}-\boldsymbol{p}-\boldsymbol{q}\right)\ \delta\left(\omega-p^0-q^0\right) \\ &\quad\times\frac{1}{E\left(q\right)}\left(\delta\left(q^0-E\left(q\right)\right)-\delta\left(q^0+E\left(q\right)\right)\right)\left(\delta\left(p^0-p\right)+\delta\left(p^0+p\right)\right) \\ &\quad\times\left(1+\tilde{n}_s\left(t,p^0,p\right)-\tilde{n}_s\left(t,q^0,q\right)\right)\ . \end{aligned} \tag{4.4.11}$$

We note that in Eq. (4.4.10) we have to evaluate the self-energies only for $\omega = k$. Taking $\omega = k$ in Eq. (4.4.11), resolving the parentheses with the δ functions and integrating over p^0 and q^0 yields terms proportional to either $\delta(k - p - E(q))$, $\delta(k - p + E(q))$, $\delta(k + p - E(q))$ or $\delta(k + p + E(q))$. Obviously

$$k + p + E(q) > 0$$

and thus we can immediately discard the term including the corresponding δ function from Eq. (4.4.11). Furthermore, the triangle inequality leads to

$$0 > k - p - E(q)$$

and

$$0 < k - p + E(q) \ .$$

Therefore, only the term including $\delta(k + p - E(q))$ remains in the self energy (4.4.11). Since

$$\tilde{n}_f(t, -\omega, k) = 1 - \tilde{n}_f(t, \omega, k) \ ,$$

at $\omega = k$ the self energy (4.4.11) reads

$$\begin{aligned} \Sigma^0_{V,\varrho}(t, k, k) &= -2\pi\eta^2 \int \frac{d^3p}{(2\pi)^3} \int d^3q \delta^3(\boldsymbol{k} - \boldsymbol{p} - \boldsymbol{q}) \, \delta(k + p - E(q)) \\ &\quad \times \frac{1}{E(q)} \left(n_s(t, q) + n_f(t, p)\right) \ . \end{aligned}$$

Proceeding along the same lines with the remaining self energies in Eq. (4.4.10), we find the Boltzmann equation for the fermions in the form:

$$\begin{aligned} \partial_t n_f(t, k) &= 2\pi\eta^2 \int \frac{d^3p}{(2\pi)^3} \int d^3q \ \delta^3(\boldsymbol{k} + \boldsymbol{p} - \boldsymbol{q}) \ \delta(k + p - E(q)) \\ &\quad \times \frac{1}{E(q)} \left(1 - \frac{\boldsymbol{kp}}{kp}\right) \left[\left(n^k_f - 1\right)\left(n^p_f - 1\right) n^q_s - n^k_f n^p_f \left(n^q_s + 1\right)\right] . \end{aligned} \quad (4.4.12)$$

As in the previous chapter, again it is pleasant to observe that the Kadanoff-Baym ansätze (4.4.1) and (4.4.4) entail the Nordheim-Uehling-Uhlenbeck quantum corrections [80–84] for the Boltzmann equations (4.4.8) and (4.4.12).

Simplifying the Collision Integral for Fermions

In order to simplify the collision integral for the fermions, we have to integrate Eq. (4.4.12) over Ω_k. On the left hand side this gives a factor of 4π. On the right hand side we evaluate the integrals over the solid angles in the order Ω_q, Ω_p, Ω_k, Ω_ξ:

$$\int d\Omega_q \ \exp(i\boldsymbol{q}\boldsymbol{\xi}) = \frac{4\pi}{q\xi} \sin(q\xi) \ ,$$

$$\int d\Omega_p \, \exp\left(-i\boldsymbol{p}\boldsymbol{\xi}\right)\left(\frac{\boldsymbol{k}\boldsymbol{p}}{kp}+1\right) = \frac{4\pi}{p\xi}\Big(\sin\left(p\xi\right) - i\cos\left(\vartheta_k\right) j\left(p\xi\right)\Big) \,,$$

$$\begin{aligned}\int d\Omega_k \, \exp\left(-i\boldsymbol{k}\boldsymbol{\xi}\right)&\left(\sin\left(p\xi\right) - i\cos\left(\vartheta_k\right) j\left(p\xi\right)\right)\\ &= \frac{4\pi}{k\xi}\Big(\sin\left(k\xi\right)\sin\left(p\xi\right) - j\left(k\xi\right) j\left(p\xi\right)\Big) \,,\end{aligned}$$

$$\int d\Omega_\xi = 4\pi \,.$$

After defining the auxiliary function

$$\begin{aligned} J_f\left(k,p,q\right) &= p\int\limits_0^\infty d\xi \, \frac{\sin\left(q\xi\right)}{k\xi}\Big(\sin\left(k\xi\right)\sin\left(p\xi\right) - j\left(k\xi\right) j\left(p\xi\right)\Big)\\ &= \frac{\pi}{16k^2}\Big(q^2-\left(k+p\right)^2\Big)\Big(\mathrm{sign}\left(k-p-q\right) - \mathrm{sign}\left(k+p-q\right)\\ &\quad - \mathrm{sign}\left(k-p+q\right) + \mathrm{sign}\left(k+p+q\right)\Big)\end{aligned}$$

and integrating over p, we eventually arrive at a form of the Boltzmann equation (4.4.12) which is suitable for an efficient numerical solution:

$$\begin{aligned}\partial_t n_f\left(t,k\right) &= \frac{2\eta^2}{\pi^2}\int\limits_0^\infty dq \, \theta\left(p_0\right) \, \frac{q}{E\left(q\right)} J_f\left(k,p_0,q\right)\\ &\quad \times\Big[\Big(n_f^k-1\Big)\Big(n_f^{p_0}-1\Big)n_s^q - n_f^k n_f^{p_0}\Big(n_s^q+1\Big)\Big] \,, \quad (4.4.13)\end{aligned}$$

where

$$p_0 = E\left(q\right) - k \,.$$

Conservation of Energy and Global Charges

Analogous to the previous chapter the conservation of the average energy density

$$E_{tot}\left(t\right) = \int \frac{d^3p}{\left(2\pi\right)^3}\Big[E\left(p\right) n_s\left(t,p\right) + 2p \, n_f\left(t,p\right)\Big] \,.$$

is guaranteed by the explicit energy-conserving δ functions in the Boltzmann equations (4.4.8) and (4.4.12). As Fig. 4.4 shows, for the initial conditions discussed in the next section our numerical algorithm indeed conserves the average energy density up to numerical errors $< 0.6\%$. As we consider systems with vanishing net charge density, due to Eq. (4.2.30) also the global charge is manifestly conserved.

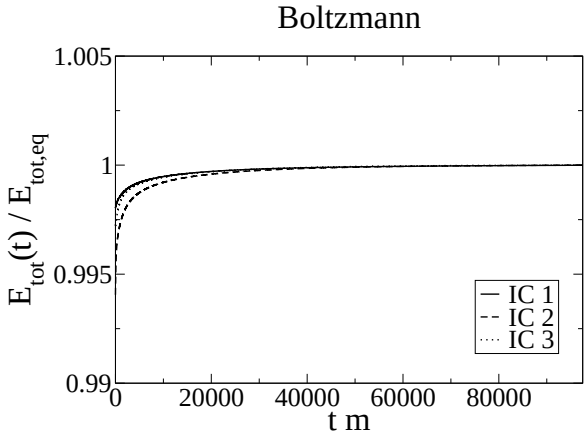

Figure 4.4: Time evolution of the average energy density for various initial conditions, cf. Fig. 4.6. Our numerical solutions of the Boltzmann equations conserve the average energy density up to numerical errors $< 0.6\%$.

4.5 Comparison of Numerical Solutions

Kadanoff-Baym Equations

In general, solving Kadanoff-Baym equations numerically is a difficult problem. Already the purely scalar case considered in the previous chapter demanded a thorough development of the algorithm and sophisticated optimizations. As compared to this, the numerical solution of the Kadanoff-Baym equations in the framework of the linear σ-model is significantly more difficult. The details of the algorithm for the scalar case and its extension to the fermionic case are discussed in the Appendix. So far we completed the implementation of the fermionic algorithm to a high degree. Unfortunately, however, there was not enough time for testing and trouble shooting, wherefore we cannot present our own numerical solutions in this subsection.

Nevertheless, the Kadanoff-Baym equations (4.2.22) through (4.2.27) have been solved numerically by the group of Jürgen Berges in Refs. [11, 35]. In Ref. [35] it was shown that the Kadanoff-Baym equations respect universality in the framework of the linear σ-model in the same way as they did in the case of the real scalar Φ^4 quantum field theory considered in the previous chapter. Provided we consider systems with equal average energy density, the late-time behavior coincides independent of the details of the initial conditions. This can be seen in Fig. 4.5 where we present numerical solutions of the Kadanoff-Baym

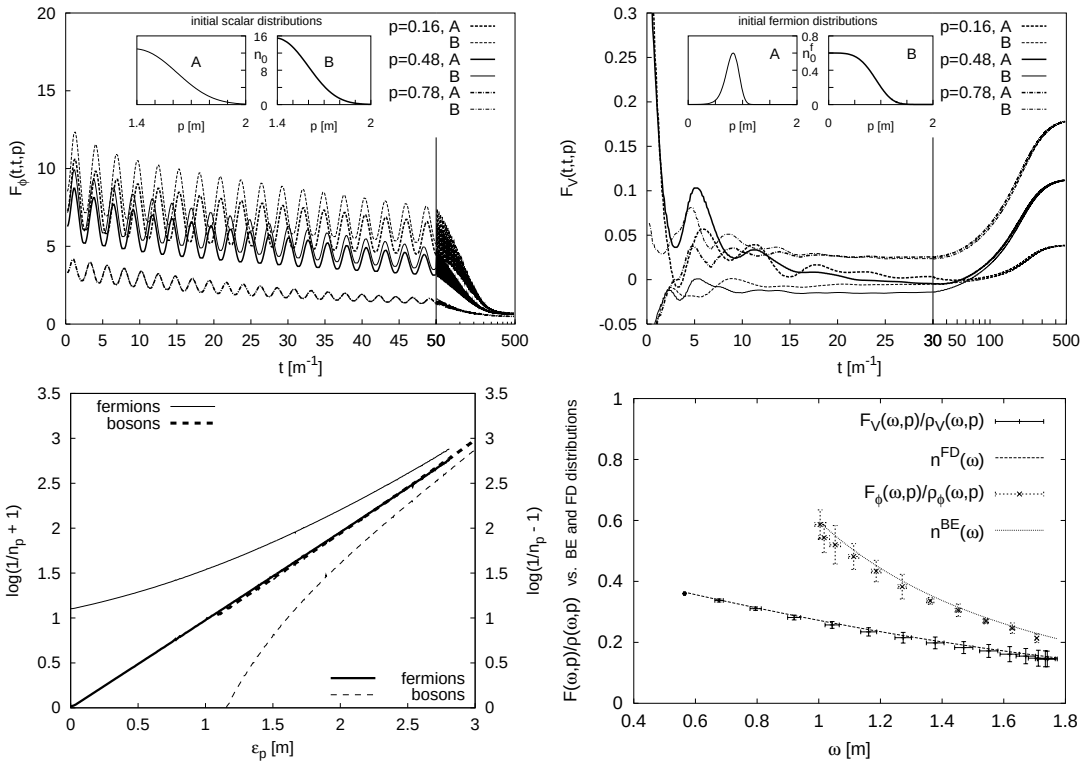

Figure 4.5: The upper plots show the time evolution of the statistical lepton and Higgs propagators for three different momentum modes and two different initial particle number distributions, which are displayed in the insets. Both initial conditions possess the same average energy density. The lower plots show the equilibrium particle number distributions. All plots have been taken from Ref. [35].

equations obtained in Ref. [35]. The upper plots show the time evolution of the statistical Higgs propagator and the space-like vector component of the statistical lepton propagator for three different momentum modes and two different initial particle number distributions. The initial particle number distributions, which are shown in the insets, possess the same average energy density. Similar to the purely scalar case, we observe that the initial conditions lead to a significantly different early-time evolution for the various momentum modes. Respecting universality, however, for each momentum mode the various propagator components approach the same late-time value. Of course, the universality observed for the various propagator components also holds for the corresponding particle number densities. The lower left plot shows that the effective particle number densities take the form of Bose-Einstein and Fermi-Dirac distribution functions after equi-

librium has effectively been reached. Due to universality one finds a universal temperature and, as we consider systems with vanishing net charge density, a universally vanishing chemical potential for scalars and fermions. The lower right plot documents that the Bose-Einstein and Fermi-Dirac distribution functions extracted from the fluctuation dissipation theorems (2.1.17) and (2.1.19) agree with the effective equilibrium particle number distributions of the lower left plot.

Additionally, in Ref. [11] it was shown that the description of nonequilibrium dynamics using Kadanoff-Baym equations comprises the phenomenon of prethermalization. This means that certain quantities, such as e.g. the ratio of pressure over energy density, approach their equilibrium values on time scales, which are dramatically shorter than the thermodynamical equilibration time. In particular, it was shown that Kadanoff-Baym equations strongly separate the time scales between kinetic and chemical equilibration. Whereas kinetic equilibration takes place on very short time scales, full thermodynamical, including chemical, equilibration is a long-term process.

In summary, concerning universality, chemical equilibration and the separation of time scales the Kadanoff-Baym equations for the linear σ-model considered in this chapter have exactly the same properties as for the real scalar Φ^4 quantum field theory considered in the previous chapter.

Boltzmann Equations

In this subsection we discuss our numerical solutions of the Boltzmann equations (4.4.9) and (4.4.13) and compare their properties with the properties of the corresponding Kadanoff-Baym equations discussed in the previous subsection. We consider three different initial conditions IC1, IC2 and IC3 which correspond to the same average energy density. Above that for the initial conditions IC1 and IC2 the sums of the initial average particle number densities agree. The corresponding initial particle number distributions are shown in Fig. 4.6.

Fig. 4.7 shows that the Boltzmann equations respect only a restricted universality. The left plot shows the time evolution of the particle number densities for a fixed momentum mode. For early times the plot emphasizes the fact that the time evolution need not be monotonous in the case of Boltzmann equations. For late times we observe that the distributions IC1 and IC2 approach the same equilibrium value for scalars and fermions, respectively. The late-time behavior of the distribution IC3 deviates significantly from the former two distributions. This can also be verified in the right plot, which exhibits the equilibrium particle number distributions. Indeed the equilibrium distributions IC1 and IC2 agree for scalars and fermions, respectively, whereas the equilibrium distributions IC3 deviate significantly from the former two. Above that, we see that the equilibrium distributions take the form of Bose-Einstein and Fermi-Dirac distribution functions. The corresponding temperatures can be read off the right plot as the inverse slope of the lines and the chemical potentials are given by the negative

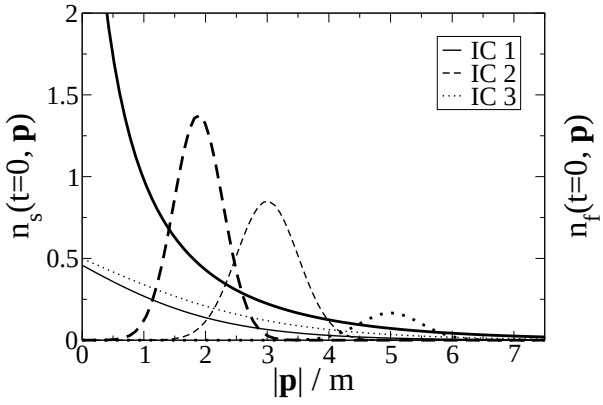

Figure 4.6: This plot shows the various initial particle number distributions, for which we solved the Boltzmann equations numerically. Thick (thin) lines correspond to scalar (fermion) particle number distributions. All initial conditions possess the same (conserved) average energy density. Above that, for the initial conditions IC1 and IC2 also the sums of the average particle numbers $N_{s,tot}(t) + N_{f,tot}(t)$ agree.

y-axis intercepts divided by the corresponding slope:

	T_s/m	T_f/m	μ_s/m	μ_f/m	μ_s/μ_f
$IC1$	1.315	1.315	0.839	0.420	1.999
$IC2$	1.315	1.315	0.839	0.420	1.999
$IC3$	1.689	1.689	−0.906	−0.453	2.001

(4.5.1)

In particular, for any given initial condition the temperatures predicted for scalars and fermions agree up to numerical errors $< 0.1\%$. Furthermore it is important to recall that the Boltzmann equations (4.4.9) and (4.4.13) include only decay and recombination processes of the form

$$1 \text{ scalar} \longleftrightarrow 2 \text{ fermions} .$$

For such a system, in equilibrium the chemical potentials are expected to satisfy the relation

$$\mu_s = 2\mu_f .$$

As one can see in the right-most column of the table in Eq. (4.5.1), this relation is indeed fulfilled up to numerical errors $< 0.1\%$. Accordingly, the Boltzmann equations lead to a classical chemical equilibrium. In contrast to this, quantum

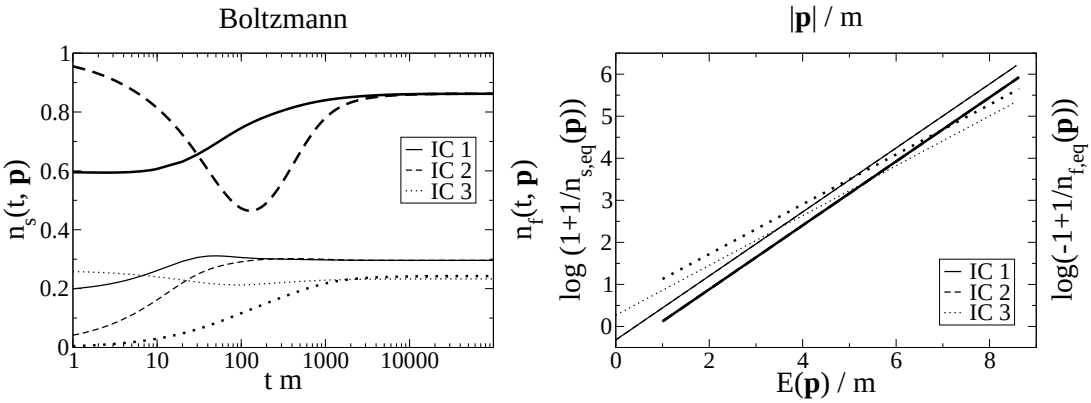

Figure 4.7: These plots show that the Boltzmann equations maintain only a restricted universality. The left plot shows the time evolution of the particle number densities $n_s(t, \boldsymbol{p})$ (thick lines) and $n_f(t, \boldsymbol{p})$ (thin lines) for a fixed momentum mode, and the right plot shows the corresponding particle number distributions after equilibrium has been reached. We observe coincident late-time behaviors for the initial conditions IC1 and IC2. The equilibrium result for the initial condition IC3 deviates from the former two.

chemical equilibrium requires that the chemical potentials vanish for systems with vanishing net charge density. In this sense, the non-vanishing chemical potentials in Eq. (4.5.1) indicate that quantum chemical equilibration is out of reach of the Boltzmann equations (4.4.9) and (4.4.13).

The reason for the observed restriction of universality and the absence of chemical equilibration can be extracted from Fig. 4.8. Due to the Yukawa coupling of the lepton doublets with the Higgs bi-doublet one of four scalars can decay into one of two fermion pairs or one of two fermion pairs may recombine to one of four scalars. Thus the linear σ-model comprises processes which can change the average scalar and fermion particle number densities

$$N_{s,tot}\,(t) = \int \frac{d^3p}{(2\pi)^3}\; n_s\,(t, \boldsymbol{p})$$

and

$$N_{f,tot}\,(t) = \int \frac{d^3p}{(2\pi)^3}\; n_f\,(t, \boldsymbol{p}) \;\; .$$

The time evolution of the average particle number densities is shown in the left plot of Fig. 4.8. As expected we find that the average particle number densities may change significantly. On the other hand, however, the sum of the average

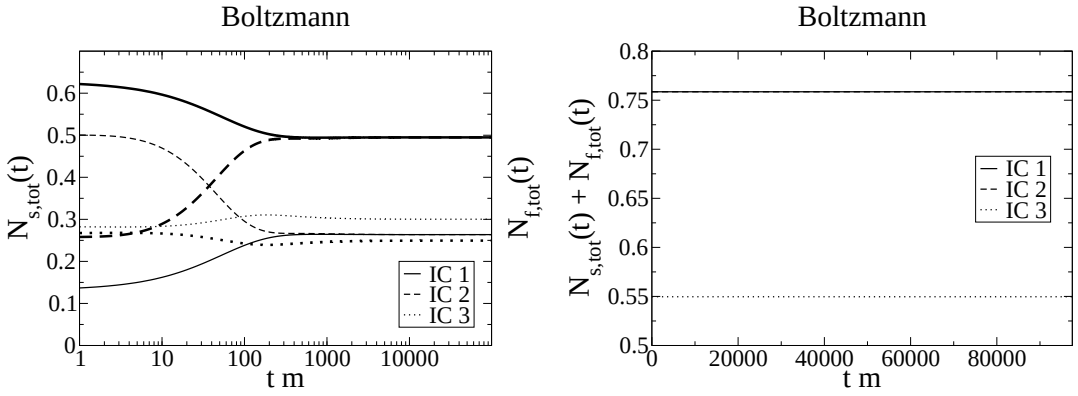

Figure 4.8: The left plot shows the time evolution of the average particle number densities $N_{s,tot}(t)$ (thick lines) and $N_{f,tot}(t)$ (thin lines) for all initial conditions. The right plot reveals that the sum of the average particle number densities is strictly conserved.

particle number densities is strictly conserved as can be seen in the right plot of Fig. 4.8. Of course, this artificial constant of motion severely restricts the evolution of the particle number distributions. Consequently the Boltzmann equations fail to describe the process of quantum chemical equilibration and respect only a restricted universality.

In Fig. 4.8 we see that the average particle number densities for the initial conditions IC1 and IC2 approach each other at times $tm \approx 1000$. Additionally, in the left plot of Fig. 4.7 the particle number distributions seem to approach each other on the same time scale. According to these observations one might be tempted to conclude that also the Boltzmann equations separate some time scales in the framework of the linear σ-model. This is, however, not the case for the following two reasons: First, there are also momentum modes which approach each other on significantly larger time scales than shown in Fig. 4.7. And second, the plots in Fig. 4.9 reveal that it takes a considerably longer time to reach kinetic equilibrium. Therefore, also in the framework of the linear σ-model Boltzmann equations do not separate any time scales.

Summary

In this chapter we reviewed the derivation of Kadanoff-Baym equations from the 2PI effective action in the framework of a chirally invariant Yukawa-type quantum field theory including fermions. We also reviewed how one can exploit symmetries in order to simplify the Kadanoff-Baym equations such that their numerical

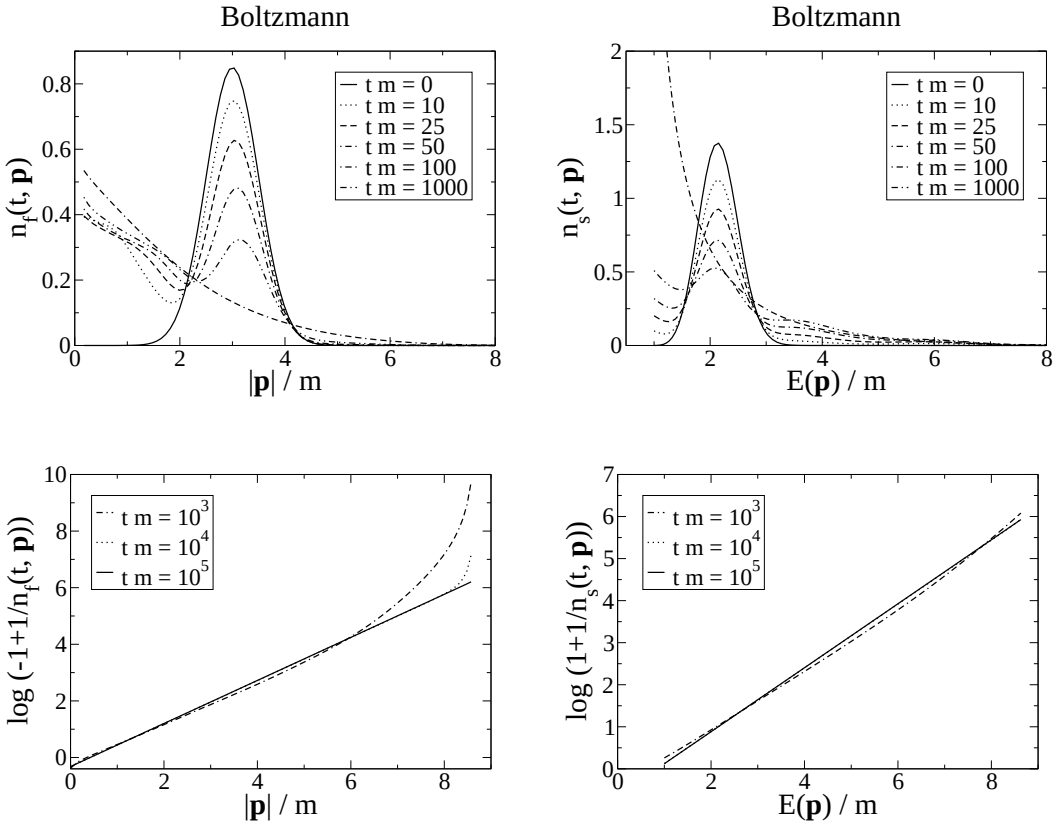

Figure 4.9: Missing separation of time scales. The scalar and fermion particle number distributions are shown at various times for the initial condition IC3.

solution becomes feasible as well as the approximations which are necessary to derive Boltzmann equations from the Kadanoff-Baym equations.

As for the purely scalar theory considered in the previous chapter, the Kadanoff-Baym equations respect full universality, including the process of quantum chemical equilibration, and strongly separate the time scales between kinetic and chemical equilibration [11, 35].

In contrast to this, the corresponding Boltzmann equations respect only a restricted universality, fail to describe the process of quantum chemical equilibration and do not separate any time scales.

Chapter 5

Conclusions and Outlook

Starting from the 2PI effective action for a real scalar Φ^4 quantum field theory and a chirally invariant Yukawa model including fermions, respectively, we reviewed the derivation of the Kadanoff-Baym equations and the approximations which are necessary to eventually arrive at Boltzmann equations. For the purely scalar theory we solved the Boltzmann and Kadanoff-Baym equations numerically for spatially homogeneous and isotropic systems in 3+1 space-time dimensions without any further approximations and compared their predictions on the evolution of systems out of thermal equilibrium for various initial conditions. For the fermionic model we solved the Boltzmann equations numerically for a highly symmetric system in 3+1 space-time dimensions and compared their solutions with the numerical solutions of the Kadanoff-Baym equations obtained by the group of Jürgen Berges.

We verified that the Kadanoff-Baym equations respect universality: For systems with equal average energy density the late time behavior coincides independent of the details of the initial conditions. In particular, independent of the initial conditions the particle number densities, temperatures, chemical potentials and thermal masses predicted for times, when equilibrium has effectively been reached, coincide. Additionally, Kadanoff-Baym equations incorporate the process of quantum chemical equilibration: For systems with vanishing net charge density the chemical potentials vanish once equilibrium has been reached. Last but not least, we observed a strong separation of time scales. We found a rapid approach to kinetic equilibrium, but only a very slow chemical equilibration.

In general Kadanoff-Baym and Boltzmann equations conserve the average energy density as well as global charges. However, the quasi-particle approximation introduces additional fake constants of motion for standard Boltzmann equations, which severely restricts the evolution of the particle number densities. As a result Boltzmann equations cannot lead to a universal quantum thermal equilibrium. Boltzmann equations maintain only a restricted universality: Only initial conditions for which the average energy density, all global charges and all fake constants of motion agree from the very beginning, lead to the same equilibrium results.

In particular, Boltzmann equations cannot describe the phenomenon of quantum chemical equilibration and, in general, will lead to non-vanishing chemical potentials even for systems with vanishing net charge density. Due to the lack of quantum chemical equilibration, the separation of time scales, which we observed for the Kadanoff-Baym equations, is absent in the case of Boltzmann equations.

Some of the approximations, which are necessary to derive Boltzmann equations from Kadanoff-Baym equations, are clearly motivated by equilibrium considerations. Taking the observed restriction of universality into account, we conclude that in the context of relativistic quantum fields one can safely apply standard Boltzmann equations only to systems which are sufficiently close to equilibrium. Accordingly, for systems far from equilibrium the results given by standard Boltzmann equations should be treated with care.

Unfortunately, solving Kadanoff-Baym equations numerically is significantly more difficult than solving the corresponding standard Boltzmann equations. However, the considerable discrepancies found for numerical solutions of Kadanoff-Baym and Boltzmann equations revealed equally significant limitations for standard Boltzmann equations. Accordingly, the importance of numerical solutions of Kadanoff-Baym equations cannot be over-estimated and it is certainly worth to face the arising difficulties.

In the present work we considered standard Boltzmann equations at lowest order in the particle number densities, and we employed the standard Kadanoff-Baym ansatz for their derivation. Our comparison of these standard Boltzmann equations with corresponding Kadanoff-Baym equations is justified by the fact that these standard Boltzmann equations are widely used in the literature. In the course of this work, however, we indicated how one can obtain Boltzmann equations beyond this standard form, and further studies are needed in order to estimate whether and in how far the situation for Boltzmann equations can be improved by including non-minimal collision terms or by employing a generalized Kadanoff-Baym ansatz.

In the future it will be important to perform a similar comparison of Boltzmann and Kadanoff-Baym equations also in the framework of gauge theories. Above that a treatment of Kadanoff-Baym equations on an expanding space-time also should reveal interesting results. This would finally enable one to establish a fully-fledged quantum mechanical treatment of leptogenesis. Independent of the comparison of Boltzmann and Kadanoff-Baym equations we are looking forward to learn to which extend an entirely non-perturbative renormalization procedure affects the results quantitatively. Above all, such a non-perturbative renormalization procedure should have a stabilizing virtue for the computational algorithms.

Appendix A

Numerical Algorithms

The numerical solution of Boltzmann and Kadanoff-Baym equations is far beyond the scope of any integrated computer software package such as Mathematica or Maple. In particular, the memory integrals in Kadanoff-Baym equations call for an enormous amount of computer memory and sophisticated optimizations of the computational algorithm in order to achieve acceptable execution times. Efficient allocation of computer memory and elaborate optimization of the employed algorithms is accomplishable only by using plain computer programming languages like C or Fortran supplemented by appropriate libraries. We implemented our numerics in C [95], supplemented by the Fastest Fourier Transform in the West [96] and the GNU Scientific Library [97]. A Fortran code for non-relativistic Kadanoff-Baym equations has been presented in Ref. [98].

A.1 Kadanoff-Baym Equations

Memory Layout

For the numerical solution of the Kadanoff-Baym equations we follow exactly the lines of Refs. [22, 34, 35, 99], i.e. for the spatial coordinates we employ a standard discretization on a three-dimensional lattice with lattice spacing a_s and N_s lattice sites in each direction. Thus, the lattice momenta are given by

$$\hat{p}_{n_j} = \frac{2}{a_s} \sin\left(\frac{\pi n_j}{N_s}\right) ,$$

where n_j, $j \in \{1, 2, 3\}$, enumerates the momentum modes in the j-th dimension. As we consider a spatially homogeneous and isotropic system, for given times (x^0, y^0) we only need to store the propagator for momentum modes with $\frac{N_s}{2} \geq n_1 \geq n_2 \geq n_3 \geq 0$. This reduces the required amount of computer memory by a factor of 48. For the practical implementation, it is convenient to map this three-dimensional structure of the considered momentum modes onto a one-dimensional

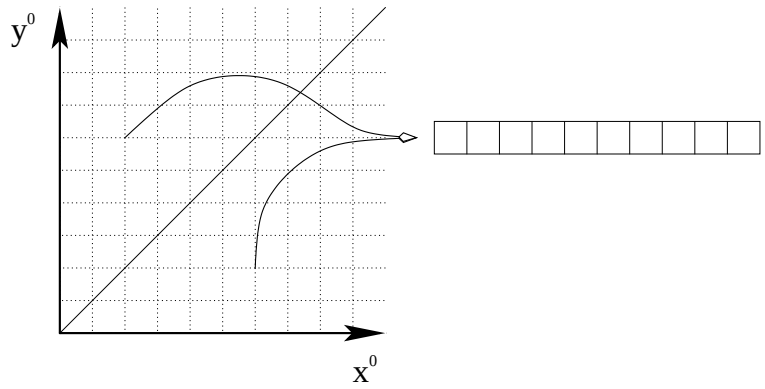

Figure A.1: Memory layout for Kadanoff-Baym equations. For each propagator component we use a matrix of pointers which aim at one-dimensional arrays containing the momentum dependence of the propagator component for the corresponding times.

array `M`. This can be achieved with the following two auxiliary functions:

$$D(j) = \sum_{k=0}^{j-1} \sum_{l=0}^{k} 1 = \frac{1}{2} j (j+1)$$

and

$$T(n) = \sum_{j=0}^{n-1} \sum_{k=0}^{j} \sum_{l=0}^{k} 1 = \frac{1}{6} n (n+1) (n+2) \ .$$

The momentum mode (n_1, n_2, n_3) can then be found at the index

$$I(n_1, n_2, n_3) = T(n_1) + D(n_2) + n_3$$

in the one-dimensional array `M`.

Now, suppose, for a given time x^0 we would like to compute the memory integrals for all[1] (x^0, y^0) with $y^0 \leq x^0$. This requires that we know the propagator for all times $(t_1, t_2) \in [0, x^0]^2$. Therefore, the discretization in time leads to a history matrix $H = \{0, a_t, 2a_t, \ldots\}^2$, where a_t is the time-step size. Exploiting the symmetry of the statistical Higgs propagator with respect to the interchange of its time arguments, we only need to store the values of the statistical Higgs propagator for all (x^0, y^0) with $x^0 \geq y^0$. In very much the same way we can exploit the corresponding anti-symmetry of the Higgs spectral-function. This reduces the memory consumption by another factor of 2. Up to subtleties to be discussed

[1] We will see in the next subsection why this is an issue.

in the following subsection, the same also holds for the various lepton-propagator components. A convenient way to implement this structure in a computer program is to use a three-dimensional array of pointers `propagator`. The first index of the `propagator` array enumerates the various propagator components, and the second and third indices parametrize the history matrix H. The afore mentioned symmetry of the statistical propagator can then be implemented in the following way: For each $(x^0, y^0) \in H$ with $x^0 \geq y^0$ an array `M` is allocated and the pointers in the `propagator` array corresponding to (x^0, y^0) and (y^0, x^0) are aimed at the same array `M`. Fig. A.1 illustrates this memory layout. The memory for the spectral function is allocated in exactly the same way. Additionally, however, one has to guarantee that for (y^0, x^0) the spectral function is accompanied by an additional minus sign.

Time Stepping and Memory Integrals

In order to discretize the second derivative with respect to time, which appears in the Kadanoff-Baym equations for the scalar propagator components, we use forward and backward derivatives [99]:

$$\begin{aligned} \partial_{x^0}^2 G\left(x^0, y^0, k\right) \quad &\rightarrow \quad \Delta_0^b \Delta_0^f G\left(x^0, y^0, \hat{\boldsymbol{k}}\right) \\ &= \quad \frac{G\left(x^0 + a_t, y^0, \hat{\boldsymbol{k}}\right) - 2G\left(x^0, y^0, \hat{\boldsymbol{k}}\right) + G\left(x^0 - a_t, y^0, \hat{\boldsymbol{k}}\right)}{a_t^2} \end{aligned}$$

Solving the discretized Kadanoff-Baym equations for $G(x^0 + a_t, y^0, \hat{\boldsymbol{k}})$ gives then something of the form

$$\begin{aligned} G\left(x^0 + a_t, y^0, \hat{\boldsymbol{k}}\right) &= 2G\left(x^0, y^0, \hat{\boldsymbol{k}}\right) - G\left(x^0 - a_t, y^0, \hat{\boldsymbol{k}}\right) \\ &\quad + a_t^2 \left[MEMINT\left(x^0, y^0, \hat{\boldsymbol{k}}\right) - \left(\hat{\boldsymbol{k}}^2 + M^2\left(x^0\right)\right) G\left(x^0, y^0, \hat{\boldsymbol{k}}\right)\right] . \end{aligned} \tag{A.1.1}$$

Suppose, for a given x^0 we know the propagator throughout the history matrix $H\left(x^0\right) = \{0, \ldots, x^0\}^2$, which is represented by the dark-gray square in Fig. A.2. The time-stepping algorithm then proceeds as follows: First of all, we compute the statistical and spectral self energies $\Pi(x^0, y^0, \hat{\boldsymbol{k}})$ for all $y^0 \leq x^0$ and all momentum modes $\hat{\boldsymbol{k}}$. Above all, here it is crucial to compute the emerging convolutions using a Fast Fourier Transform algorithm[2] [96]. Then we can compute the memory integrals and apply Eq. (A.1.1) for all (x^0, y^0) with $y^0 \leq x^0$ and all momentum modes $\hat{\boldsymbol{k}}$ as indicated by steps 1, 2 and 3 in Fig. A.2. In order to compute the

[2]Never convolve by hand! The Fastest Fourier Transform in the West offers nice algorithms for real-valued even functions in arbitrary dimension!

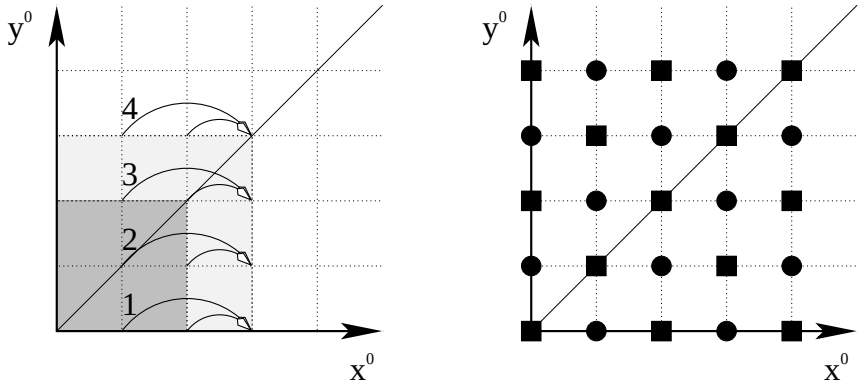

Figure A.2: In order to evolve the Kadanoff-Baym equations one step from x^0 to $x^0 + a_t$ we have to advance the propagators for all (x^0, y^0) with $y^0 \leq x^0 + a_t$ in the order specified in the left figure. The right figure illustrates additional subtleties involved in the memory layout for the fermion-propagator components. Due to the leap-frog algorithm space-like (time-like) vector components of the lepton propagator are stored at even (odd) relative times, which are indicated by squares (circles).

memory integrals we employ a simple trapezoidal rule:

$$\begin{aligned}
&\int_0^{y^0} dz^0 \; \Pi_F\left(x^0, z^0, k\right) G_\varrho\left(z^0, y^0, k\right) \\
&\quad \rightarrow \;\; \frac{1}{2}\Pi_F\left(x^0, 0, \hat{\boldsymbol{k}}\right) G_\varrho\left(0, y^0, \hat{\boldsymbol{k}}\right) + \sum_{z_0 = a_t}^{y^0 - a_t} \left[\Pi_F\left(x^0, z^0, \hat{\boldsymbol{k}}\right) G_\varrho\left(z^0, y^0, \hat{\boldsymbol{k}}\right)\right] \\
&\qquad + \frac{1}{2}\Pi_F\left(x^0, y^0, \hat{\boldsymbol{k}}\right) G_\varrho\left(y^0, y^0, \hat{\boldsymbol{k}}\right)
\end{aligned}$$

Note that the upper boundary term of the memory integral vanishes because of the anti-symmetry of the spectral function. As a matter of fact, the upper boundary terms of all memory integrals vanish! After all, we now know the propagators for all $(x^0 + a_t, y^0)$ with $y^0 \leq x^0$. At this point it is important to take the (anti-)symmetry of the various propagator components into account, due to which we also know the propagators for $(y^0, x^0 + a_t)$. As the upper boundary terms of all memory integrals vanish, we do not need to compute any self energy for $(x^0, x^0 + a_t)$, and we immediately can compute the memory integrals and apply Eq. (A.1.1) (step 4 in Fig. A.2), thereby completing the history matrix $H\left(x^0 + a_t\right)$ which is represented by the light gray box in Fig. A.2.

As already indicated earlier, things are a bit more subtle in the case of the fermion propagator. The first-order derivative with respect to time, which appears in the Kadanoff-Baym equations for the fermions, can be discretized in a symmetric way according to

$$\partial_{x^0} S\left(x^0, y^0, k\right) \quad \rightarrow \quad \frac{S\left(x^0 + a_t, y^0, \hat{\boldsymbol{k}}\right) - S\left(x^0 - a_t, y^0, \hat{\boldsymbol{k}}\right)}{2a_t}$$

Solving the discretized Kadanoff-Baym equations for $S(x^0 + a_t, y^0, \hat{\boldsymbol{k}})$ gives then something of the form

$$\begin{aligned} S_V^0\left(x^0 + a_t, y^0, \hat{\boldsymbol{k}}\right) &= S_V^0\left(x^0 - a_t, y^0, \hat{\boldsymbol{k}}\right) \\ &+ 2a_t \left[MEMINT\left(x^0, y^0, \hat{\boldsymbol{k}}\right) - \hat{k} S_V\left(x^0, y^0, \hat{\boldsymbol{k}}\right)\right] . \end{aligned} \tag{A.1.2}$$

and

$$\begin{aligned} S_V\left(x^0 + a_t, y^0, \hat{\boldsymbol{k}}\right) &= S_V\left(x^0 - a_t, y^0, \hat{\boldsymbol{k}}\right) \\ &+ 2a_t \left[MEMINT\left(x^0, y^0, \hat{\boldsymbol{k}}\right) + \hat{k} S_V^0\left(x^0, y^0, \hat{\boldsymbol{k}}\right)\right] . \end{aligned} \tag{A.1.3}$$

Thus, in the discretized Kadanoff-Baym equations we need the various propagator components only at every second point in the history matrix. As already explained in Chapter 4 the effective particle number density for the fermions is obtained from $S_{V,F}(t, t, k)$. Therefore, the above discretization of the Kadanoff-Baym equations for fermions suggests to store the space-like (time-like) vector components of the statistical fermion propagator only for even (odd) relative times $x^0 - y^0$, which corresponds to a generalized leap-frog algorithm [35, 99]. Applying this leap-frog algorithm to the memory integrals, one observes that one also has to put space-like (time-like) vector components of the fermion spectral-function at even (odd) relative times.

History Cut-Off

Obviously, the memory layout described in previous subsections calls for an enormous amount of computer memory. Therefore it is impossible to evolve the Kadanoff-Baym equations up to reasonable times keeping the complete history matrix of all propagator components in memory. Fortunately, according to Fig. 3.4 correlations between earlier and later times are damped exponentially, which allows us to introduce a history cut-off. A convenient way to implement this history cut-off is to use a history matrix of fixed size

$$H = \{0, a_t, 2a_t, \ldots, (N_t - 1)\, a_t\}^2$$

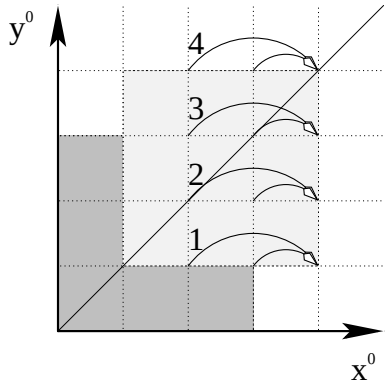

Figure A.3: Due to the history cut-off the history matrix possesses a maximal size. Once the history matrix is filled completely, it starts moving forward along the bisecting line of the x^0-y^0 plane. The history matrix at time $x^0 = t$ $(t + a_t)$ is represented by the dark gray (light gray) square.

and to store the propagator components at indices $(x^0 \mod N_t, y^0 \mod N_t)$. The time-stepping algorithm and the computation of the memory integrals described in the previous subsection can easily be adjusted to account for this history cut-off. After the history matrix is filled completely, at each time x^0 we advance the Kadanoff-Baym equations only for times $y^0 \in \{x^0 - N_t + a_t, \ldots, x^0 + a_t\}$ in the order specified in Fig. A.3. As indicated by the gray squares in Fig. A.3, the history cut-off amounts to shifting history matrix along the bisecting line of the x^0-y^0-plane. In order to give an impression on the consumption of computer memory, it might be illustrative to put together some numbers: In the purely scalar case there are 2 propagator components, the statistical propagator and the spectral function. Our numerical solutions were achieved with $N_t = 500$ and $N_s = 32$. Due to isotropy, for $N_s = 32$ there are 969 independent momentum modes. Thus using double precision requires

$$2 \times \frac{500 \times 501}{2} \times 969 \times 8 \text{ Bytes} = 1.9 \text{ GBytes} .$$

This number is doubled in the case of the linear σ-model. There one has 6 propagator components. However, due to the leap-frog algorithm the 4 fermion-propagator components can be stored in an alternating fashion, such that they only require as much computer memory as the 2 scalar propagator components.

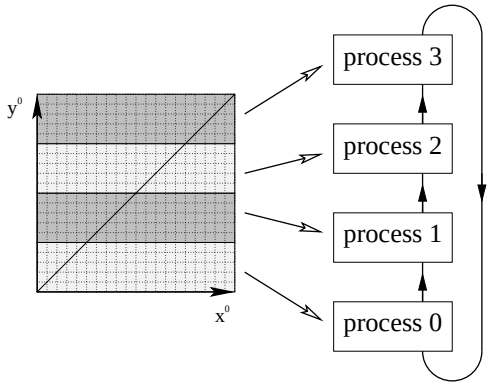

Figure A.4: This is how a parallel distributed-memory algorithm could look like. The history matrix is distributed among a number of processes, which communicate their achievements.

Parallelization

The enormous amount of computer memory and computing power that are needed to solve the Kadanoff-Baym equations numerically cry for a parallel distributed-memory algorithm. Such an algorithm can be realized using the Parallel Virtual Machine [100] or the Message Passing Interface [101, 102]. For the special algorithm presented here, the user interface offered by MPI is probably more convenient than the PVM3 alternative. In any case, we will start a number of processes on various computers, which then communicate their achievements.

The sequential algorithm described in the previous subsections was designed to run on a single computer. Therefore memory consumption was a critical issue and we had to exploit the (anti-)symmetry of the various propagator components in order to reduce the required amount of memory by a factor of 2. For the parallel algorithm described in this subsection, however, it is convenient to abstain from this reduction of memory. Instead we will allocate memory for the complete history matrix. The increasing requirement of computer memory can easily be compensated by an increasing number of participating computers. Suppose, we started P processes on P identical computers. For simplicity of the algorithm and in order to achieve an optimal work-load balance P must be a divisor of the size of the history matrix N_t. Then we divide the history matrix in P equally sized stripes parallel to the x^0-axis and each of the P processes allocates the memory needed for one of those stripes. Fig. A.4 adumbrates the situation for the case $P = 4$. As compared to the previous subsection the time-stepping algorithm has to be generalized in the following way: Each process computes the self energies $\Pi(x^0, y^0, \hat{\boldsymbol{k}})$ for all times y^0 which belong to his history-matrix stripe. The self-

energies are then distributed to all processes in the ring-like fashion indicated in Fig. A.4. The computation of the memory integrals and the evolution of the Kadanoff-Baym equations according to steps 1, 2 and 3 of Fig. A.2 can then be performed by all processes simultaneously. Next, taking their (anti-)symmetry properties into account the obtained propagator components $G(x^0 + a_t, y^0, \hat{\boldsymbol{k}})$ are sent to the process maintaining the history-matrix stripe which contains the time $y^0 = (x^0 + a_t) \mod N_t$. Performing step 4 of Fig. A.2 this process then completes the time-stepping procedure.

A.2 Boltzmann Equations

As we saw in the previous section, in order to discretize Kadanoff-Baym equations we can rely on the well-defined scheme offered by standard lattice field theory. Unfortunately, the energy conserving δ function in the Boltzmann equations (3.3.4), (4.4.8) and (4.4.12) prevent us from using these standard lattice techniques for these Boltzmann equations. The reason is the following: Having resolved the momentum conserving δ function, one can also resolve the energy conserving δ function by performing the integral over one of the remaining momentum modes. This requires to look for zeros of the argument of the energy conserving δ function with respect to this particular momentum mode. These zeros might well fall between two lattice sites. Hence, computing the collision integral requires the use of interpolation techniques in order to determine the particle number distribution for these in-between lattice sites. These interpolation techniques imply a continuity assumption for the particle number distribution which contradicts the strict lattice discretization as offered by lattice field theory. Apart from this principal obstacle, there is also a practical reason which encourages us to use different discretization schemes for both types of equations: The collision integral in Eq. (3.3.4) is no convolution. Consequently, Fast Fourier Transformation algorithms are not applicable, and the numerical computation of the collision integral becomes rather expensive. In order to reduce the complexity of our Boltzmann numerics we exploited isotropy, which allowed us to simplify the Boltzmann equations (3.3.4), (4.4.8) and (4.4.12) analytically and lead us to Eqs. (3.3.7), (4.4.9) and (4.4.13). In the discretized Boltzmann equations (3.3.7), (4.4.9) and (4.4.13) the momenta are of the form

$$p_n = \frac{\sqrt{12}}{a_s N_s} n \, .$$

We use the same value for a_s as for the Kadanoff-Baym equations. This ensures that the largest available momentum is the same as for the Kadanoff-Baym equations. Of course, the number of momentum bins N_s need not be the same as for the Kadanoff-Baym equations, which just means that we approach the physically relevant infinite volume limit independently for both types of equations.

In order to compute the collision integral in Eq. (3.3.7) we proceed as follows: For fixed (k, p, q) we determine r_0, which of course need not be one of the discretized momenta given above. Obviously, the function $D\,(k, p, q, r_0)$ can be evaluated for any value of r_0. In order to obtain the particle number density for an arbitrary r_0 we use a cubic spline interpolation [97]. Thus, for given (k, p, q) the integrand is known to any given accuracy and for given k we can simply sum over p and q. The computation of the collision integrals in Eqs. (4.4.9) and (4.4.13) proceeds along the same lines, except that we have to compute only a one-dimensional integral. In order to advance the particle number distributions in time we use a Runge-Kutta-Cash-Karp routine with adaptive step-size control [97].

Bibliography

[1] M. Fukugita and T. Yanagida, *Baryogenesis without Grand Unification*, Phys. Lett. **B174** (1986) 45.

[2] W. Buchmüller, P. Di Bari, and M. Plümacher, *Leptogenesis for pedestrians*, Ann. Phys. **315** (2005) 305, `hep-ph/0401240`.

[3] Wilfried Buchmüller and Stefan Fredenhagen, *Quantum mechanics of baryogenesis*, Phys. Lett. **B483** (2000) 217, `hep-ph/0004145`.

[4] A. D. Sakharov, *Violation of CP Invariance, C Asymmetry, and Baryon Asymmetry of the Universe*, JETP Lett. **5** (1967) 24.

[5] I. Arsene et al. (BRAHMS), *Quark gluon plasma and color glass condensate at RHIC? The perspective from the BRAHMS experiment*, Nucl. Phys. **A757** (2005) 1, `nucl-ex/0410020`.

[6] B. B. Back et al. (PHOBOS), *The PHOBOS perspective on discoveries at RHIC*, Nucl. Phys. **A757** (2005) 28, `nucl-ex/0410022`.

[7] J. Adams et al. (STAR), *Experimental and theoretical challenges in the search for the quark gluon plasma: The STAR collaboration's critical assessment of the evidence from RHIC collisions*, Nucl. Phys. **A757** (2005) 102, `nucl-ex/0501009`.

[8] K. Adcox et al. (PHENIX), *Formation of dense partonic matter in relativistic nucleus nucleus collisions at RHIC: Experimental evaluation by the PHENIX collaboration*, Nucl. Phys. **A757** (2005) 184, `nucl-ex/0410003`.

[9] Tomislav Prokopec, Michael G. Schmidt, and Steffen Weinstock, *Transport equations for chiral fermions to order h-bar and electroweak baryogenesis*, Ann. Phys. **314** (2004) 208, `hep-ph/0312110`.

[10] Tomislav Prokopec, Michael G. Schmidt, and Steffen Weinstock, *Transport equations for chiral fermions to order h-bar and electroweak baryogenesis. II*, Ann. Phys. **314** (2004) 267, `hep-ph/0406140`.

[11] J. Berges, S. Borsányi, and C. Wetterich, *Prethermalization*, Phys. Rev. Lett. **93** (2004) 142002, hep-ph/0403234.

[12] A. H. Mueller and D. T. Son, *On the equivalence between the Boltzmann equation and classical field theory at large occupation numbers*, Phys. Lett. **B582** (2004) 279, hep-ph/0212198.

[13] Sangyong Jeon, *The Boltzmann equation in classical and quantum field theory*, Phys. Rev. **C72** (2005) 014907, hep-ph/0412121.

[14] Gordon Baym and Leo P. Kadanoff, *Quantum Statistical Mechanics* (Benjamin, New York, 1962)

[15] P. Danielewicz, *Quantum Theory of Nonequilibrium Processes I*, Annals Phys. **152** (1984) 239.

[16] Yu. B. Ivanov, J. Knoll, and D. N. Voskresensky, *Resonance Transport and Kinetic Entropy*, Nucl. Phys. **A672** (2000) 313, nucl-th/9905028.

[17] J. Knoll, Yu. B. Ivanov, and D. N. Voskresensky, *Exact Conservation Laws of the Gradient Expanded Kadanoff-Baym Equations*, Annals Phys. **293** (2001) 126, nucl-th/0102044.

[18] Jean-Paul Blaizot and Edmond Iancu, *The quark-gluon plasma: Collective dynamics and hard thermal loops*, Phys. Rept. **359** (2002) 355, hep-ph/0101103.

[19] Radu Balescu, *Equilibrium and Nonequilibrium Statistical Mechanics* (Wiley, New York, 1975)

[20] S. R. De Groot, W. A. Van Leeuwen, and Ch. G. Van Weert, *Relativistic Kinetic Theory. Principles and Applications* (North-Holland, Amsterdam, Netherlands, 1980)

[21] H. J. Kreuzer, *Nonequilibrium Thermodynamics and its Statistical Foundations* (Clarendon, Oxford, 1981)

[22] Jürgen Berges, *Controlled nonperturbative dynamics of quantum fields out of equilibrium*, Nucl. Phys. **A699** (2002) 847, hep-ph/0105311.

[23] Gert Aarts and Jürgen Berges, *Nonequilibrium time evolution of the spectral function in quantum field theory*, Phys. Rev. **D64** (2001) 105010, hep-ph/0103049.

[24] Edward W. Kolb and Stephen Wolfram, *Baryon Number Generation in the Early Universe*, Nucl. Phys. **B172** (1980) 224.

[25] Edward W. Kolb and Michael S. Turner, *The Early Universe* (Addison-Wesley, 1990)

[26] P. Danielewicz, *Quantum Theory of Nonequilibrium Processes II. Application to Nuclear Collisions*, Annals Phys. **152** (1984) 305.

[27] H. S. Köhler, *Memory and correlation effects in nuclear collisions*, Phys. Rev. **C51** (1995) 3232

[28] H. S. Köhler, *Memory and correlation effects in the quantum theory of thermalization*, Phys. Rev. **E53** (1996) 3145

[29] K. Morawetz and H. S. Köhler, *Formation of correlations and energy-conservation at short time scales*, Eur. Phys. J. **A4** (1999) 291, `nucl-th/9802082`.

[30] S. Juchem, W. Cassing, and C. Greiner, *Quantum dynamics and thermalization for out-of-equilibrium ϕ^4-theory*, Phys. Rev. **D69** (2004) 025006, `hep-ph/0307353`.

[31] Manfred Lindner and Markus Michael Müller, *Comparison of Boltzmann equations with quantum dynamics for scalar fields*, Phys. Rev. **D73** (2006) 125002, `hep-ph/0512147`.

[32] Markus Michael Müller, *Comparing Boltzmann vs. Kadanoff-Baym*, J. Phys. Conf. Ser. **35** (2006) 390.

[33] Jürgen Berges and Jürgen Cox, *Thermalization of quantum fields from time-reversal invariant evolution equations*, Phys. Lett. **B517** (2001) 369, `hep-ph/0006160`.

[34] Jürgen Berges, *Introduction to nonequilibrium quantum field theory*, AIP Conf. Proc. **739** (2005) 3, `hep-ph/0409233`.

[35] Jürgen Berges, Szabolcs Borsányi, and Julien Serreau, *Thermalization of fermionic quantum fields*, Nucl. Phys. **B660** (2003) 51, `hep-ph/0212404`.

[36] Gordon Baym and Leo P. Kadanoff, *Conservation Laws and Correlation Functions*, Phys. Rev. **124** (1961) 287

[37] Gordon Baym, *Selfconsistent approximation in many body systems*, Phys. Rev. **127** (1962) 1391.

[38] Yu. B. Ivanov, J. Knoll, and D. N. Voskresensky, *Self-consistent approximations to non-equilibrium many-body theory*, Nucl. Phys. **A657** (1999) 413, `hep-ph/9807351`.

[39] R. Jackiw, *Functional evaluation of the effective potential*, Phys. Rev. **D9** (1974) 1686.

[40] John M. Cornwall, R. Jackiw, and E. Tomboulis, *Effective Action for Composite Operators*, Phys. Rev. **D10** (1974) 2428.

[41] E. Calzetta and B. L. Hu, *Nonequilibrium quantum fields: Closed-time-path effective action, Wigner function and Boltzmann equation*, Phys. Rev. **D37** (1988) 2878.

[42] Gert Aarts and Jürgen Berges, *Classical aspects of quantum fields far from equilibrium*, Phys. Rev. Lett. **88** (2002) 041603, `hep-ph/0107129`.

[43] Gert Aarts and Jose M. Martínez Resco, *Transport coefficients from the 2PI effective action*, Phys. Rev. **D68** (2003) 085009, `hep-ph/0303216`.

[44] Steven Weinberg, *The Quantum Theory of Fields 1: Foundations* (Cambridge University Press, 1995)

[45] N. P. Landsman and C. G. van Weert, *Real and Imaginary Time Field Theory at Finite Temperature and Density*, Phys. Rept. **145** (1987) 141.

[46] Joseph I. Kapusta, *Finite Temperature Field Theory* (Cambridge University Press, 1989)

[47] Jean Zinn-Justin, *Quantum Field Theory and Critical Phenomena* (Oxford University Press, 1989)

[48] Michel LeBellac, *Thermal Field Theory* (Cambridge University Press, 1996)

[49] Takeo Matsubara, *A New approach to quantum statistical mechanics*, Prog. Theor. Phys. **14** (1955) 351.

[50] A. J. Niemi and G. W. Semenoff, *Finite Temperature Quantum Field Theory in Minkowski Space*, Ann. Phys. **152** (1984) 105.

[51] Antti J. Niemi and Gordon W. Semenoff, *Thermodynamic Calculations in Relativistic Finite Temperature Quantum Field Theories*, Nucl. Phys. **B230** (1984) 181.

[52] Ryogo Kubo, *Statistical mechanical theory of irreversible processes. 1. General theory and simple applications in magnetic and conduction problems*, J. Phys. Soc. Jap. **12** (1957) 570.

[53] Paul C. Martin and Julian S. Schwinger, *Theory of many particle systems. I*, Phys. Rev. **115** (1959) 1342.

[54] Julian S. Schwinger, *Brownian motion of a quantum oscillator*, J. Math. Phys. **2** (1961) 407.

[55] L. V. Keldysh, *Diagram technique for nonequilibrium processes*, Sov. Phys. JETP **20** (1965) 1018.

[56] Pradip M. Bakshi and Kalyana T. Mahanthappa, *Expectation value formalism in quantum field theory. 1*, J. Math. Phys. **4** (1963) 1.

[57] Pradip M. Bakshi and Kalyana T. Mahanthappa, *Expectation value formalism in quantum field theory. 2*, J. Math. Phys. **4** (1963) 12.

[58] Victor Korenman, *Nonequilibrium Quantum Statistics; Application to the Laser*, Ann. Phys. **39** 72

[59] R. A. Craig, *A Variational Relationship for Nonequilibrium, Real Time Quantities*, Ann. Phys. **40** 416

[60] R. A. Craig, *Perturbation Expansion for Real-Time Green's Functions*, J. Math. Phys. **9** 605

[61] Victor Korenman, *On Perturbation Expansions for Real-Time Green's Functions*, J. Math. Phys. **10** 1387

[62] Kuang-chao Chou, Zhao-bin Su, Bai-lin Hao, and Lu Yu, *Equilibrium and Nonequilibrium Formalisms made Unified*, Phys. Rept. **118** (1985) 1.

[63] J. M. Luttinger and J. C. Ward, *Ground state energy of a many fermion system. 2*, Phys. Rev. **118** (1960) 1417.

[64] Jürgen Berges, *n-PI effective action techniques for gauge theories*, Phys. Rev. **D70** (2004) 105010, `hep-ph/0401172`.

[65] Cyrano de Dominicis and Paul C. Martin, *Stationary Entropy Principle and Renormalization in Normal and Superfluid Systems. Algebraic Formulation*, J. Math. Phys. **5** 14

[66] Cyrano de Dominicis and Paul C. Martin, *Stationary Entropy Principle and Renormalization in Normal and Superfluid Systems. Diagrammatic Formulation*, J. Math. Phys. **5** 31

[67] Jean-Paul Blaizot, Edmond Iancu, and Urko Reinosa, *Renormalization of phi-derivable approximations in scalar field theories*, Nucl. Phys. **A736** (2004) 149, `hep-ph/0312085`.

[68] Hendrik van Hees and Jörn Knoll, *Renormalization in self-consistent approximations schemes at finite temperature. I: Theory*, Phys. Rev. **D65** (2002) 025010, `hep-ph/0107200`.

[69] Hendrik van Hees and Jörn Knoll, *Renormalization of self-consistent approximation schemes. II: Applications to the sunset diagram*, Phys. Rev. **D65** (2002) 105005, `hep-ph/0111193`.

[70] Hendrik van Hees and Jörn Knoll, *Renormalization in self-consistent approximation schemes at finite temperature. III: Global symmetries*, Phys. Rev. **D66** (2002) 025028, `hep-ph/0203008`.

[71] J. Berges, Sz. Borsányi, U. Reinosa, and J. Serreau, *Renormalized thermodynamics from the 2PI effective action*, Phys. Rev. **D71** (2005) 105004, `hep-ph/0409123`.

[72] Jürgen Berges, Szabolcs Borsányi, Urko Reinosa, and Julien Serreau, *Nonperturbative renormalization for 2PI effective action techniques*, Annals Phys. **320** (2005) 344, `hep-ph/0503240`.

[73] Urko Reinosa, *Nonperturbative renormalization of Phi-derivable approximations in theories with fermions* (2005), `hep-ph/0510119`.

[74] Urko Reinosa and Julien Serreau, *2PI effective action for gauge theories: Renormalization* (2006), `hep-th/0605023`.

[75] Alejandro Arrizabalaga, Jan Smit, and Anders Tranberg, *Equilibration in φ^4 theory in 3+1 dimensions*, Phys. Rev. **D72** (2005) 025014, `hep-ph/0503287`.

[76] Jürgen Berges and Markus M. Müller, *Nonequilibrium quantum fields with large fluctuations*, in *Progress in Nonequilibrium Green's Functions 2* (edited by M. Bonitz and D. Semkat, World Scientific Publ., Singapore, 2003), 367, `hep-ph/0209026`.

[77] Jürgen Berges, Szabolcs Borsányi, and Christof Wetterich, *Isotropization far from equilibrium*, Nucl. Phys. **B727** (2005) 244, `hep-ph/0505182`.

[78] Jürgen Berges and Szabolcs Borsányi, *Range of validity of transport equations* (2005), `hep-ph/0512155`.

[79] P. Lipavský, V. Špička, and B. Velický, *Generalized Kadanoff-Baym ansatz for deriving quantum transport equations*, Phys. Rev. **B10** (1986) 6933

[80] Ludwig Boltzmann, *Weitere Studien über das Wärmegleichgewicht unter Gasmolekülen*, Wien. Ber. **66** (1872) 275

[81] L. W. Nordheim, *On the Kinetic Method in the New Statistics and Its Application in the Electron Theory of Conductivity*, Proc. Roy. Soc. Lond. **A119** (1928) 689

[82] E. A. Uehling and G. E. Uhlenbeck, *Transport Phenomena in Einstein-Bose and Fermi-Dirac Gases. I*, Phys. Rev. **43** (1933) 552

[83] L. D. Landau, E. M. Lifshitz, and L. P. Pitaevskii, *Course of Theoretical Physics 10: Physical Kinetics* (Pergamon Press, Oxford, 1981)

[84] Wim Botermans and Rudi Malfliet, *Quantum transport theory of nuclear matter*, Phys. Rept. **198** (1990) 115.

[85] Markus Michael Müller, *Kinetic equations from the two-particle-irreducible 1/N- expansion* (2002), `hep-ph/0303221`.

[86] Margaret E. Carrington and Stanislaw Mrowczynski, *Transport theory beyond binary collisions*, Phys. Rev. **D71** (2005) 065007, `hep-ph/0406097`.

[87] Steffen Weinstock, *Boltzmann collision term*, Phys. Rev. **D73** (2006) 025005, `hep-ph/0510417`.

[88] Francois Fillion-Gourdeau, Jean-Sebastien Gagnon, and Sangyong Jeon, *All orders Boltzmann collision term from the multiple scattering expansion of the self-energy* (2006), `hep-ph/0603212`.

[89] A. D. Dolgov, S. H. Hansen, and D. V. Semikoz, *Non-equilibrium corrections to the spectra of massless neutrinos in the early universe*, Nucl. Phys. **B503** (1997) 426, `hep-ph/9703315`.

[90] L. D. Landau and E. M. Lifshitz, *Course of Theoretical Physics 5: Statistical Physics, Part 1* (Pergamon Press, Oxford, 1980)

[91] N. G. Deshpande, J. F. Gunion, B. Kayser, and Fredrick I. Olness, *Left-right symmetric electroweak models with triplet Higgs*, Phys. Rev. **D44** (1991) 837.

[92] Julian S. Schwinger, *A Theory of the fundamental interactions*, Annals Phys. **2** (1957) 407.

[93] J. C. Polkinghorne, *Renormalization of Axial Vector Coupling*, Nuovo Cim. **8** (1958) 179 and 781

[94] Murray Gell-Mann and M Levy, *The axial vector current in beta decay*, Nuovo Cim. **16** (1960) 705.

[95] Brian W. Kernighan and Dennis M. Ritchie, *The C Programming Language, Second Edition, ANSI C* (Prentice-Hall International, Englewood Cliffs, New Jersey 07632)

[96] Matteo Frigo and Steven G. Johnson, *FFTW Reference Manual* (Version 3.1, 2006)

[97] Mark Galassi et al., *GNU Scientific Library Reference Manual* (Version 1.5, 2004). See also [103].

[98] H. S. Köhler, N. H. Kwong, and Hashim A. Yousif, *A Fortran Code for solving the Kadanoff-Baym equations for a homogeneous fermion system*, Comp. Phys. Comm. **123** (1999) 123

[99] István Montvay and Gernot Münster, *Quantum fields on a lattice* (Cambridge University Press, 1994)

[100] Al Geist et al., *PVM 3 User's Guide and Reference Manual* (Version 3.4.5, 1994)

[101] MPI Forum, *MPI-2: Extensions to the Message-Passing Interface* (1997)

[102] William Gropp et al., *MPICH2 User's Guide* (Version 1.0.3, 2005)

[103] William H. Press et al., *Numerical Recipes in C* (Cambridge University Press, 1988)

Danksagung
(engl. Acknowledgments)

"The world is coming to an end. Please log off."

/usr/bin/fortune

Bevor ich diese Arbeit endgültig schließe, möchte ich mich noch bei allen Menschen bedanken, die zum Gelingen dieser Arbeit sowie zu meiner persönlichen Weiterentwicklung während der letzten dreieinhalb Jahre beigetragen haben.

Vor allem ist hier mein Doktorvater Manfred Lindner zu nennen, der es mir ermöglicht hat meine Doktorarbeit in diesem äußerst wichtigen, interessanten und abwechslungsreichen Gebiet zu verfassen. Insbesondere genoß ich die mir gewährte Freiheit bei meiner Arbeit ebenso wie gewinnbringende Diskussionen und die optimale Arbeitsumgebung. Für all dies meinen herzlichsten Dank.

Diskussionen mit Andreas Hohenegger haben wesentlich zu meinem Verständnis von Boltzmanngleichungen und ihrer numerischen Lösung beigetragen. Desweiteren waren Mathias Garny und Michael Schmidt stets für Diskussionen über praktische Fragen zu (nicht)perturbativen Methoden in der Quantenfeldtheorie zu begeistern. Hierfür meinen besten Dank!

Ein besonderer Dank geht auch an Stefan Recksiegel, der mir immer sehr geduldig die Feinheiten der Computeradministration nähergebracht hat. Dadurch hat er meine Vertrautheit mit diesen Gerätschaften deutlich gesteigert, wovon sowohl unser Cluster als auch meine Numerikprogramme profitiert haben.

Ich möchte an dieser Stelle sämtlichen Leuten an unserem Lehrstuhl (Diplomanden, Doktoranden, Postdocs, Gäste, ... einfach zu viele um alle einzeln zu nennen) für das angenehme Arbeitsklima danken. Besonders hervorheben muß ich hier jedoch meine beiden Büromitbewohner: zum einen Jörn Kersten, mit dem ich auch die eine oder andere Bergtour und Skifahrt unternehmen durfte, und zum anderen Florian Bauer, mit dem ich unbeirrbar die Tradition der mittäglichen Kaffeepause am Leben erhielt. Die fast regelmäßig abgehaltenen Kartrennen der 'Formula Φ' werden mir ebenso in guter Erinnerung bleiben wie deren phantastische Auswertung durch Mark Rolinec.

Diese Arbeit wurde finanziell getragen vom Max-Planck-Institut für Physik

(Werner-Heisenberg-Institut) in München und vom Sonderforschungsbereich 375 für Astroteilchenphysik der Deutschen Forschungsgemeinschaft.

Selbstverständlich möchte ich auch meinen lieben Eltern herzlichst danken, die mich in vielfältigster Art und Weise wann immer möglich unterstützen. Nach 30 Jahren habe ich nun endlich meinen berufsqualifizierenden Abschluß erlangt.